

THE OXIDATION OF HYDROGEN CHLORIDE
IN A MICROWAVE DISCHARGE

by

William W. Cooper IV

S.B., Massachusetts Institute of Technology
(1963)

S.M., Massachusetts Institute of Technology
(1964)

Submitted in Partial Fulfillment
of the Requirements for the
Degree of Doctor of Science

at the

MASSACHUSETTS INSTITUTE OF TECHNOLOGY

November, 1966

Signature of Author:.....
Department of Chemical Engineering
November 14, 1966

Certified by:.....
Thesis Supervisor

.....
Thesis Supervisor

Accepted by:.....
Chairman,
Departmental Committee on Graduate Theses

ABSTRACT

THE OXIDATION OF HYDROGEN CHLORIDE
IN A MICROWAVE DISCHARGE

by

William W. Cooper IV

Submitted to the Department of Chemical Engineering
on November 14, 1966, in partial fulfillment of the
requirements for the degree of Doctor of Science.

The microwave discharge has been investigated as a low temperature medium for carrying out the oxidation of hydrogen chloride. The reactor consisted of a straight quartz tube with provision for either air or oil cooling. A Raytheon PGM 100 generator provided continuous wave power at 2450 megacycles per second. A tapered waveguide terminating section coupled the power into the plasma.

Using oxygen and hydrogen chloride feeds mixed in stoichiometric proportions, conversions of over 50% of the hydrogen chloride to chlorine were obtained. The observed variations in yield as the absorbed power ranged from 100 to 700 watts and the pressure, from 4 to 40 millimeters of mercury are interpreted in terms of the ratio of electric field strength to pressure, E/p , as being the proper variable for control of the chemical products from the discharge. Operation with air instead of oxygen is possible but with a reduction in yields. The best energy efficiencies obtained show 2.3 kilowatt-hours of energy absorbed in the discharge per pound of chlorine produced.

Studies made when only one of the reactant gases was subjected to the discharge followed by mixing downstream with the other indicate that the active initiating species is either the oxygen or hydrogen atom.

The success of this work points to a general applicability of the low temperature plasma technique for carrying out chemical reactions with favorable thermodynamics but poor kinetics.

Thesis Supervisors:

Harold S. Mickley
Ford Professor of
Chemical Engineering

Raymond F. Baddour
Professor of
Chemical Engineering

Department of Chemical Engineering
Massachusetts Institute of Technology
Cambridge, Massachusetts
November 14, 1966

Professor Edward N. Hartley
Secretary of the Faculty
Massachusetts Institute of Technology
Cambridge, Massachusetts

Dear Professor Hartley:

In accordance with the regulations of the Faculty, I herewith submit a thesis entitled "The Oxidation of Hydrogen Chloride in a Microwave Discharge," in partial fulfillment of the requirements for the degree of Doctor of Science at the Massachusetts Institute of Technology.

Respectfully submitted,

William W. Cooper IV

ACKNOWLEDGMENTS

The author wishes to express his appreciation and thanks to his advisors, Professors Harold S. Mickley and Raymond F. Baddour for their suggestions and assistance during the course of this work. He also would like to acknowledge the value of many critical discussions with Mr. Alexis T. Bell and Dr. Peter H. Dundas both on the theoretical and practical aspects of the work.

Thanks are also due the National Science Foundation for its support of both the work and the author through a Cooperative Graduate Fellowship.

The loan of the spectrograph by Professor Richard C. Lord of the Department of Chemistry and his assistance in interpreting spectra are gratefully acknowledged. Harry C. Greenlaw, Jr. generously contributed his knowledge and facilities for the development of the spectroscopic plates.

Al Merrill assisted with the construction of various pieces of the experimental apparatus in the Chemical Engineering Shop.

Finally, the author would like to thank his wife, Martha, for bearing with him and providing her support during the course of the research and writing.

TABLE OF CONTENTS

	<u>Page</u>
I. SUMMARY	
A. Introduction	1
B. Apparatus and Procedure	2
C. Results and Conclusions	3
II. INTRODUCTION	
A. Background	9
B. Previous Work	12
C. Discharge Excitation	18
D. Objectives	
1. Areas of Investigation	24
2. System	25
III. APPARATUS	
A. General Description	27
B. Microwave Equipment	27
C. Gas Feed System	32
D. Sample System	33
E. Reactor and Cooling System	33
F. Calorimeter	34
G. Spectrograph	37
H. Resonant Cavity	37
IV. PROCEDURE	
A. Mixed Feed	40
B. Separated Feed	44

	C. Measurements	
	1. Temperature	44
	2. Spectra	45
	3. Energy Balance	46
	4. Calorimeter	46
	5. Cavity	47
V.	RESULTS	
	A. Mixed Feed	48
	B. Separated Feed	57
	C. Measurements	67
VI.	DISCUSSION OF RESULTS	
	A. Premixed Reactants	
	1. Effects of Pressure and Power	78
	2. Economics	84
	3. Quench	90
	B. Separated Feed	
	1. Reactors	92
	2. Kinetics	94
	3. Recombination	97
	4. Diffusion	99
	5. Mass Balance	102
	6. Test of the Diffusion, Wall Recombination Model	104
	7. Recommendations for Future Work	105
	C. Measurements and Errors	
	1. Temperature	107

2.	Spectra	108
3.	Power Measurements	109
4.	Calorimetry	110
5.	Tunable Cavity	112
VII.	CONCLUSIONS	116
VIII.	RECOMMENDATIONS	117
APPENDIX A.		
A.	Details of Calculations for Oxygen Discharge	118
B.	Details of Calculations for Hydrogen Chloride	120
C.	Calculation of δ	131
APPENDIX B.	Thermodynamics	132
APPENDIX C.		
A.	Reynolds Number	135
B.	Estimate of Diffusivity	136
APPENDIX D.		
A.	Derivation of Diffusion Equation	137
B.	Average over the Radius	141
C.	Magnitude of Terms	141
D.	Approximation for a_i	142
APPENDIX E.	Error Estimate of Measured Temperature	145

APPENDIX F.	
A. Wet Analysis	147
B. Energy Balance	148
C. Calorimetry	150
D. Voltage Standing Wave Ratio and Absorbed Power Calculation	151
APPENDIX G. Technique of Electric Field Measurement	153
APPENDIX H. Nomenclature	156
APPENDIX I. Location of Original Data	159
APPENDIX J. Literature Citations	160
APPENDIX K. Biographical Note	165

LIST OF FIGURES

<u>Figure Number</u>		<u>Page</u>
1.	Conversion Versus Pressure	6
2.	Oxygen Atom Decay	8
3.	Hydrogen Atom Decay	8
4.	Schematic of Apparatus	28
5.	Experimental Equipment	29
6.	Thermowell Reactor	35
7.	Tungsten-Filament Calorimeter, Disassembled	36
8.	Tunable Resonant Cavity	38
9.	Resonant Cavity Partially Disassembled	39
10.	Schematic of Purge System	43
11.	Conversion Versus Power at 20 mm Hg Pressure	49
12.	Conversion Versus Power at 10 mm Hg Pressure	50
13.	Conversion Versus Pressure	51
14.	The Effects of Using Air as the Oxidizer	55
15.	Effect of Nitrogen Quench	56
16.	The Three Designs of Separated Feed Reactor	58
17.	Conversion Versus Position of HCl Input with Impinging Flow Reactor	59
18.	Conversion Versus Position of HCl Input with Lateral Injection Reactor	60
19.	Conversion Versus Position of HCl Input with Side Wall Injection Reactor	62
20.	Oxygen Atom Concentration Versus Time of Flight	63

LIST OF FIGURES (Continued)

<u>Figure Number</u>		<u>Page</u>
21.	Conversions versus Position of O ₂ Input	64
22.	Hydrogen Atom Concentration versus Time of Flight	66
23.	Temperature Profile below an Oxygen Discharge	68
24.	Temperature Profile below an Hydrogen Chloride Discharge	69
25.	Spectra of the Discharges	70
26.	Cavity Resonant Curve with Iris Coupling	75
27.	Cavity Resonant Curve with Loop Coupling	76
28.	Cavity Resonant Curve with Iris Coupling and Microwave Absorbent Material	77
29.	Dissociative Attachment Cross Section of Oxygen	79
30.	Phase Curve	114
A-1.	Oxygen Velocity Time Data at 10 mm Hg	121
A-2.	Oxygen Velocity Time Data at 20 mm Hg	122
A-3.	Hydrogen Chloride Velocity Time Data at 10 mm Hg	127
A-4.	Hydrogen Chloride Velocity Time Data at 20 mm Hg	128
B-1.	Conversion versus Equilibrium Temperature	133
B-2.	Temperature Profiles	134
D-1.	Annular Volume Element	137
D-2.	Transcendental Equation Plot	143
F-1.	Bayol-35, Physical Property Data	149
G-1.	Resonance Curve	154

LIST OF TABLES

<u>Table Number</u>		<u>Page</u>
I.	Diameter and Flow Effects (mixed feed)	53
II.	Energy Balance	72
III.	Calorimetric Data	73
IV.	Energy Requirements	87
A-1.	Oxygen Atom Data at 10 mm Hg Pressure	123
A-2.	Oxygen Atom Data at 20 mm Hg Pressure	124
A-3.	Hydrogen Atom Data at 10 mm Hg Pressure	129
A-4.	Hydrogen Atom Data at 20 mm Hg Pressure	130

I. SUMMARY

A. Introduction

As electricity in its various forms has become progressively cheaper, interest in using it as a chemical processing tool has correspondingly increased. Strictly electrolytic techniques for the production of chlorine and aluminum have been in use for many years, but more recently interest has been drawn to the high temperature d.c. plasma arc. This unit has been developed with some success for the production of acetylene by the cracking of methane. There are, however, three inherent disadvantages in arc processes. First they are limited to those reactions which possess favorable high temperature thermodynamics or kinetics such that the desirable products may be removed by a fast quench step. Second, the presence of electrodes presents a contamination problem. And finally, most of the energy required to heat the entire reactant stream to these very high temperatures, 2,000 to 10,000 °K, is lost as far as useful chemical work is concerned.

An examination of most chemical processes shows that they are concerned with supplying either the free energy or activation energy of reaction. When this energy is supplied as heat there is commonly a conflict between thermodynamically favorable operation and reasonable rates. It would be

desirable then to be able to form the active species required for reaction at low temperature.

The plasma arc reactor has demonstrated that electron bombardment will serve to produce the necessary active species at high temperature; however, this same activation may be obtained at low temperatures, under 1,000 °K, in a glow discharge. The use of microwaves provides a convenient means for excitation of such a discharge without the use of electrodes. In the microwave discharge the high electron temperature serves to activate the reactants while the low gas temperature may provide favorable thermodynamics.

The reaction studied in this work was the oxidation of hydrogen chloride to form chlorine and water. This reaction falls into a class characterized by favorable thermodynamics but poor kinetics. In general practice, such processes are usually coaxed along with the aid of a catalyst and the application of heat.

B. Apparatus and Procedure

The microwave discharge was excited by a PGM 100 Raytheon generator. A tapered waveguide terminating section provided the coupling between the microwaves and the cold plasma. Hydrogen chloride mixed stoichiometrically with oxygen was passed through the discharge. Samples were collected in

liquid nitrogen cold traps; and after warming, analysis proceeded by potassium iodide titration of the free chlorine.

The mechanism of the reaction was investigated using a reactor which allowed one gas to be passed through the discharge zone while the other was mixed downstream with it. A knowledge of the temperature profiles and the distance allowed a calculation of the time of flight from the discharge zone to the input position of the second gas. From this number and the conversions, a recombination coefficient characteristic of the particular active species was obtained.

C. Results and Conclusions

Conversions of over 50% of the hydrogen chloride to chlorine were obtained in a mixed feed, flow system. Under the usual operating flow rate of 2.90×10^{-4} moles per second, the lowest energy requirement was 3.7 kilowatt-hours absorbed in the discharge per pound of chlorine formed. By simply increasing the flow rates by a factor of four this lowest value was reduced to 2.3 kilowatt-hours per pound. Limitations in the trapping ability of the liquid nitrogen sampling system prevented further increases in flow rates with any additional efficiencies.

Work was carried out with reactors of three different diameters, 2, 11, and 22 millimeters. No effect of this diameter on conversion was noted, nor was there any great

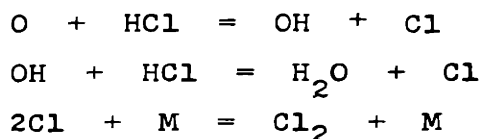
effect on the minimum power required to break down the gas. This minimum was only 17% higher with the 22 millimeter diameter reactor than with the 2 millimeter one. The observation of an increase rather than a decrease in breakdown power as the reactor diameter was made larger indicated that the discharge was recombination or attachment rather than diffusion controlled.

At the sacrifice of some of the yield, it was found to be possible to operate with air as the oxidizer rather than pure oxygen. At 10 millimeters mercury pressure and an absorbed power of 300 watts, the yield fell from 45% to 28% when air was used; but at 20 millimeters under the same conditions, the decline was from 48% to 42%. There was evidence that oxides of nitrogen were being formed indicating that the nitrogen in the air was competing with the hydrogen chloride for the available oxygen.

Efforts to quench the reaction by adding nitrogen downstream from the discharge resulted in no increase in yields. In fact as the input position of the nitrogen was brought closer to the discharge zone, the yields declined toward those obtained when air was used as the oxidizer. The lack of any increase in yield as a result of this rapid cooling tends to indicate that the extent of reaction is being controlled by the quantity of active species formed in the discharge.

In accord with results found by other workers (1) studying the dissociation of hydrogen, the power-pressure data are consistent with the hypothesis that it is the ratio of the electric field strength to pressure which is the proper variable for controlling the yields. Figure 1 shows data taken at two different power levels as the pressure was varied from four to forty torr. The positions of the maxima occur at what are estimated to be the same value of this proper variable. Efforts to measure the electric field strength directly using cavity techniques were not successful.

When oxygen alone was passed through the discharge, the results are consistent with the mechanism below which postulates oxygen atoms as the required initiating species.



As shown in Figure 2, the oxygen atom concentration decayed semilogarithmically independent of pressure indicating a wall loss process. The surface recombination coefficient calculated from the data was 13.1×10^{-4} compared with a literature value of 7.1×10^{-4} for a similar quartz surface.

By subjecting only the hydrogen chloride to the discharge data were obtained which are consistent with the following initiating mechanism (2).

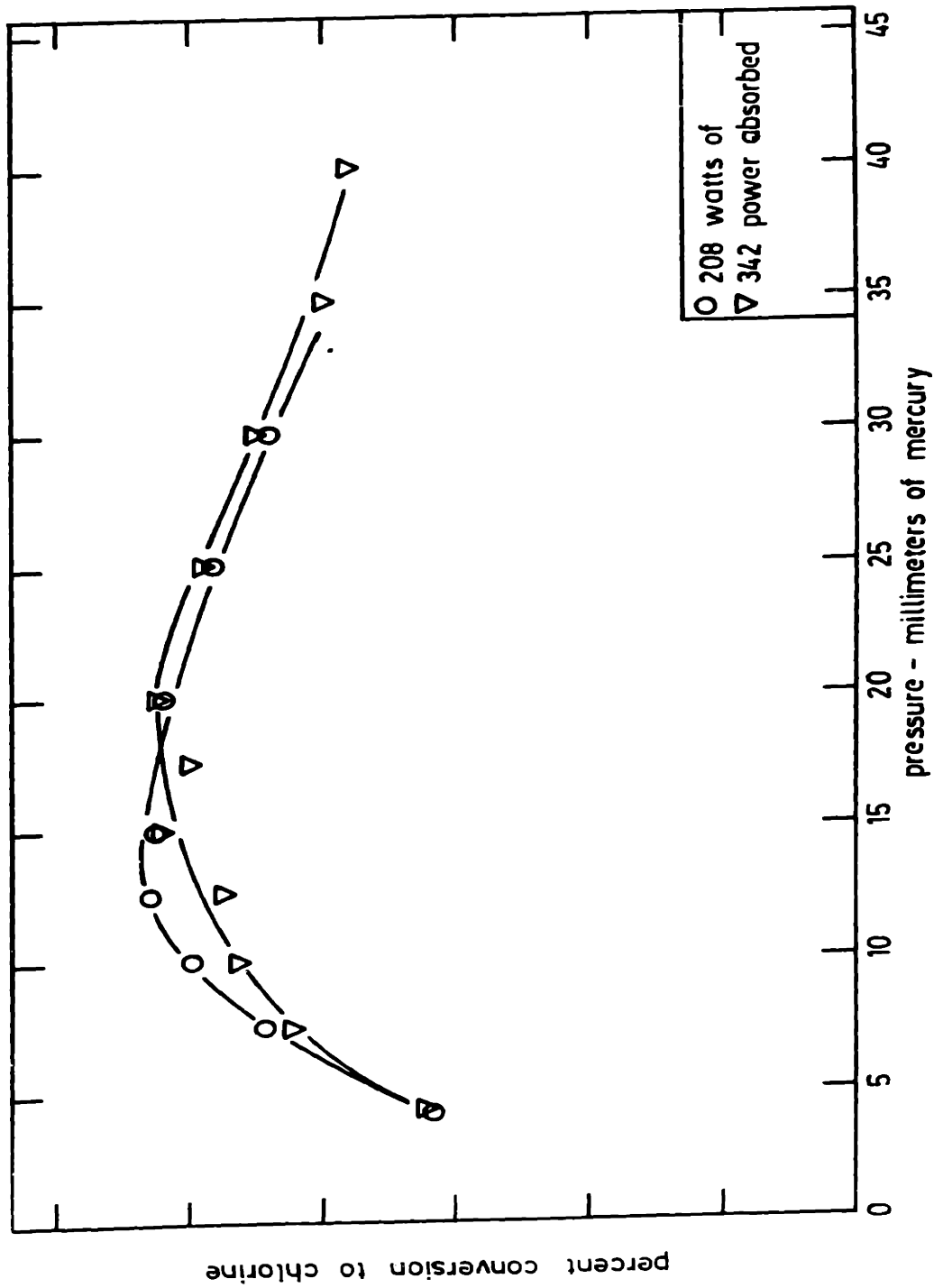
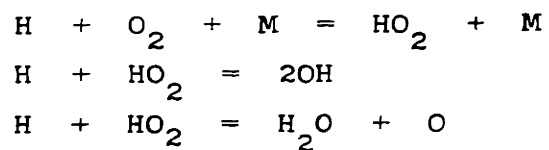


FIGURE 1. CONVERSION VERSUS PRESSURE WITH A MIXED FEED



The decay data in Figure 3 show a slope 2.8 times that in Figure 2. This steeper slope is to be expected if hydrogen atoms are the active species.

Spectra taken of the discharge region support these hypotheses by revealing the presence of hydrogen and oxygen atoms and hydroxyl radicals.

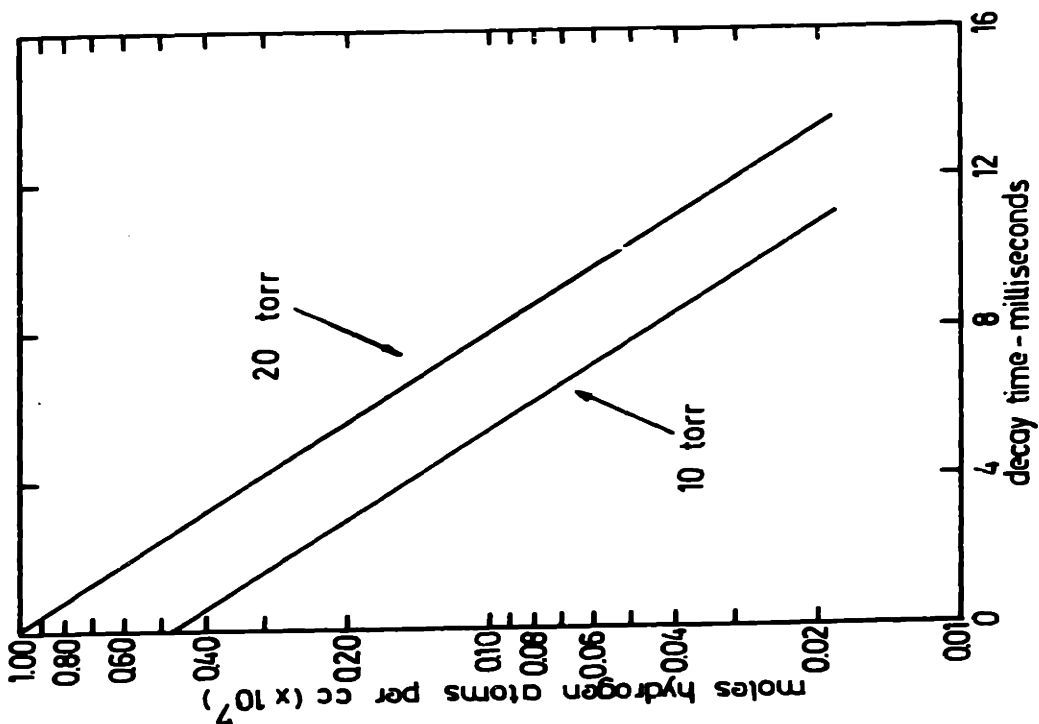


FIGURE 3. HYDROGEN ATOM DECAY

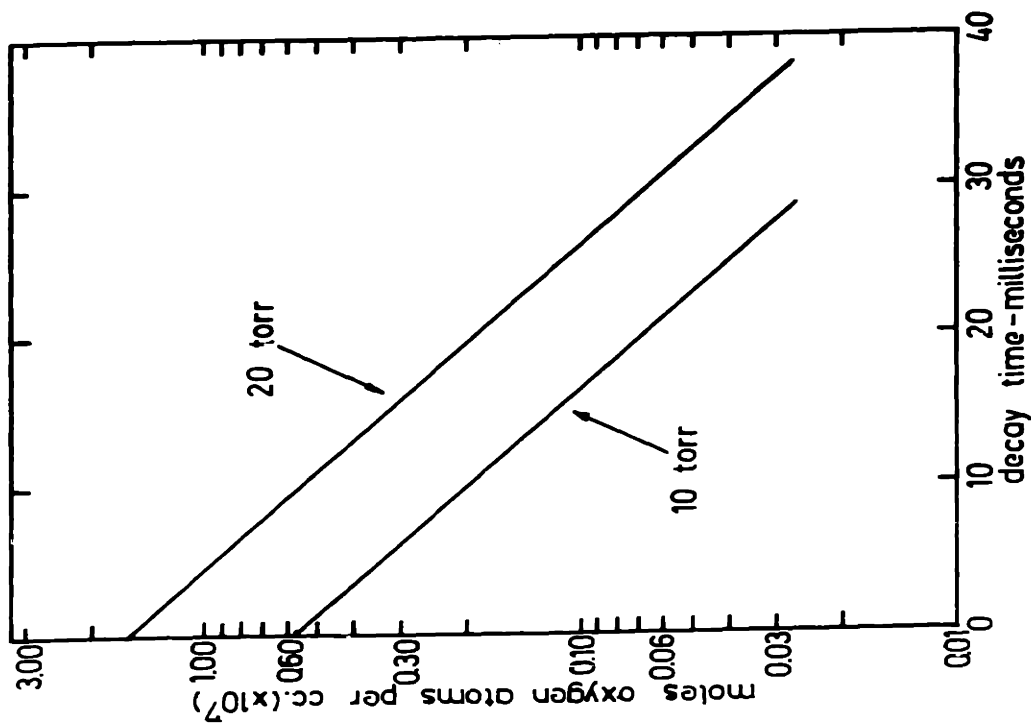


FIGURE 2. OXYGEN ATOM DECAY

II INTRODUCTION

A. Background

Chemical processing usually requires an energy input to the reactant materials either as free energy of reaction or as activation energy. Although heat is the most common form of this energy, electricity is sometimes used as in the electrolytic processes for the production of aluminum or chlorine. Commonly there is a conflict between the reasonable rates obtainable at high temperatures and the favorable thermodynamics existing at low temperatures. The usual method of circumventing this problem is via a catalyst as in the oxidation of sulphur dioxide to the trioxide in sulphuric acid manufacture. Even with such catalysts some heating of the materials is generally required.

From a kinetic viewpoint, the heat added to initiate a reaction serves to produce the necessary active species that starts the reaction sequence. Since high temperatures are often unfavorable thermodynamically for the overall reaction, some method of producing this initiator at low temperatures is desirable. Also since chemical reactions are concerned only with the atom's outer electron shells, funneling the energy directly into these bonding electrons should be a more efficient way to carry out reaction.

Work done with d.c. arcs has shown that chemical reactions may be carried out in high temperature plasmas, and thus that the necessary activation or free energy can be supplied via electronic excitation. The fact that these processes do operate at very high gas temperatures of from 2,000 to 10,000 °K restricts their applicability. They can be used only when the thermodynamics are favorable at these temperatures or the kinetic sequence is such that the desired product may be removed in a quench step. Work done by Iwasyk (3), Blanchet (4), Bronfin (5), and Leutner (6) are good examples of the application of this arc technology. A further drawback to the arc as a processing tool is the d.c. nature of the discharge. This means that electrodes must be present to supply the electrons continually being swept across the reaction volume. These can present a serious contamination problem and if metal, may be catalytic.

These problems associated with arc processes may be avoided through the use of an electrodeless discharge. Here the discharge is contained within a dielectric vessel and requires no electrodes in the discharge zone. Furthermore, such a discharge is a non-equilibrium phenomenon in that the electron temperature is not equal to the gas temperature. This difference provides the opportunity for the excitation of active chemical species through electron collision without the gas temperature's being raised. This

type of discharge presents a promising medium for carrying out reaction because of its relatively low gas temperatures and its high concentration of chemically active species (7).

The work reported here was carried out in a microwave discharge at 2450 megacycles per second. This corresponds to a free space wavelength of slightly over 12 centimeters. Although McCarthy (7) indicates that a microwave discharge is a particularly rich source of chemically excited species, the physics show no reason why microwaves should be any better for excitation than any other high frequency. As long as this frequency is high enough so that all free electrons are not swept out of the discharge volume over the period of a half cycle, there should be no difference in discharges. If these electrons are all lost over this time period and must be replaced in each half cycle, then the discharge is indistinguishable from a d.c. glow discharge.

The frequency is unimportant because the excitation is via a collisional process and the molecule excited knows only that it was struck by an electron of a certain energy, not how the electron gained this energy. This picture is in direct contrast to various quantum absorption processes such as photochemical reactions. There a selectivity is obtained by radiation of the reactants at the particular frequency whose quanta correspond in energy to the desired process.

B. Previous Work

Although microwave power sources were developed for radar applications during World War II and the physical mechanism of gaseous breakdown was studied extensively during the next decade (8, 9, 10), their use as a means of providing active species for a chemical reaction was not reported until 1954 in a paper by McCarthy (7). Certainly part of the reason for a lack of interest in them as a chemical processing tool arose from the costs associated with this type of power. Nevertheless since that time, there have been a number of investigations into the phenomena involved when microwaves are used to break down a gas into a plasma which provides a source of excited species for chemical reaction.

The production of atomic hydrogen in a microwave discharge has been reported by Shaw (11) and Bak and Rastrup-Anderson (12). Conversions of up to 90% of the molecules to atoms were reported. In a separate paper, Shaw (13) notes that water vapor appears to have a catalytic effect on the production of hydrogen atoms. He obtained his best results at a flow rate of 10^{-5} moles per second, an input power of 100 watts, a pressure of 0.5 torr, and a frequency of 3,000 megacycles per second. He also found that as he increased the flow rates the yield of atoms increased but the extent of dissociation dropped to 25% at a flow of

1.5×10^{-4} moles per second.

Young et al (14) studied the dissociation of nitrogen molecules to the atoms in a microwave discharge. They found that the nitrogen atom density was increased by two orders of magnitude when SF₆ was added in minute amounts to the feed stream. Similar results were obtained when oxygen or nitric oxide was the added gas. They concluded that small amounts of impurities largely determine the degree of dissociation of the nitrogen in the discharge.

The dissociation of oxygen in a microwave discharge has been studied by Elias et al (15) and by Kaufman and Kelso (16). Although exact mechanisms are not determined, the latter workers note the apparant importance of impurities particularly nitrogen in determining the oxygen atom yields. In addition to atoms Foner and Hudson (17) report the $^1\Delta_g$ metastable oxygen molecule to be a product of the microwave discharge in oxygen.

The halogens have also been subjected to the influence of a microwave discharge. Ogryzlo (18) reports obtaining large concentrations of chlorine, bromine, and iodine atoms in a flow system. The rapid surface recombination of these atoms was prevented by the used of various acid poisons on the reactor walls.

As mentioned above, McCarthy (7) did some of the earliest work in the area of microwave plasma chemistry. In particular his work involved the synthesis of acetylene from methane and the production of nitric oxide from nitrogen and oxygen.

In addition to these two syntheses, he studied free radical production in oxygen, nitrogen, and hydrogen discharges. He presented evidence which indicated that the active species from the discharge are free radicals and not charged particles. To correlate the data obtained, he proposed two empirical parameters, one applicable for molecular dissociation and the other for synthesis. The correlation made there is the only work known to the author in which an attempt has been made to relate the electrical parameters of the discharge to the chemical reaction occurring. McCarthy also notes that the most efficient operation is obtained when the discharge is operated on the verge of extinction.

McTaggart (19) found that a 2450 megacycle discharge decomposed carbon dioxide and deposited elemental carbon of amorphous structure on the reactor walls. The effluent gases contained oxygen and carbon monoxide in addition to carbon dioxide. When power levels just sufficient to maintain the discharge were used, red deposits of carbon suboxide were formed. Hydrogen added to the input carbon dioxide produced three different types of deposits on the tube walls. The first was a yellow polymeric material with an empirical formula of $C_{25}H_{35}O$. The other two deposits were both carbon, but one appeared as rings while the other was a amorphous formation. The gaseous products from the discharge contained water and formaldehyde. In further work,

McTaggart (20,21) reports the reduction of the alkali and alkaline earth halides to the metals by bombarding them with the products of a microwave discharge in hydrogen.

Further work with hydrocarbon systems in a microwave discharge was done by Vastola and Wightman (22). They found hydrogen to be the major gaseous product when methane, ethane, and ethylene were passed through the discharge. A polymeric film of amorphous structure was also formed which absorbed added hydrogen until the H/C ratio approached 1.6. The lack of any mention of acetylene production from methane is in contrast with the results McCarthy (7) reported. When acetylene, benzene or naphthlene were subjected to the discharge no gaseous products were produced. These compounds also yielded a polymeric material which took up hydrogen until the H/C ratio approached 1.6.

Heterogeneous reactions of solid carbon and the products of a microwave discharge in hydrogen, oxygen, or water vapor were investigated by Vastola, Walker, and Wightman(23). Small amounts of hydrocarbons were formed when solid carbon was placed directly inside the hydrogen discharge. Carbon monoxide was the major product when the solid carbon was placed either inside or downstream from an oxygen discharge. The products of the water discharge reacted with the carbon to yield hydrogen and carbon monoxide.

Twenty-five individual components were detected by

Coates (24) in the product mixture issuing from a microwave discharge in n-hexane. He explained the relatively large concentrations of branched products in the $C_6 - C_8$ category by the stability of the isobutyl radical in the discharge zone. The product distribution reportedly was unaffected as the power level was varied from 25 to 125 watts.

The work of Streitwieser and Ward (25) is unique in that they are the only workers that feel a charged molecular anion, not a free radical, is the important energy carrier. They passed toluene vapor in a helium carrier gas through the discharge zone and found benzene, ethylbenzene, styrene, and phenylacetylene to be the products. Because there were only minor amounts of xylenes and biaryls, they felt that free radicals were not important intermediates. In light of the work of McTaggart (19) and Vastola and Wightman (22), the lack of any mention of a polymeric material's being formed is somewhat surprising.

Smith and Engelhardt (26) investigated the reactions of SF_4 in a microwave discharge using a reactor lined with alumina. They found a 59% conversion of the SF_4 with an 80% yield of SF_6 . Other products included SOF_2 , SCF_4 , SO_2 , and SiF_4 . Emeleus and Tittle (27) also investigated sulphur fluoride chemistry in a microwave discharge. They studied the reaction of SF_6 with chlorine and oxygen and reported the formation of pentafluoro-sulphur chloride and sulphur oxide tetrafluoride.

Digermanium hexachloride was prepared from germanium tetrachloride in a microwave discharge by Shriver and Jolly (28). Frazer and Holzmann (29) report that a microwave synthesis of diboron tetrachloride from boron trichloride is the best method of preparing that compound. Their work is somewhat unusual in that the entire system was maintained at -78.5°C with the product being collected at -111.9°C .

Work done by Root(30) on the reaction of tetrafluoromethane in a microwave discharge showed the formation of a fluoro-carbon wax product. Infrared spectra showed the molecule to have carbonyl bonds and a repeating CF_2 unit.

C. Discharge Excitation

The conditions for breakdown of a gas to form a plasma have been derived by a number of workers (8, 31) and will not be discussed in detail here. Basically the criterion is that the rate of electron production equal the rate of loss from diffusion, recombination, and attachment. In this section the emphasis is placed on the chemical excitation occurring in the plasma.

Consider a solitary electron which is subjected to an oscillating high frequency electric field. Let this field have components only in the "z" direction. It can then be written as:

$$E = E_0 \sin \omega t \quad (1)$$

If Newton's second law is written for this sole electron, the following equation results:

$$F = m d^2 z / dt^2 = -q E_0 \sin \omega t \quad (2)$$

The work done on the electron in a time "dt" as it moves a distance "dz" under the influence of the field can be expressed as:

$$dW = F \cdot dz = -q E_0 \sin \omega t dz \quad (3)$$

Considering the electron to have no initial velocity, the integration of Equation (2) once results in:

$$dz/dt = (q E_0 / \omega) (\cos \omega t - 1) \quad (4)$$

When Equation (4) is substituted into Equation (3) there results:

$$dW = (-q^2 E_0^2 / \omega) (\sin \omega t \cos \omega t - \sin \omega t) dt \quad (5)$$

If this expression for the work done by the field on the electron is integrated over the period of a cycle, that is from $t = 0$ to $t = 2\pi/\omega$, the net work is zero. Hence, the electron experiences no net energy gain from the field.

The situation changes markedly when the electron can undergo collisions. In this case Equation (2) must be rewritten to include the effects of momentum transfer on collision. It then becomes (42):

$$m d^2z/dt^2 + m\gamma_m v = -qE_0 \sin \omega t \quad (6)$$

In terms of the electron's velocity this is a first order equation.

$$dv/dt + \gamma_m v = (-qE_0/m) \sin \omega t \quad (7)$$

Again assuming that the initial velocity at time $t = 0$ is zero, integration of Equation (7) yields:

$$\frac{dz}{dt} = \frac{(-qE_0/m)(\gamma_m \sin \omega t - \omega \cos \omega t - \omega)}{(\omega^2 + \gamma_m^2)} \quad (8)$$

Substituting Equation (8) into Equation (3) and integrating from $t = 0$ to $t = 2\pi/\omega$ results in the following expression for the work done on the electron over the period of a cycle:

$$W = \frac{q^2 E_0^2 \pi \gamma_m}{m \omega (\omega^2 + \gamma_m^2)} \quad (9)$$

Since the frequency of the field is related to the radian frequency by the simple relation: $f = \omega/2\pi$, the power input to this electron is given by the product of the work per cycle and the frequency. The resulting equation for the

power input per electron is:

$$P = \frac{q^2 E_0^2}{2m \gamma_m} \left(\frac{v_m^2}{v_m^2 + \omega^2} \right) \quad (10)$$

Thus it is shown that when an electron can undergo collisions it is capable of picking up energy from the applied electric field. Physically this pick-up results from the electron's obtaining a component of velocity perpendicular to the direction of the field. Work is done on the electron as the field tries again to orient it to oscillate parallel with the field vector. One further point which should be noted about the derivation given is that it assumes that the collisions experienced by the electrons are perfectly elastic so that the absolute magnitude of the kinetic energy of the system is unchanged on collision.

Through a series of these elastic collisions, the electrons progressively gain energy until finally they have enough energy to undergo an inelastic collision. The result of such a collision is the excitation of the atom or molecule with which the electron collides. In this way, the active chemical species which cause reaction are produced in the plasma.

Vasilev (32) has performed an energy balance on these colliding electrons. From this calculation he has determined the fraction of the energy transferred on collision which goes into the excitation of a particular level of the struck

molecule. He has shown that the distribution of this energy among the various possible levels for excitation is a function only of the electron temperature. Hence, this is the important parameter that determines the products from a chemical reaction carried out in an electric discharge. Since the average energy of the electrons is related to their temperature and kinetic energy by the equation:

$$\epsilon_0 = (3/2)kT_e = \frac{1}{2}m\bar{v}^2 \quad (11)$$

the variable which controls the electrons' energy will control their temperature.

Massey and Cannon (33) have developed the equations necessary to determine this important physical parameter. Equation (10) may be rewritten in terms of an effective field strength as:

$$E_{\text{eff}}^2 = E_0^2 \gamma_m^2 / (\gamma_m^2 + \omega^2) \quad (12)$$

and the collision frequency may be written in terms of its cross section as:

$$\gamma_m = \bar{v}NQ \quad (13)$$

In these equations \bar{v} is the average electron speed; N, the gas density; and Q the elastic collision cross section. Finally a quantity " δ " is defined as the fraction of an electron's energy which is transferred upon collision. For a perfectly elastic collision $\delta \cong 2m/M$. At steady state there is a balance between the rate at which energy is being imparted to the electrons from the field and the rate at which the electrons are passing it on to the particles with

which they collide. This balance may be expressed as:

$$q^2 E_{\text{eff}}^2 / 2m \nu_m = \delta \nu_m \epsilon_o \quad (14)$$

Rearrangement of Equation (14) gives:

$$\epsilon_o = q^2 E_{\text{eff}}^2 / 2m \delta \nu_m^2 \quad (15)$$

The use of Equations (11) and (13) transform Equation (15) to:

$$\epsilon_o^2 = q^2 E_{\text{eff}}^2 / 4N^2 Q^2 \delta \quad (16)$$

Then using the perfect gas laws, the number density of molecules may be expressed as:

$$N = (6.02 \times 10^{23}) / (2.24 \times 10^4) (p/p_o) (T_o/T_g) \quad (17)$$

In Equation (17), p_o and T_o are the standard pressure and temperature. The average electron energy in ergs then becomes:

$$\epsilon_o = (qp_o) / 2 \delta^{1/2} T_o (2.7 \times 10^{19}) (E_{\text{eff}}/p) (T_g/Q) \quad (18)$$

Equation (18) demonstrates the importance of the ratio of the electric field strength to pressure as the proper variable for determining the products of chemical synthesis in an electrical discharge. Since under the conditions of operation, the electron collision frequency is approximately 10^{11} per second and the microwave radian frequency is 10^{10} per second, the effective field is very nearly the same as the applied field, E_o ; and no correction via Equation (12) is necessary. Brown and MacDonald (34) have shown the importance of the ratio of the electric field strength to pressure as a variable in correlating breakdown data.

If this variable, commonly denoted E/p , is in fact important chemically, the yields from a reaction in a discharge should correlate with it. Work carried out by Lunt and Meek (1) showed that this was in fact the case for hydrogen molecule dissociation. In their work on the production of hydrogen atoms in the positive column of a d.c. discharge, they found that the atom production was maximized when E/p was held at 30 volts/cm/mm-Hg.

D. Objectives

1. Areas of Investigation With the exception of the work by McCarthy (7), the microwave discharge and the chemical processes occurring there have been treated as a "black box." No attention has been given to the control of the active species produced or how to maximize production of those considered desirable for the reaction under study. The theoretical considerations presented in Section C. above indicate that by regulating the ratio of the electric field strength to pressure, the energy of the plasma's electrons may be controlled. Since the cross sections for the various excitation processes are a function only of the electrons' kinetic energy, the product distribution from the discharge will be determined by control of this energy. Within the limitations imposed by the available equipment, work was done to test the hypothesis that E/p does govern chemical synthesis in a microwave discharge.

Because operation under the wrong electrical conditions would favor competing processes via the production of other active species, a knowledge of the kinetics of the process occurring is desirable. With this knowledge, E/p can be controlled so that the operation yields the maximum amount of the desired initiator with a minimum amount of side reaction precursors. Previous work has not dealt in detail with the mechanisms of the chemical processes. Because of

the high energy nature of the discharge itself, it is difficult to make direct chemical measurements in that zone, but spectroscopy provides a useful tool for revealing what species are present. Efforts were also directed toward using decay techniques to determine the product which was responsible for initiating reaction. With this information considered as a whole, a kinetic mechanism could be constructed.

2. System The oxidation of hydrogen chloride provides in many ways an ideal system for study. The reaction as shown below:



is thermodynamically favorable and free from side reactions but will not readily proceed because of kinetic hinderances. During the late 1800's and early 1900's, this process assisted by a copper chloride catalyst was a commercially important method of chlorine production. With the advent of the electrolytic cell, brine electrolysis replaced it as the major process for chlorine manufacture. Recently interest in this Deacon Reaction has increased markedly as hydrogen chloride from chlorination processes has become a troublesome by-product. However, most efforts in this area have been directed toward the development of a better catalyst

to take advantage of the favorable thermodynamics at low temperatures.

The use of a low temperature plasma presents another way of carrying out this process in a region where the thermodynamics are favorable. While in an overall chemical sense, the microwave discharge supplies the necessary activation energy for the reaction, from a kinetic viewpoint the plasma provides the active species able to initiate the reaction. Because low temperature thermodynamics are favorable, there is no necessity for a rapid quench step to freezeout the products at some favorable high temperature equilibrium point.

III APPARATUS

A. General Description The system pictured schematically in Figure 4 allowed the passage of the reactant hydrogen chloride and oxygen to a region of high microwave power level. Here these gases were broken down under the influence of the field to form a plasma which provided the active species for reaction. The products from this discharge region were collected in a cold trap immersed in liquid nitrogen. The microwave power, pressure, and gas flow rates were the controllable variables.

B. Microwave Equipment A close-up photograph of the microwave power control system is shown in Figure 5. Here the generator, a Raytheon model PGM-100, is pictured at the far left. The magnetron was capable of a continuous wave power output of from 500 to 1,000 watts at 2450 megacycles per second. Power was fed into RG104/U waveguide for transmission to the discharge which provided the load.

Inserted in the waveguide closest to the generator was a 12 decibel, water cooled, isolator section which served to absorb reflected power. This section was necessary to prevent possible damage to the magnetron from the reflected wave's interaction with it.

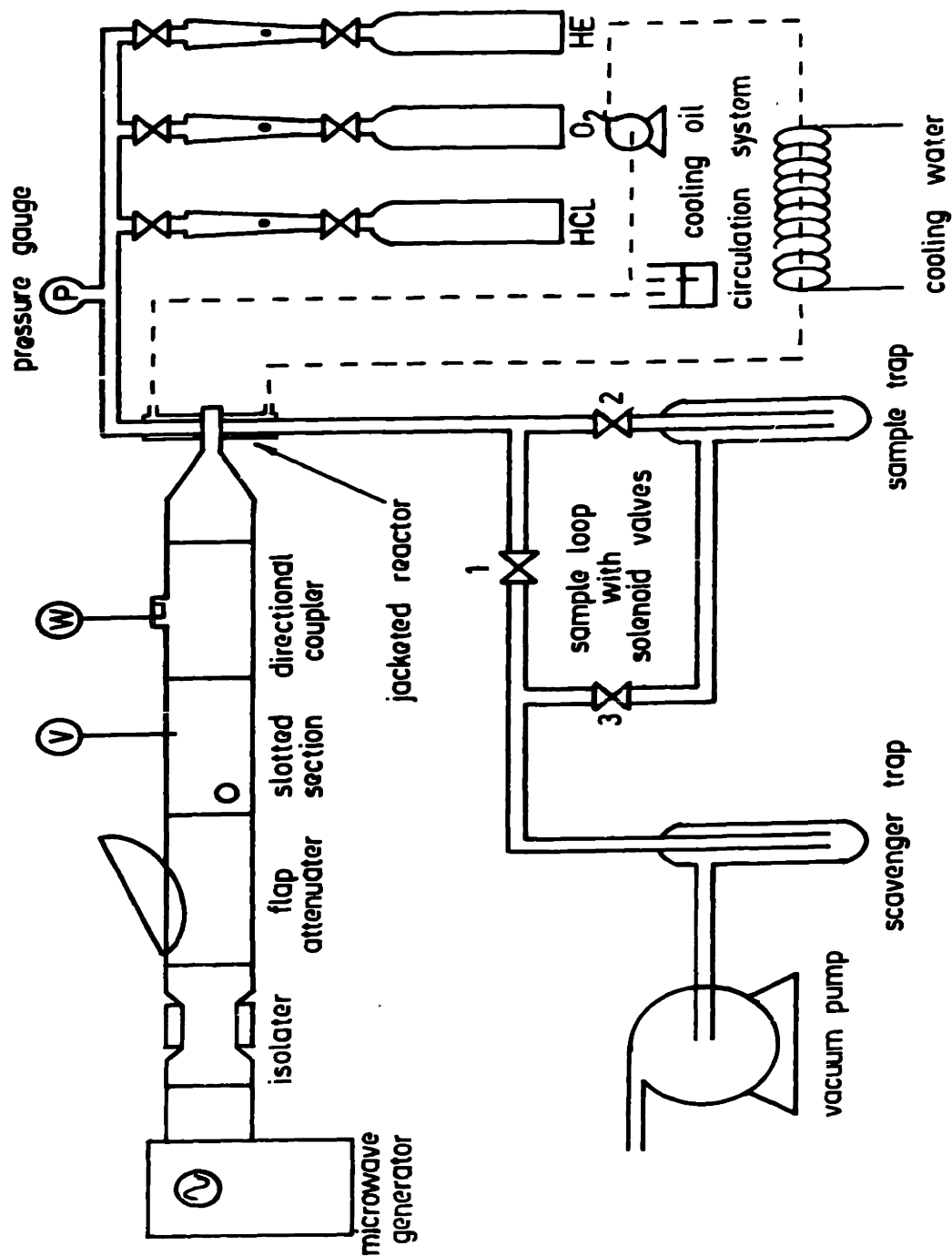


FIGURE 4. SCHEMATIC OF APPARATUS

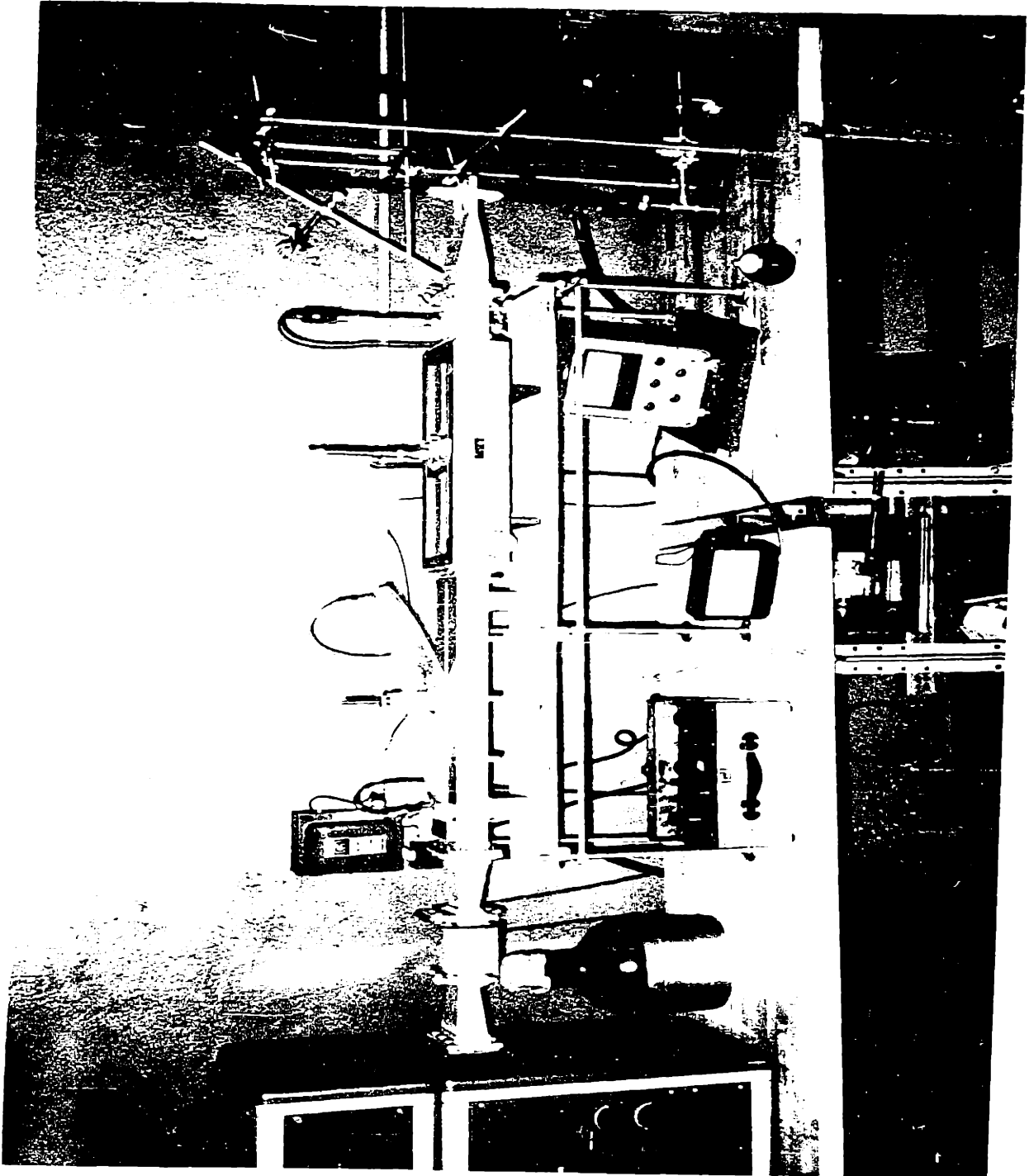


FIGURE 5. EXPERIMENTAL EQUIPMENT

Because the generator itself was capable of operation at an output power level of no less than 500 watts, it was necessary to insert an attenuator in the transmission line. This served to reduce the effective output for low power measurements. This section was formed from a piece of waveguide which had a $\frac{1}{4}$ inch slot cut lengthwise along the top side. Water flowing through a hollowed out, semi-circular, plexiglas flap designed to fit into this slot provided the actual attenuation. The depth to which the flap protruded into the waveguide was adjustable by means of a screw and knurled nut arrangement. With it fully lowered into the guide, the power transmitted to the load could be reduced to zero; and when fully removed, the section had no effect at all. Each side of the centrally cut slot was built up for one half inch to prevent power loss by radiation.

Inserted in the line after the flap type attenuator was a slotted section. This piece of equipment contained a fine wire probe which protruded slightly into a slot cut along the top of the waveguide. A carriage assembly allowed this probe to be traversed along the length of the guide. Since the probe was sensitive to the electric field strength in the guide, it was possible to measure the relative intensity of the maxima and minima of the standing wave in the guide. This measurement was not made directly

but rather by a null method using a pancake attenuator. The voltage standing wave ratio (VSWR) was calculated from these measurements. This provided a direct measure of how well the load was matched to the waveguide.

A loop type directional coupler was used to measure the power incident on the discharge region. This coupler had a directionality in excess of 30 Db. and a coupling coefficient of 49.2 Db. The signal received by this unit was fed into a PRD model #650 microwave power meter. The reading on this meter provided a direct indication of the power incident on the discharge zone. To obtain the power actually absorbed in the plasma, this meter reading was multiplied by the factor: $4(\text{VSWR})/(\text{VSWR} + 1)^2$.

The terminating power transfer section was a tapered piece of waveguide shorted at the far end. A slot was cut in this to accommodate the reactor tube. The operation of this section has been described by Fehsenfeld, Evenson, and Broida (35). The reactor tube was positioned $\frac{1}{4}$ wavelength back from the shorted end so that it would be subjected to the maximum field strength. The reactor tube was passed perpendicularly through the slot so that the electric field was aligned with its axis.

C. Gas Feed System USP grade oxygen taken from the same tank was used for all runs. The anhydrous hydrogen chloride used was supplied by the Matheson Company at a marked purity of 99%. No effort was made to further purify this gas. A pressure, as indicated by mercury manometers, of very slightly over one atmosphere was maintained in the feed system. The flow rates which varied from 85 to 1360 milliliters per minute were monitored on the appropriate Matheson #600 series rotameters. These meters all were independently calibrated and found to agree reasonable well with the calibration supplied by the manufacturer. Stainless steel Nupro fine metering valves controlled the flow rates and provided the constriction across which the pressure was reduced from one atmosphere to that of the operating conditions. From these valves the gases passed into a manifold where they were mixed. The manifold was connected to the quartz reactor tube with a short length of 7/16 inch rubber vacuum tubing.

A Wallace and Tiernan FA-160 absolute pressure gauge which had a range from 0 to 50 millimeters of mercury was used for pressure measurement. A 5/8 inch oriface, vee stem valve equipped with micrometer threads provided the fine throttling necessary for pressure control. The source of the low pressure was a high-capacity Kinney mechanical vacuum pump.

D. Sample System As can be seen in Figure 4, the sample system consisted of a bypass loop leading through 19 millimeter diameter pyrex cold traps. Three Asco solenoid valves were positioned so that the entire product stream could be directed through the traps which themselves were maintained at 77°K by liquid nitrogen. The valves were connected to 5/8 inch monel pipe which provided the structure for the system. Other connections to the reactor and the pump were made with 7/16 inch inside diameter rubber vacuum hose. Except for the reactor itself, nowhere in the system was there a constriction smaller than $\frac{1}{2}$ inch diameter.

E. Reactor and Cooling System The reactor consisted of a 61 centimeter length of 11 millimeter inside diameter quartz tubing. For mixed feed work this tube was jacketed with a large concentric, glass tube connected as a laboratory condenser. A paraffinic petroleum distillate, Bayol 35, marketed by Esso, was circulated through the intervening annular region to provide cooling for the central reactor tube. This non-polar hydrocarbon was essentially transparent to the microwaves. The oil was passed in a closed system through the tube side of a heat exchanger containing water on the shell side. This circulation maintained an oil temperature no higher than 30°C.

A reactor incorporating a thermowell for temperature determination in the region below the plasma is shown in Figure 6. An iron-constantan thermocouple inserted into the well provided the means for making the actual measurements.

Three different designs of separated flow reactors were built. The main feature of each of these was that it allowed one of the reactant gases to be passed through the discharge region while the other unactivated gas was mixed downstream with it. Because of the drastic effect the design had on the results, these are further discussed in the results section and are pictured there in Figure 16.

F. Calorimeter The calorimeter design was copied exactly from that reported by Shaw (36). Each filament was constructed from the double helix, tungsten wire in an hundred watt light bulb. The supporting wires were all glass coated to prevent surface recombination there. The photograph in Figure 7 shows the general layout and dimensions. Each of the three wires is at an angle of 120° to the others and could be connected separately as one arm in a wheatstone bridge circuit.

william w. cooper Sc.D. thesis 9/30/66

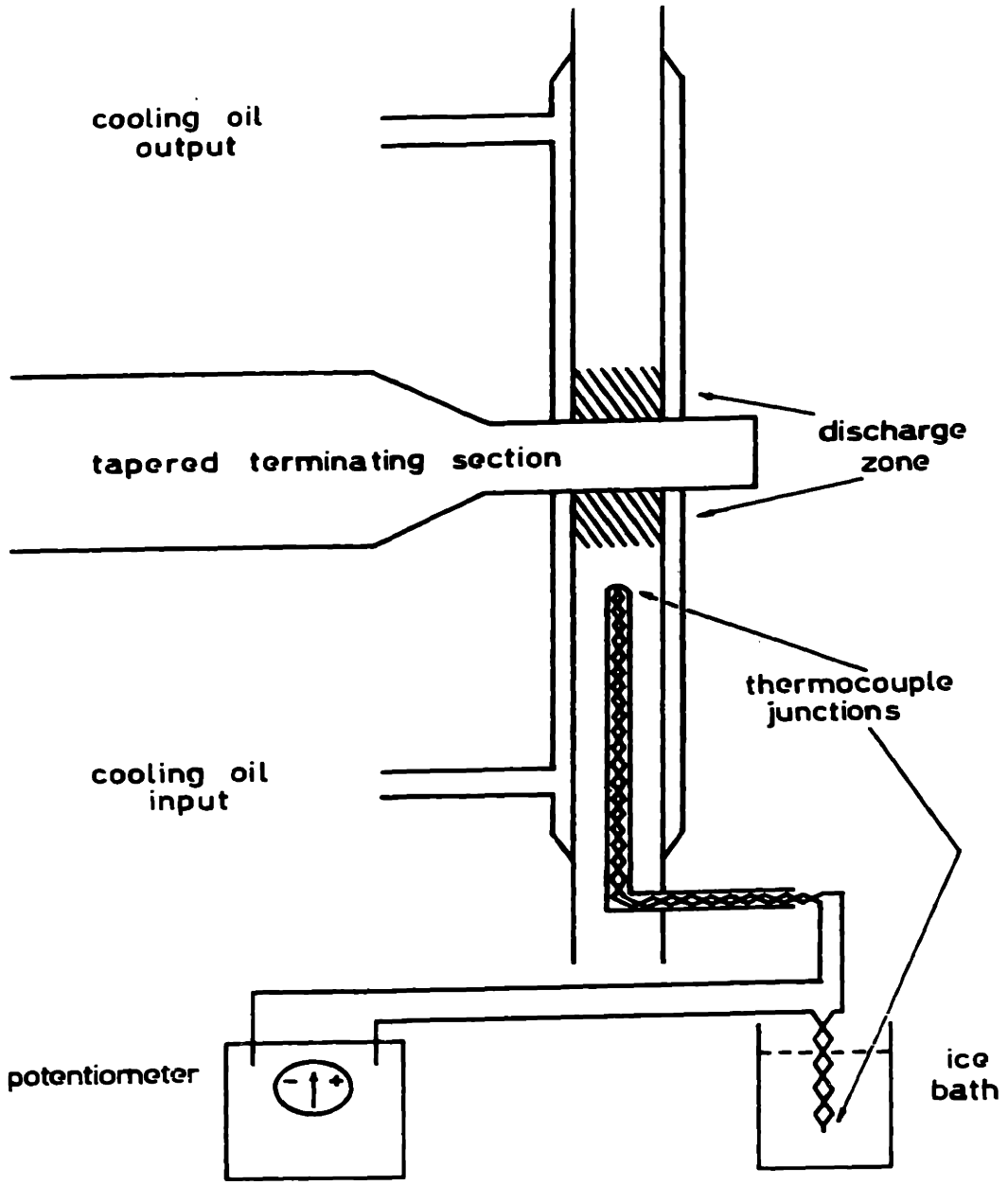


FIGURE 6. THERMOWELL REACTOR

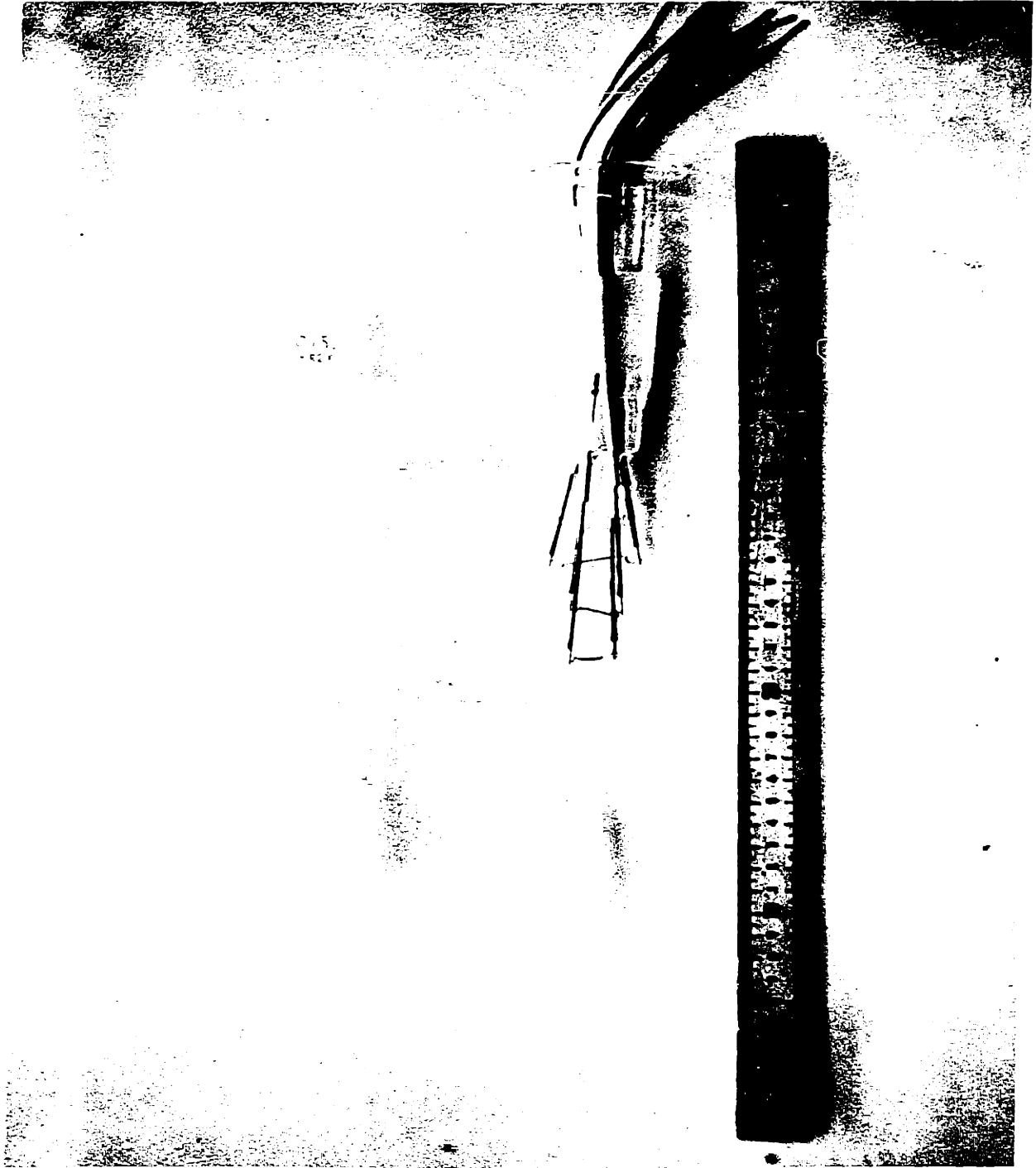


FIGURE 7 TUNGSTEN - FILAMENT CALORIMETER , DISASSEMBLED

G. Spectrograph A Bausch and Lomb medium optical spectrograph was used to separate the spectral components of the light emitted from the discharge. These were focused on Kodak type 103A-0 glass plates which are sensitive to wavelengths from 2100 to 5300 angstroms. The images on the developed plates were printed on Kodak Kodabromide F-5 high contrast paper.

H. Resonant Cavity This cavity was designed and built by Bell (37) who made it available to the author. Figure 8 shows the general layout and important dimensions. Because of its high "Q" characteristics over a wide frequency range and the ease with which it is tuned, the resonant mode was designed to be the TE_{111} . The characteristic feature of a cavity operating in this mode (59) is its ability to be tuned by changing the position of a piston within it. This motion was accomplished by turning a threaded nut which forced a screw-shaft-plunger assembly to move. The construction material was brass except for the piston itself which was copper. The photograph in Figure 9 shows the separate parts with the cavity partially disassembled. Coupling to the waveguide was through either an iris or loop.

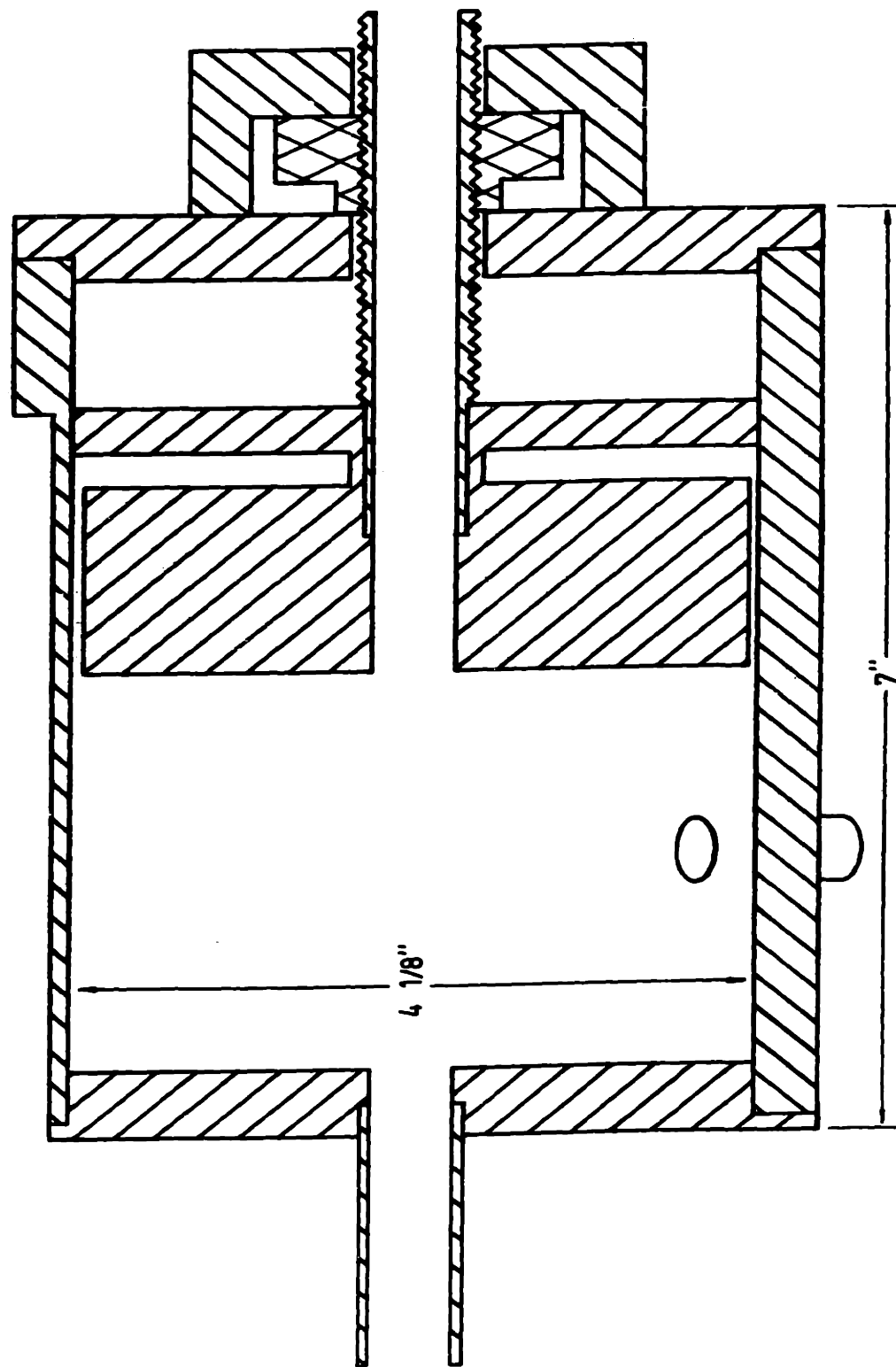


FIGURE 8. TUNABLE RESONANT CAVITY full scale

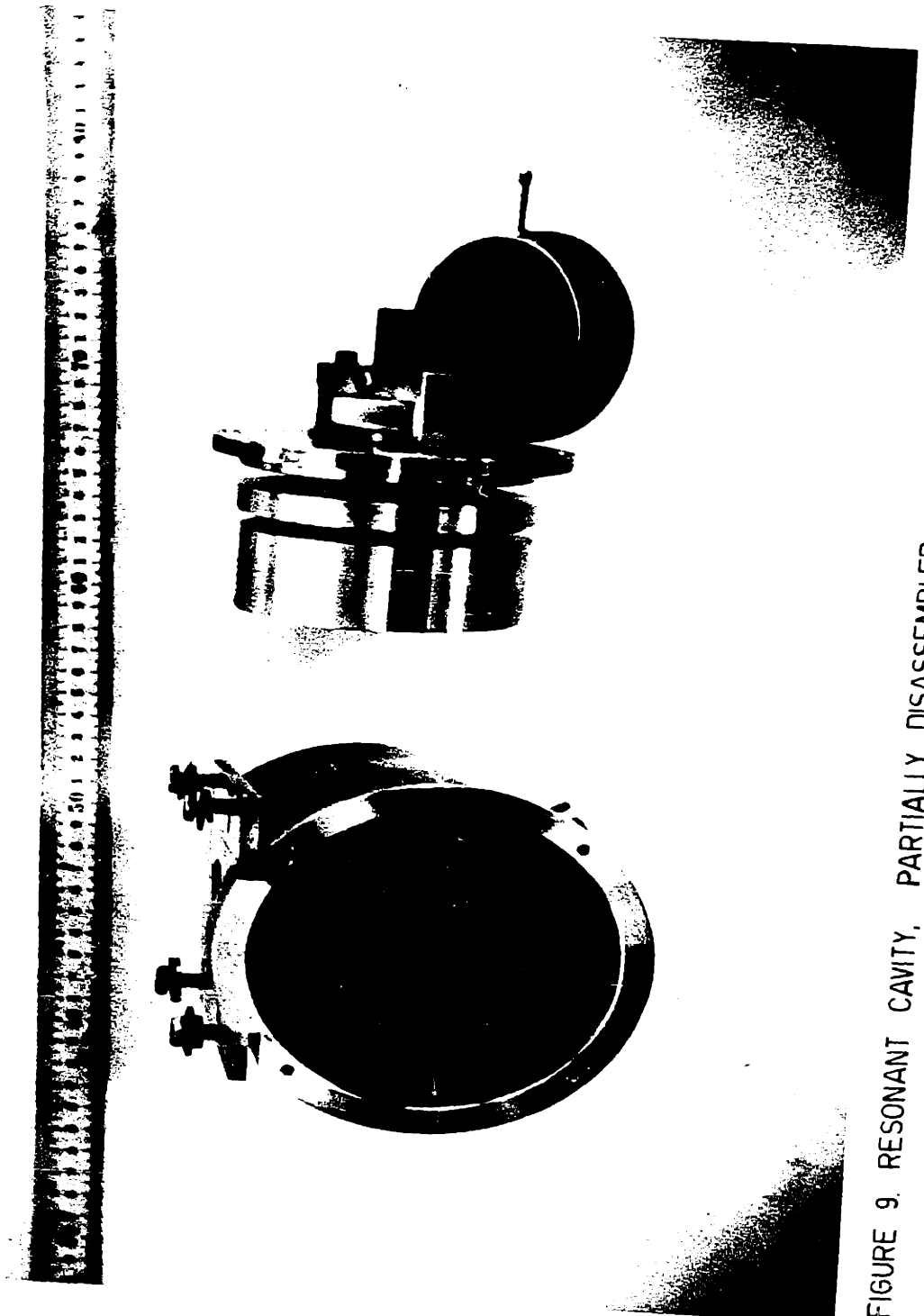


FIGURE 9. RESONANT CAVITY, PARTIALLY DISASSEMBLED

IV PROCEDURE

A. Mixed Feed

All mixed feed data were taken using the oil jacketed reactor; however, test runs showed that the results were no different if an uncooled reactor was used.

After the reactor was installed, the run was begun by pumping the system down to as low a pressure as possible. When the system was operating properly, this meant a zero pressure reading on the Wallace and Tiernan gauge. After being so evacuated, the system was sealed off from the pump by closing the large throttling valve. The pressure gauge was then monitored for any rise in pressure which would indicate a leak. If any rise was less than one tenth of one percent of the rate of rise attained when oxygen was fed in at the flow rate of the experiment, it was ignored and the work proceeded. If the leak rate was greater than this, the equipment was shut down and the source of the leak determined and eliminated.

After this leak test procedure, helium was admitted to the system with the valves open into the sample loop until the pressure rose to that of the planned run. When this pressure had been reached, it was held for at least ten minutes. This procedure allowed the gas in the sample traps to cool and contract. After the necessary time had elapsed,

the valves to the sample loop were closed and the pressure lowered in the rest of the system.

Following this trap pressurization procedure, the reactant gases were allowed to flow into the system at the desired rate as indicated on the rotameters. These gases were mixed in the manifold connecting the stainless steel metering valves and allowed to flow through the reactor and the rest of the system. At this point the microwave power was turned on and the discharge lighted by means of a Tesla coil. (Sometimes the discharge ignited spontaneously.) The throttling valve was then turned back until the system again reached operating pressure.

After operating pressure had been reached, the various electrical measurements were made. These were the incident power and the voltage standing wave ratio. These values in addition to the pressure and the flow rates were recorded.

When all measurements were completed, the sample valves were opened and the gases allowed to flow through the cold traps for a specified time. The traps froze out all the products from the discharge reaction. After the allowed time, the sample valves were closed and the flows and power shut off. Helium was then purged through the system for a few minutes at the operating pressure. Since the throttling valve was open and the pump operating, this procedure removed any residual products in the line. Following this purge, a single sample valve (labeled #3 in Figure 1)

was opened and the throttling valve closed completely. Helium was allowed to continue flowing into the system until it reached atmospheric pressure.

At atmospheric pressure, the sample trap was removed and stoppered. It was then placed in a nitrogen purge system shown schematically in Figure 10 and allowed to slowly warm. As the products came off, they were passed through a caustic solution which thoroughly scrubbed out all components. When the trap was warm, green chlorine vapor could be observed in it. At this point, the nitrogen purge stream was turned on and allowed to flow for 20 minutes. This process completely removed all chlorine from the trap and forced it into the caustic solution. When the trap was removed from the apparatus, a small amount of distilled water was shaken up in it and tested with potassium iodide-starch indicator paper. A negative result indicated a thorough flushing of the chlorine from the trap.

Analysis of the products proceeded by the Pontius method (38). The pH of the caustic solution was adjusted to eight by adding a small amount of six normal sulphuric acid. A few drops of starch solution were added to the solution and 0.1 normal potassium iodide titrated in until a blue color appeared. This was the end point and the amount of potassium iodide solution added was noted. The conversion to chlorine was determined from

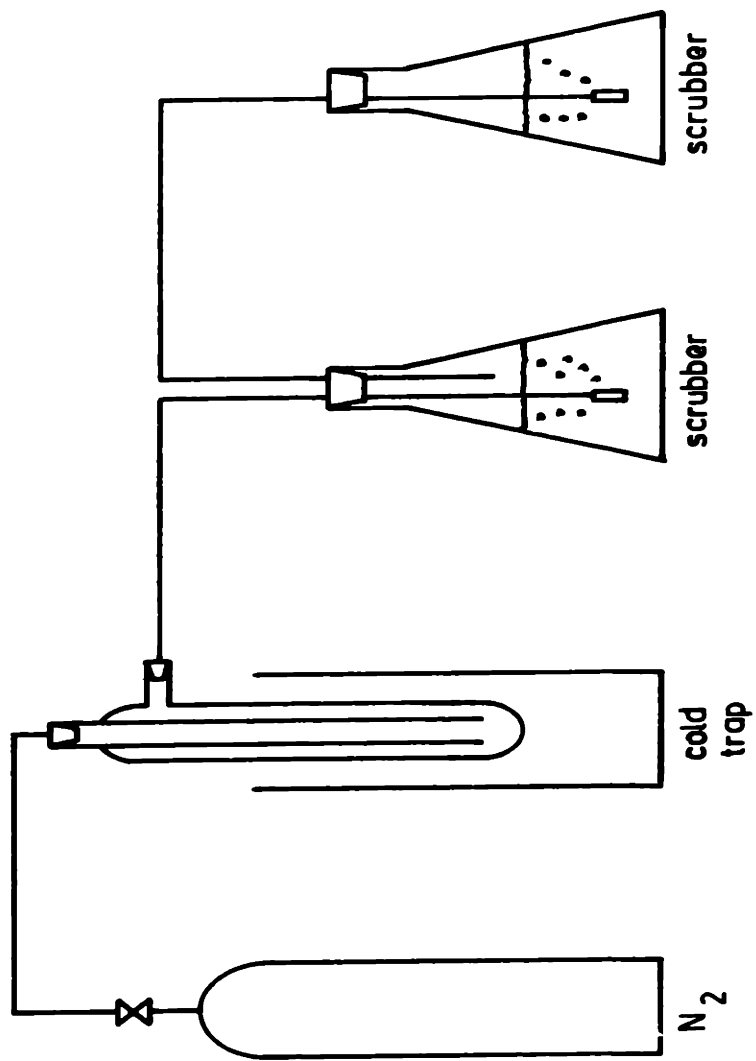


FIGURE 10. SCHEMATIC OF PURGE SYSTEM

this number. (See Appendix F.)

B. Separated Feed The operating and analysis procedure with the reactant feed streams separated was exactly the same as that outlined above for mixed feeds. The difference in this case was that the gas not passed through the discharge was not mixed in the manifold, but fed directly to the side arm of the dual gas reactor. Here it was mixed downstream from the plasma with the discharge products of the second gas. The distance between this input position and the base of the discharge could be varied by moving the reactor either up or down.

C. Measurements

1. Temperature The thermowell reactor shown in Figure 6 was used for all temperature measurements. An iron-constantan thermocouple was inserted into the well and the junction pressed firmly against the tip. The reactor was positioned so that the end of the thermowell was as far from the discharge as possible. A reference junction maintained at 0 °C. by an ice water bath was used in conjunction with a potentiometer to measure the millivolt output from the thermocouple. Standard calibration tables

were used to convert the millivolt readings into temperatures. When the temperature at a position closer to the discharge was desired, the whole thermowell reactor was moved upward. Care was taken to see that the thermocouple junction was kept firmly pressed against the tip of the well. In this way temperature profiles of the region downstream from the discharge were plotted out. (See Appendix B.) Tests made with microwave power present by no discharge showed that any errors from pick-up of this energy were negligible. Appendix A. discusses the possible error arising from recombination on the quartz probe.

2. Spectra A plain quartz tube reactor was used when spectra of the discharge zone were being taken. A system of chromium mirrors and glass lenses were used to focus the light on the slit of the spectrograph. The use of the glass lenses resulted in the light's being cut off for wavelengths shorter than 3100 Angstroms. The operating procedure consisted of setting the discharge conditions and flow rates to be identical with those used under normal operating conditions and focusing the light on the slit. The shutter was then opened and the plate exposed from one to twenty minutes. All of the spectroscopic work was carried out with the room darkened.

3. Energy Balance To carry out this balance the flow rate of the cooling oil circulating pump was carefully measured. Runs were then made using the oil jacketed reactor. An enthalpy balance was set up on the assumption that all of the energy input to the gas from the microwaves left in the oil and that all the enthalpy released on reaction was also given up to the cooling oil. The overall temperature change in the gas was found to be negligible, but the temperature change of the cooling oil was measureable with iron-constantan thermocouples. A knowledge of this temperature change, the physical properties of the oil (See Figure F-1), the flow rates and the extent of reaction enabled the balance to be set up. A sample calculation is presented in Appendix F.

4. Calorimeter The operation of this calorimeter is based on the fact that the resistance of the wires is solely a function of their temperature. The atomic products from the discharge find the metal surface very favorable for recombination and in doing so heat the wire by releasing the enthalpy of recombination. To operate the instrument, the discharge was turned on and the atoms formed allowed to heat the filament by their recombination. Under these conditions the Wheatstone Bridge in which the filament

was one arm was balanced and the voltage and current through one filament recorded. The discharge was then turned off and the bridge rebalanced under these conditions. The result of this rebalance was that the filament was restored to the same resistance and temperature as it had when recombination was occurring there. Since the temperature conditions are the same the difference in electrical power dissipated in the filament with and without the discharge is proportional to the rate at which atoms are recombining there. (See Appendix F.)

5. Cavity To use the tunable resonant cavity, it was necessary to first remove the tapered coupling section and substitute the cavity as the terminating unit on the waveguide. Coupling with the microwave field was accomplished either through the use of an iris or a loop. After being connected to the waveguide, the cavity had its piston moved to the fully extended position; and the microwave power was turned on. The probe on the slotted section was tuned to a minimum and its position noted. Next the voltage standing wave ratio was measured. After these measurements were completed, the piston was moved inward and the process repeated. In this way, data on the voltage standing wave ratio and the position of the voltage minimum were obtained as functions of plunger location.

V. RESULTS

A. Mixed Feed

With a total molar flow rate of 2.90×10^{-4} moles per second and both reactant gases combined in a 4:1 stoichiometric ratio, conversions of hydrogen chloride to chlorine ranged from a high of 53% to a low of 30%. The work was done at pressures extending from four to forty millimeters of mercury with from 111 to 709 watts of power absorbed in the discharge.

At a pressure of 20 millimeters of mercury, the power absorbed in the discharge region had little effect on the yields; whereas at 10 millimeters, there was a definite trend toward lower yields at higher powers. These effects are illustrated in Figures 11 and 12 where the percent conversion to chlorine has been plotted against the watts of power absorbed in the discharge. The fairly large scatter of the data results from the fluctuations in the flow rates caused by the slight pressure variations in the system during operation. This effect is more severe at the lower pressure where the change is a larger percentage of the total.

Figure 13 shows how the absolute pressure level in the system, again with a stoichiometric feed of oxygen

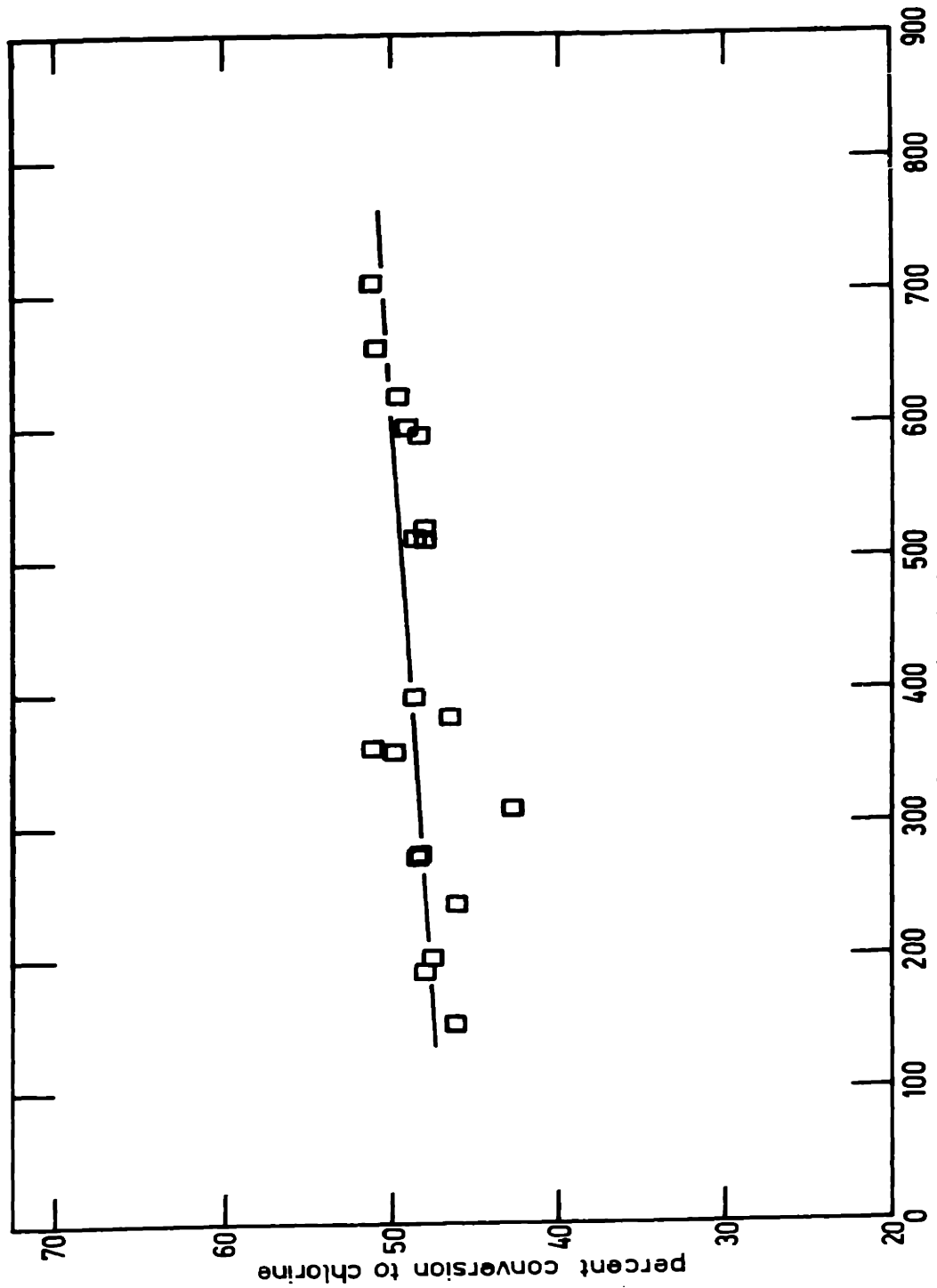


FIGURE 11. CONVERSION VERSUS POWER AT 20 mm Hg PRESSURE WITH A MIXED FEED OF 0.579×10^{-4} MOLES PER SEC. O_2 AND 2.32×10^{-4} MOLES PER SEC. HCL

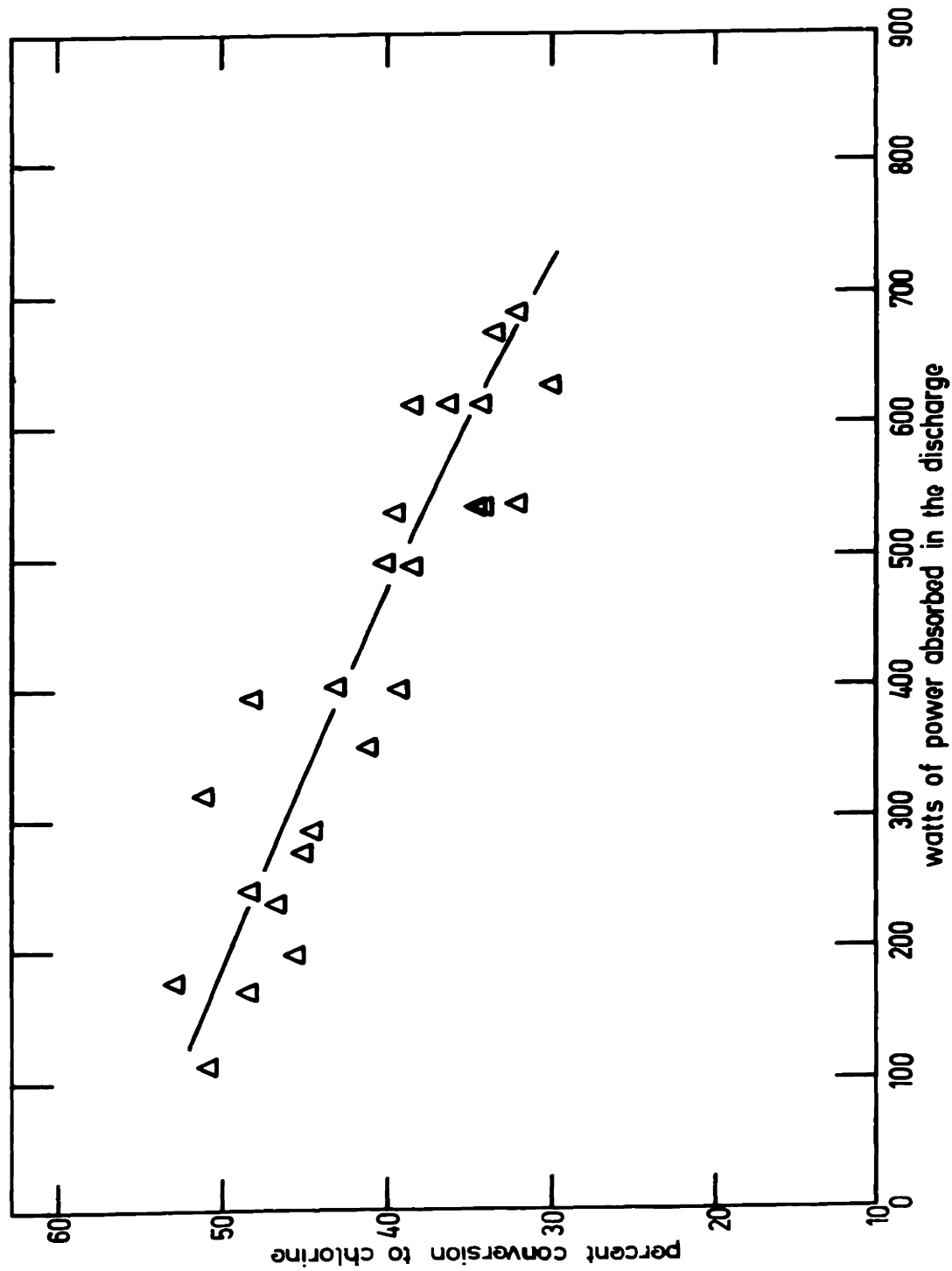


FIGURE 12. CONVERSION VERSUS POWER AT 10 mm Hg PRESSURE WITH A MIXED FEED OF 0.579×10^{-4} MOLES PER SEC. O_2 AND 2.32×10^{-4} MOLES PER SEC. HCL

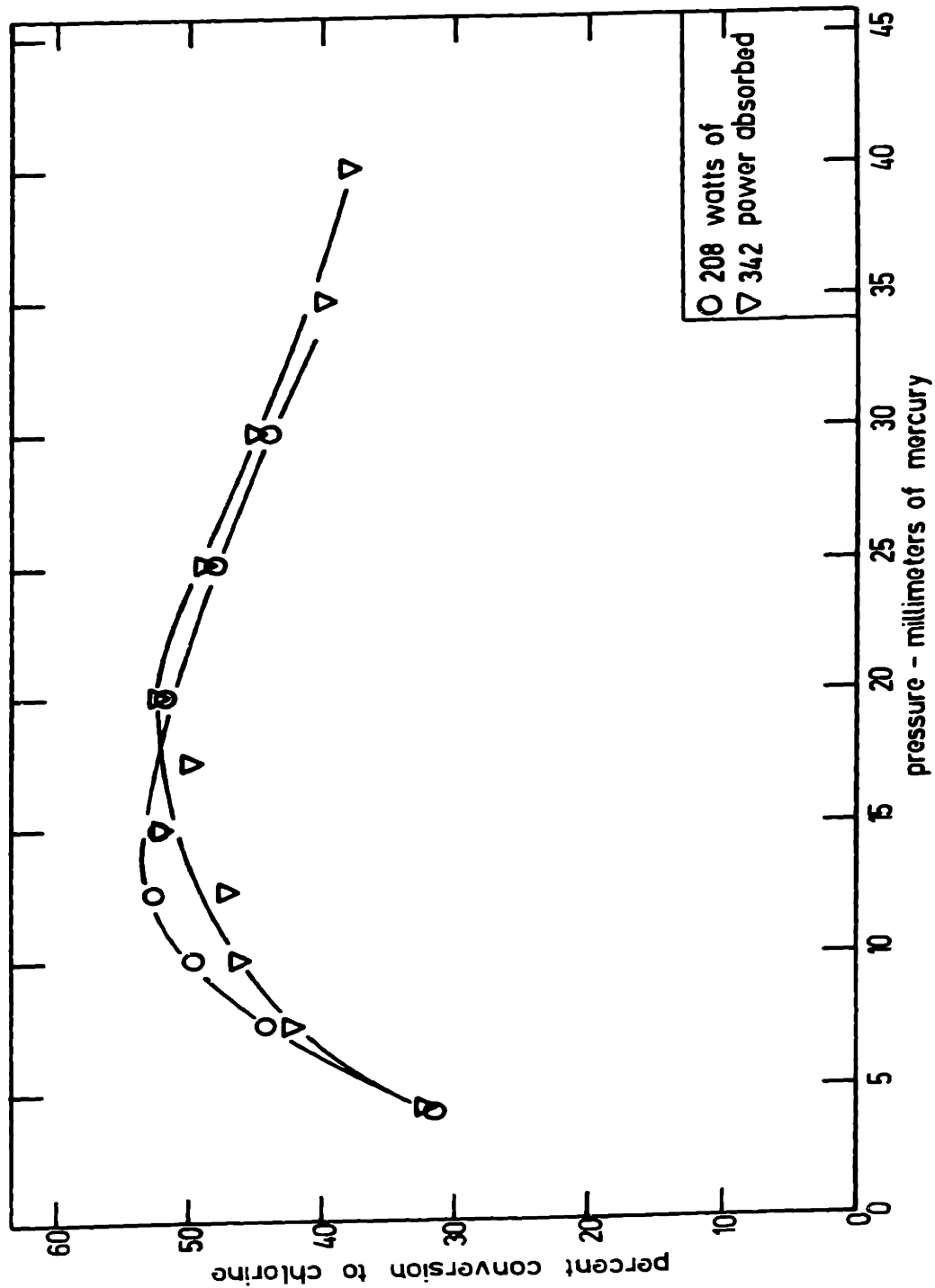


FIGURE 13. CONVERSION VERSUS PRESSURE WITH A MIXED FEED OF 0.341×10^{-4} MOLE/SEC. O_2 AND 1.37×10^{-4} MOLES/SEC. HCL

and hydrogen chloride, affected the yields. There are two broad maxima, one near 14 millimeters of mercury and the other near 20 millimeters.

The diameter of the quartz reaction tube had little effect on either the yields or the energy requirements for maintaining the discharge. As shown in Table I, a tenfold diameter variation caused very little change in the range of conversions. The apparent exception at a diameter of 22 millimeters and a pressure of 20 torr can be explained as a channeling effect since the discharge did not completely fill the cross section of the reactor. Data in Table I also show that increasing the diameter from 2 to 22 millimeters resulted in only a 17% increase in the power required to maintain the discharge.

Increasing the flow rate of the gases through the discharge resulted in a small increase in the power required for breakdown. The increased power was more than compensated by the larger flow and a net decrease resulted in the power consumption per pound of chlorine formed. At the usual atmospheric flow rate of 340 milliliters of hydrogen chloride per minute, the lowest energy requirement was 3.7 kilowatt-hours per pound of chlorine produced. This best value dropped to 2.3 kilowatt-hours per pound when the flow rates were quadrupled.

Efforts to use air as the oxidant rather than pure

TABLE I
Diameter and Flow Effects (mixed feed)

Reactor Diam. mm	Flow Rate ml/min @ 1 atm HCl	Flow Rate O ₂	Press mm Hg	Minimum Power to Maintain Discharge Watts	Range of Absorbed Power Watts	Range of Conversions Percent
2.0	340	85	20	127	127 - 382	34.8 - 50.2
11	340	85	20	151	151 - 709	42.8 - 51.3
11	340	85	10	111	111 - 687	29.9 - 52.7
22	340	85	20	149	149 - 275	36.3 - 37.2 *
22	340	85	10	132	132 - 472	48.8 - 51.9
11	680	170	10	-	165	47.6
11	680	170	20	185	185 - 420	38.5 - 48.2
11	1360	340	10	170	170 - 384	21.3 - 37.9 #
11	1360	340	20	179	179 - 420	23.1 - 51.1

* The low yields result from the discharge's not completely filling the cross section of the reactor at this higher pressure and large diameter. Reactant gases may pass through the discharge region without actually passing through the discharge.

The low yields reflect the inability of the cold trap to collect all the products at this high flow rate and lower pressure.

oxygen were successful, but at the sacrifice of some of the chlorine yield. Figure 14 compares results with an air feed with those obtained under similar conditions with oxygen. In these runs, the air feed was adjusted so that there was always a stoichiometric amount of oxygen present. As can be readily seen from Figure 14, the penalty for using air as the oxidizer is greater at 10 millimeters pressure than at 20.

The reactor shown in Figure 16-A was used to quench the products of the discharge by adding nitrogen downstream. The nitrogen flow rate was 425 milliliters per minute at one atmosphere, equal to the sum of the hydrogen chloride and oxygen flows through the discharge. Figure 15 shows the decline in yield from 50% to 44% as the input positions of the cooling nitrogen was brought closer to the discharge region. The dotted line at 41.3% indicates the average yield when air was used as the oxidant at 20 millimeters pressure.

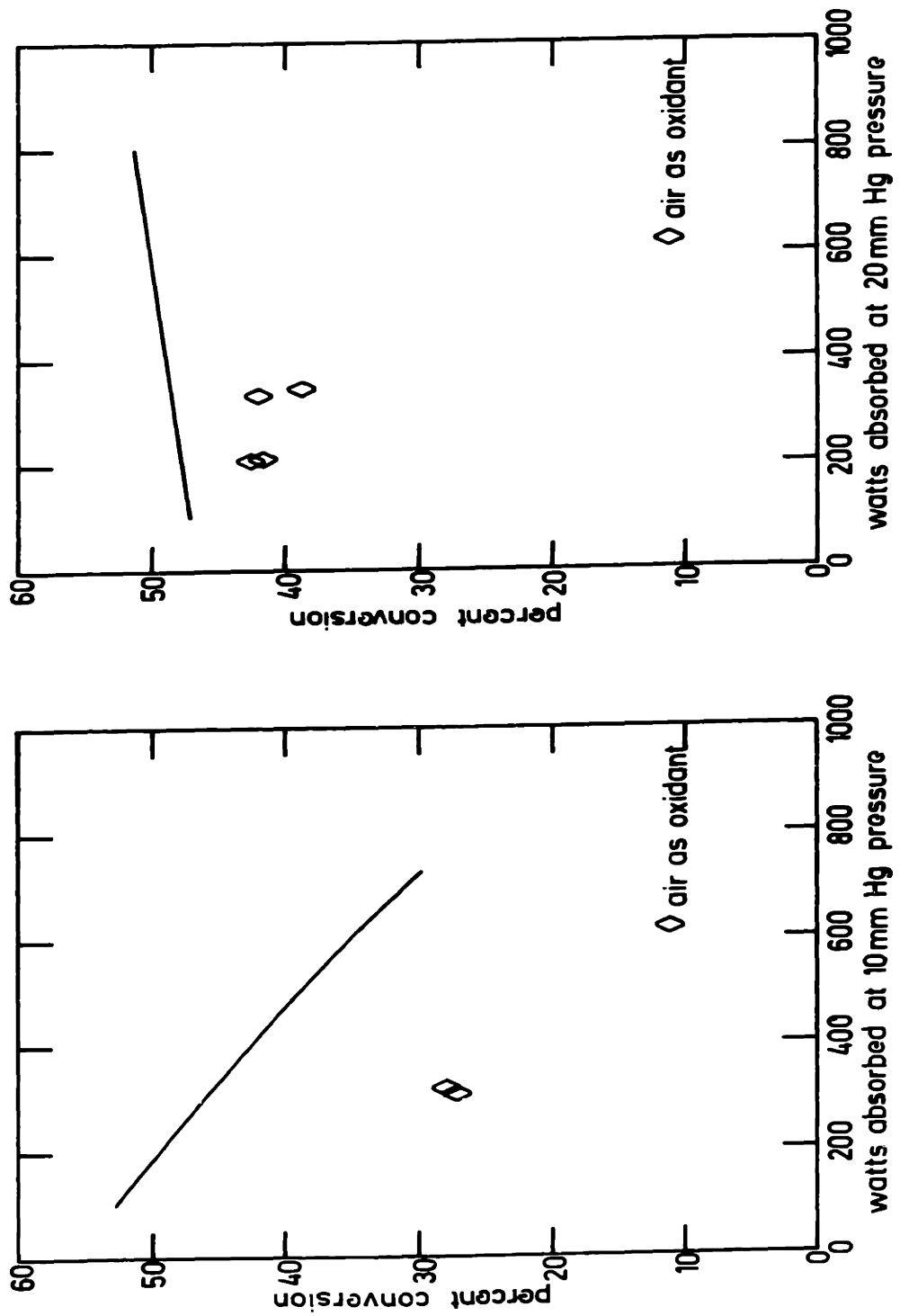


FIGURE 14. THE EFFECTS OF USING AIR AS THE OXIDIZER

william w. cooper iv Sc.D. thesis 10/6/66

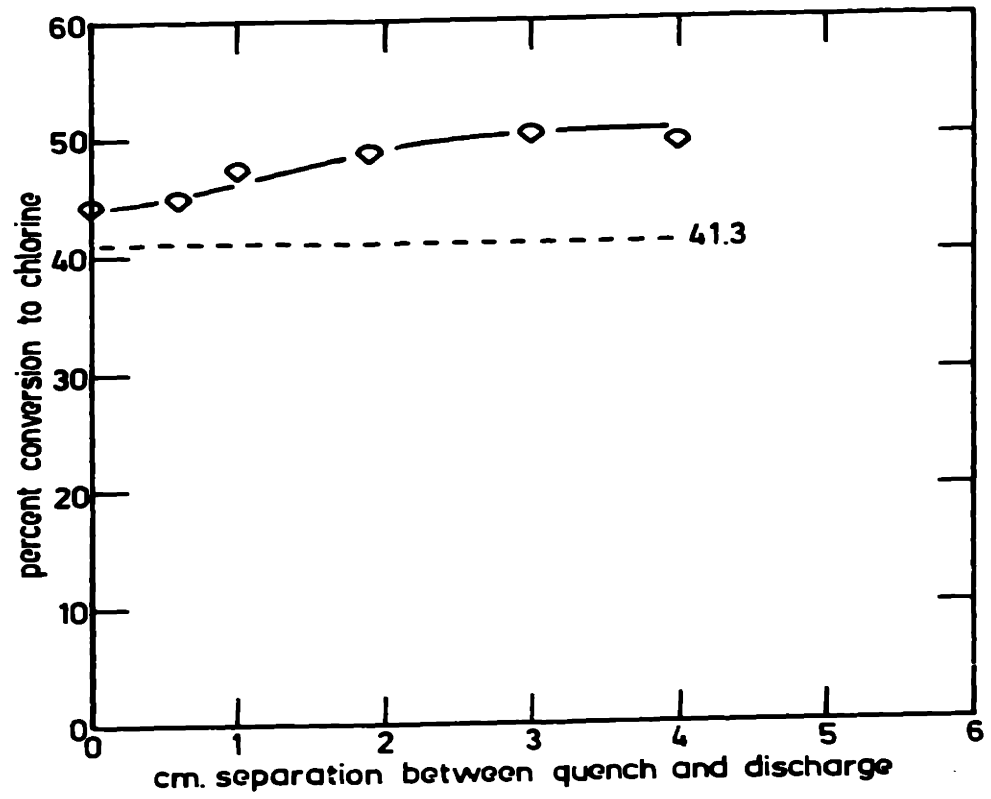


FIGURE 15. EFFECT OF NITROGEN QUENCH
20 mm. HG. pressure

B. Separated Feed

Three different designs of reactor, all shown in Figure 16, were used to pass oxygen only through the discharge and mix it downstream with hydrogen chloride. In all these runs the oxygen flow rate was held constant at 0.579×10^{-4} moles per second and the hydrogen chloride flow rate, constant at 2.32×10^{-4} moles per second. The power incident on the discharge region was maintained at 416 watts.

The results of those runs made with the impinging flow design of Figure 16-A are shown in Figure 17 where the conversion to chlorine has been plotted on a semi-logarithmic scale against the input position of the hydrogen chloride. At zero separation, there is a difference in magnitude of 8% between the yields at the two pressures compared to a difference in Figures 11 and 12 of 5% with mixed feed at the same average absorbed power of 345 watts. With this reactor, the change in pressure of operation had no effect on the slope of the straight line in Figure 17.

When the reaction tube shown in Figure 16-B was used the yields fell off from 32% to 3.5% as the input position of the hydrogen chloride was moved from zero to one centimeter away from the discharge zone. Figure 18

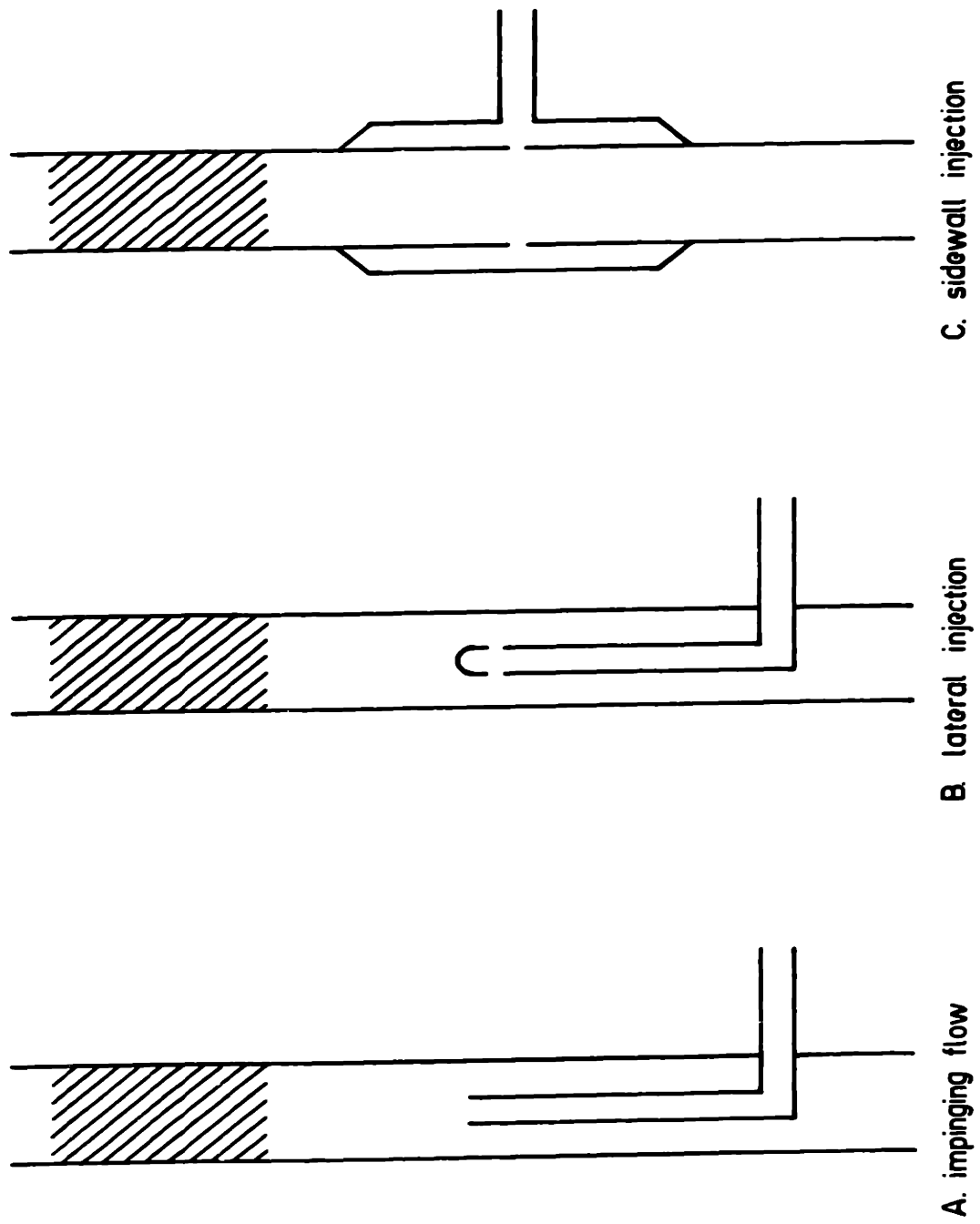


FIGURE 16. THE THREE DESIGNS OF SEPARATED FEED REACTOR

william w. cooper iv Sc.D. thesis 10/6/66

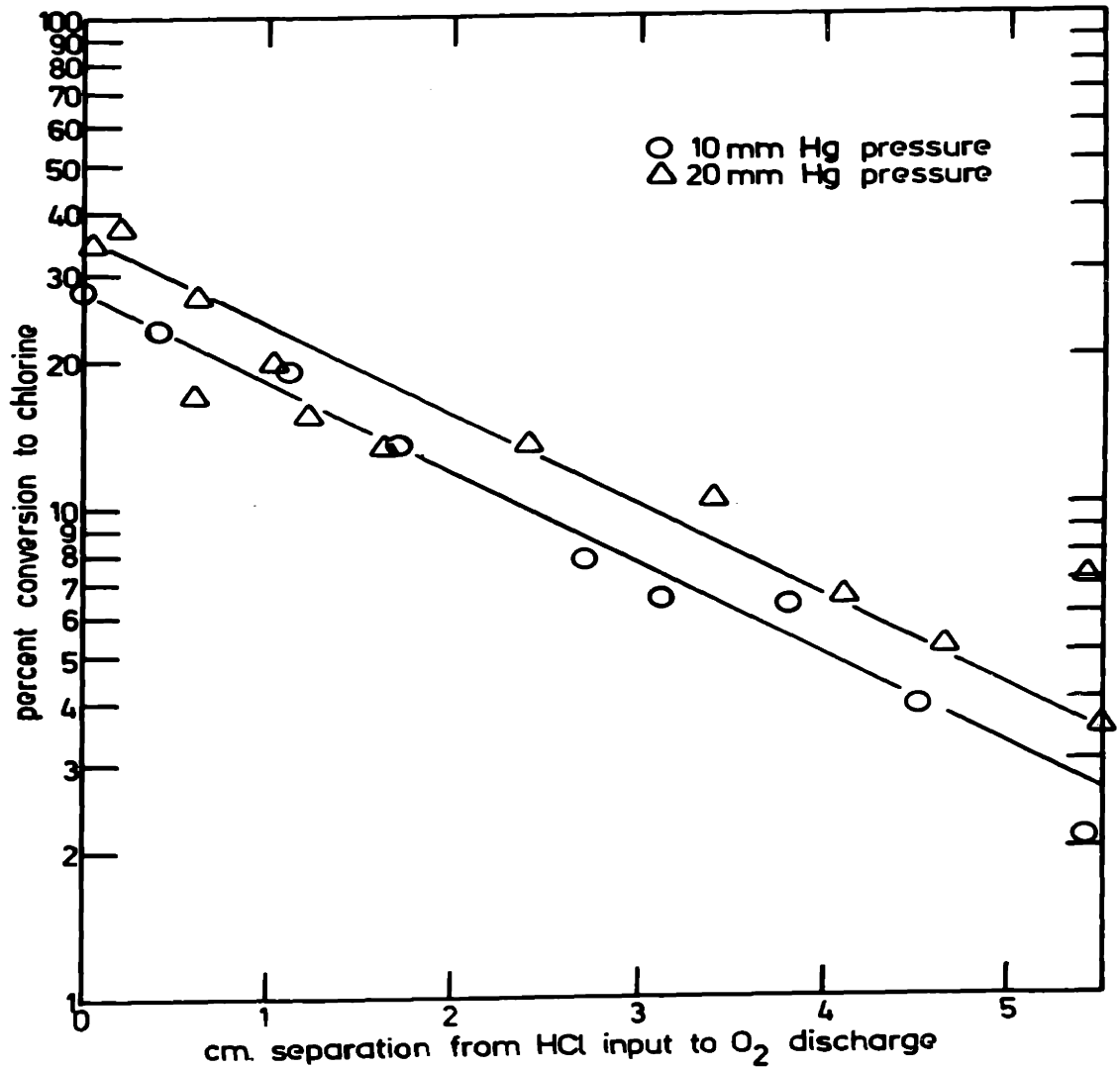


FIGURE 17. CONVERSION VERSUS POSITION OF HCL INPUT with impinging flow reactor at 345 watts absorbed and flows of 0.579×10^{-4} moles/sec O₂ and 2.32×10^{-4} moles/sec HCl

william w. cooper iv Sc.D. thesis 10/6/66

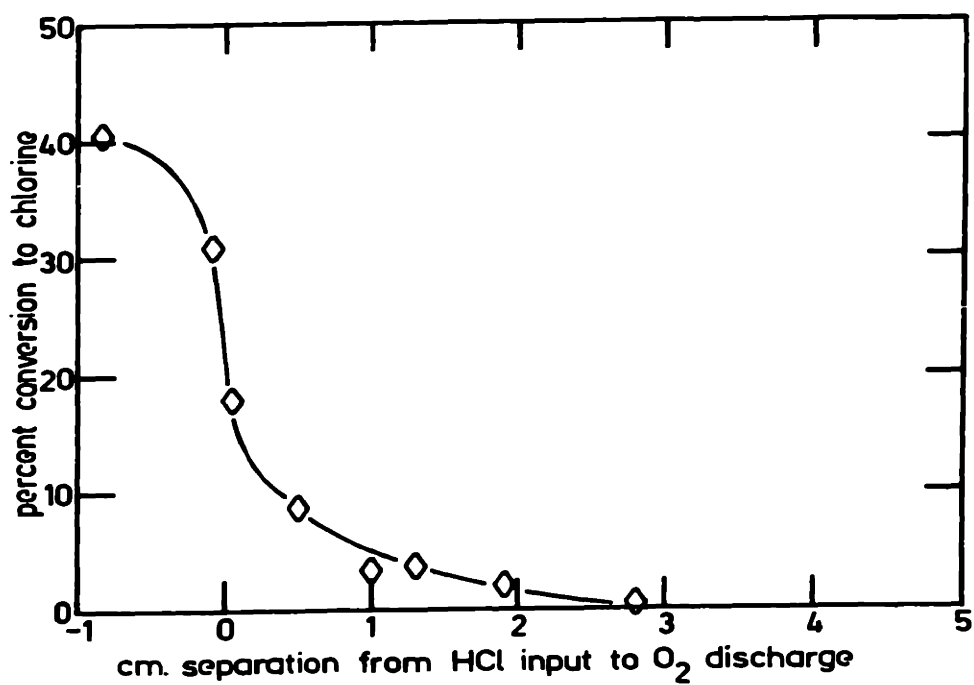


FIGURE 18. CONVERSION VERSUS POSITION OF HCL INPUT with lateral injection reactor at 20 mm. Hg., 327 watts absorbed, and flows of 0.579×10^{-4} moles/sec O₂ and 2.32×10^{-4} moles/sec. HCl

illustrates this effect. Because of the lack of success with this reactor design, only one series of runs was made and that was at 20 millimeters pressure.

More extensive data were taken using the side-wall injection design shown in Figure 16-C. Data taken with this reactor when oxygen alone was subjected to the discharge followed by injection of hydrogen chloride at various positions downstream are shown in Figure 19. In this figure, the percent conversion on the ordinate is plotted against the distance of separation between the discharge and the point of hydrogen chloride injection on the abscissa. The plot shows an increase in the slope as the pressure increased from 10 to 20 millimeters. At zero separation there is an 18% difference in yields at the two pressures compared to only 8% with the impinging design and 5% with mixed flow. These data have been replotted in Figure 20 so that the ordinate reflects the oxygen atom concentration and the abscissa, the time of flight from the base of the discharge to the hydrogen chloride input position. (For the details of the calculations see Appendix A.) After this transformation, the data for the two pressures plot as parallel lines with a slope of 107 reciprocal seconds.

Using this reactor, similar experiments were carried out with the flows reversed. Figure 21 shows these results

william w. cooper iv Sc.D. thesis 10/8/66

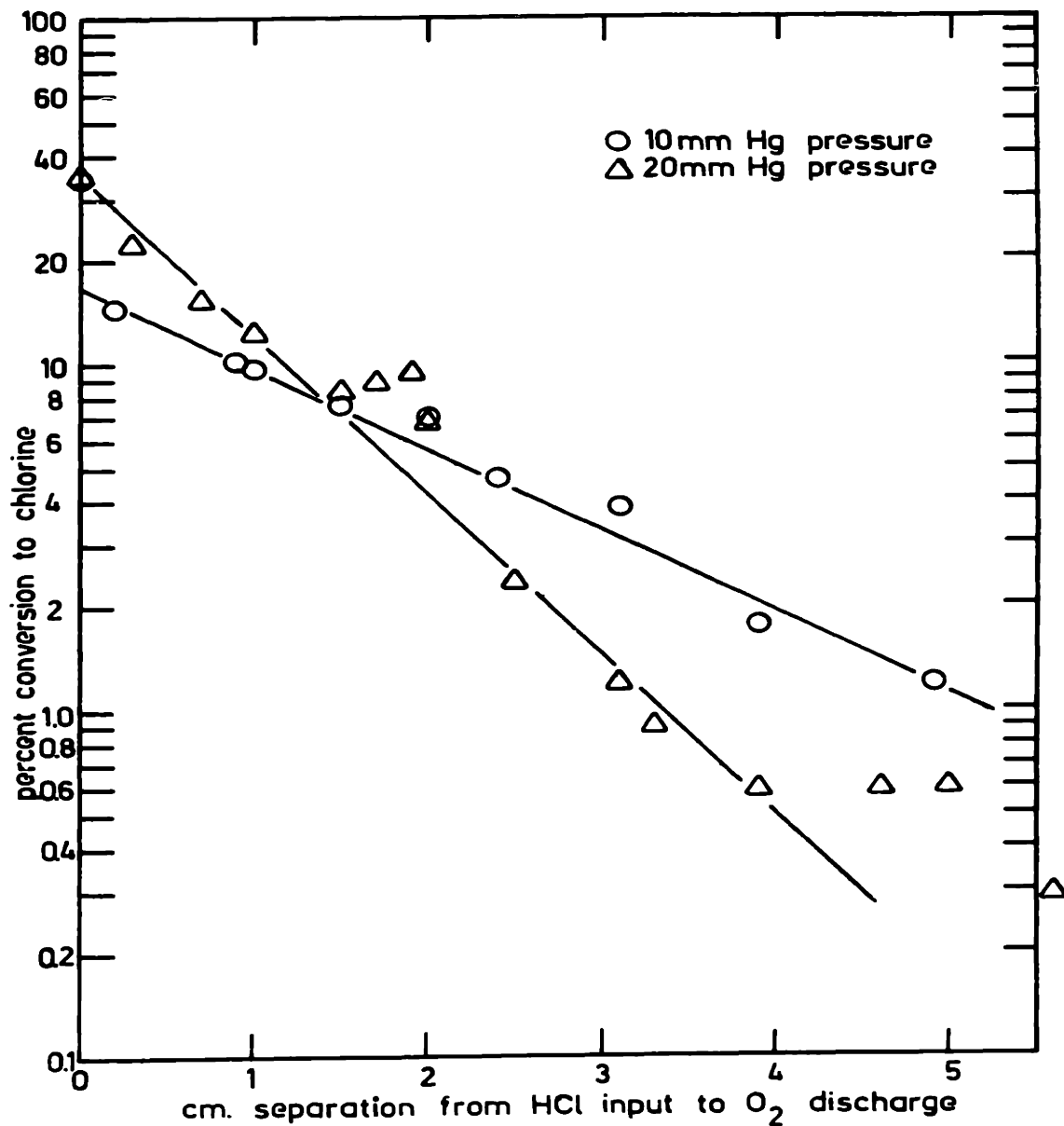


FIGURE 19. CONVERSION VERSUS POSITION OF HCL INPUT with side-wall injection reactor at 327 watts absorbed and flows of 0.579×10^{-4} moles/sec. O₂ and 2.32×10^{-4} moles/sec HCl

williamw cooper iv Sc.D. thesis 10/8/66

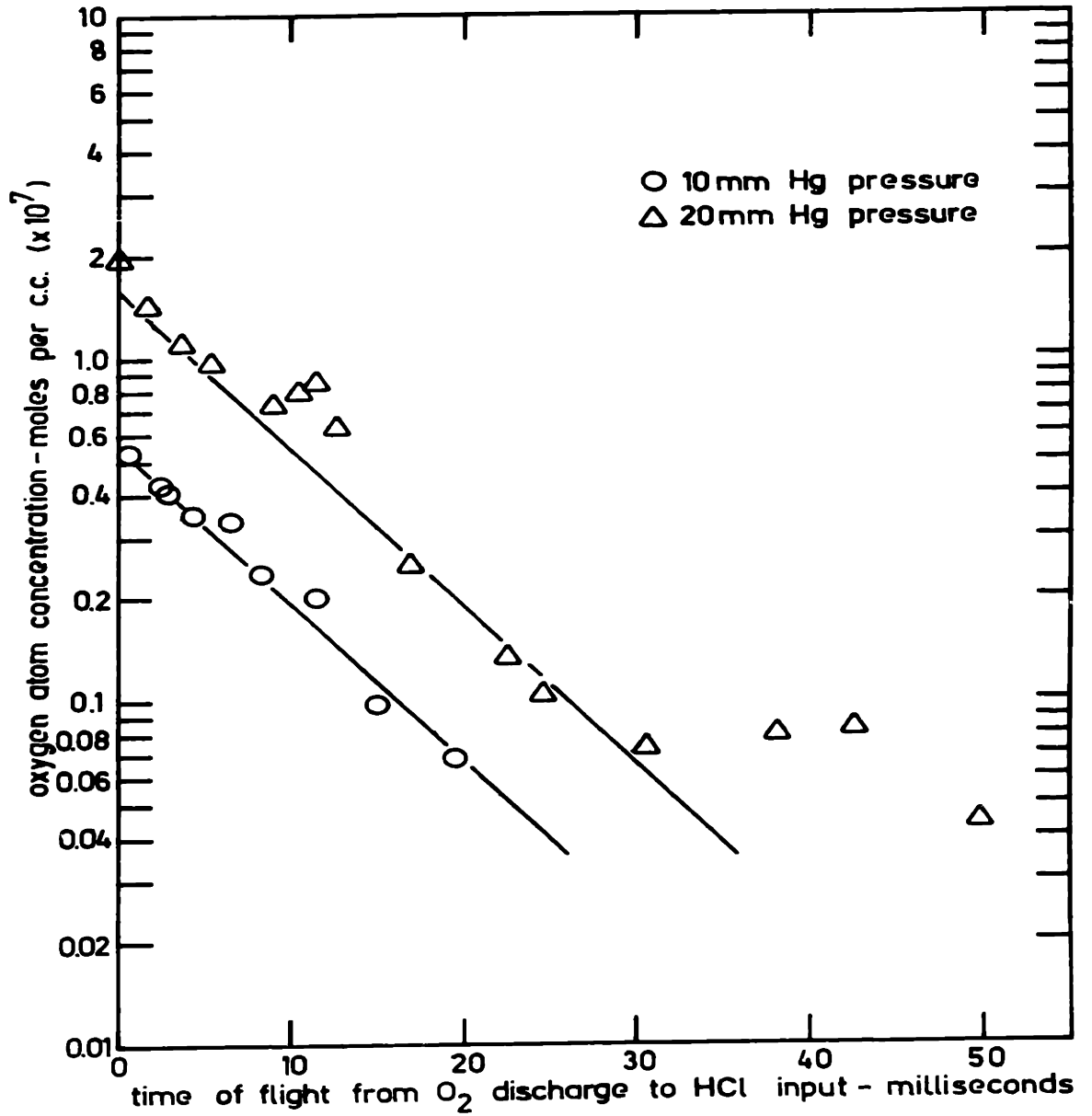


FIGURE 20. OXYGEN ATOM CONCENTRATION VERSUS TIME OF FLIGHT with side-wall injection reactor at 327 watts absorbed and flows of 0.579×10^{-4} moles/sec. O_2 and 2.32×10^{-4} moles/sec. HCl

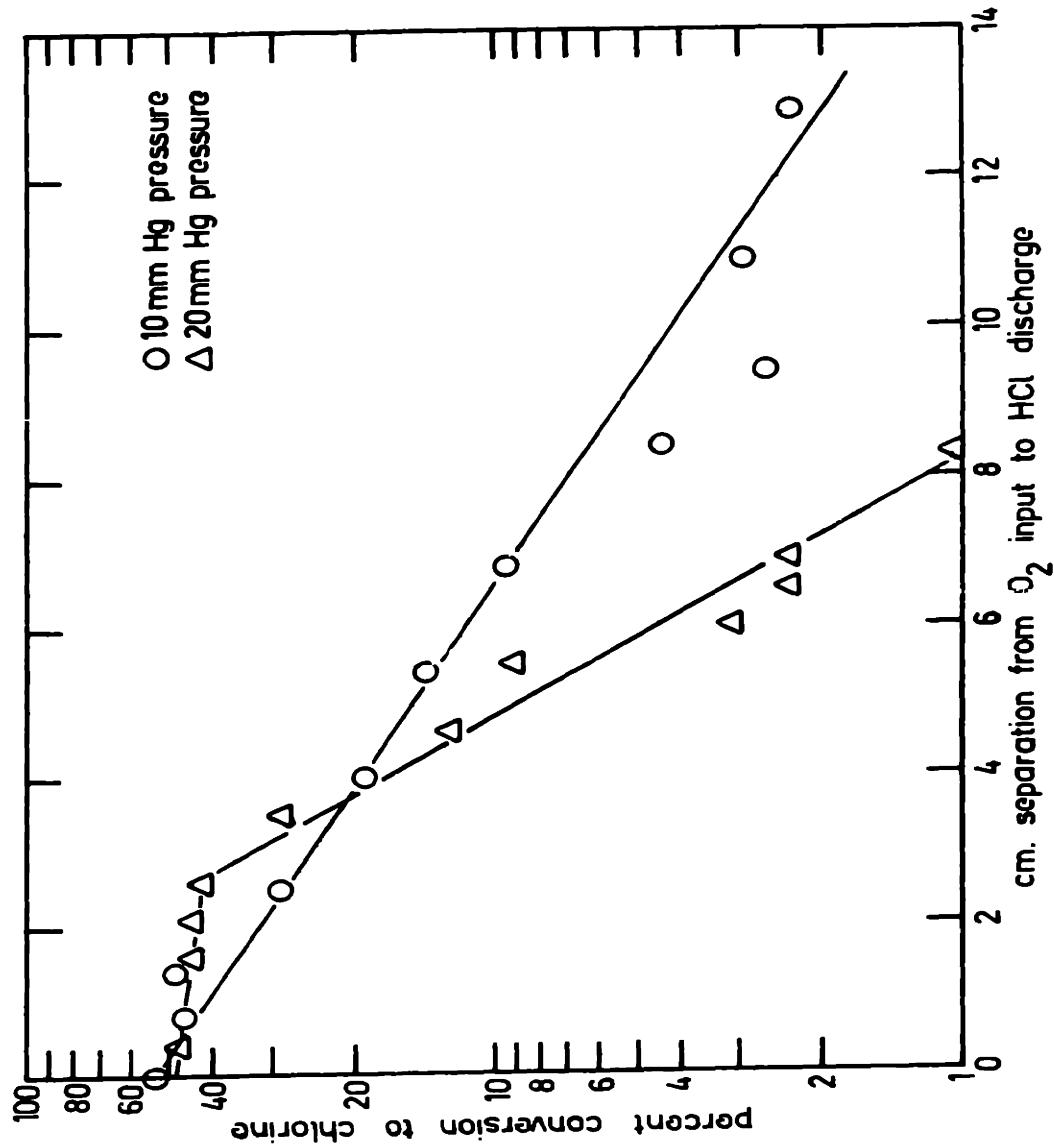


FIGURE 21. CONVERSION VERSUS POSITION OF O₂ INPUT with side-wall injection reactor at 318 watts absorbed and flows of 0.579 x 10⁻⁴ moles/sec O₂ and 2.32 x 10⁻⁴ moles/sec HCl

when hydrogen chloride was the gas subjected to the discharge and oxygen was added downstream. Here the yields at zero separation are approximately 50% at both pressures. The data in Figure 21, the distance plot, have been replotted on a time scale in Figure 22 by the same method used for the oxygen. (See Appendix A.) Again the lines at the two pressures became parallel on this type of plot; but in this case, the slope is 298 reciprocal seconds.

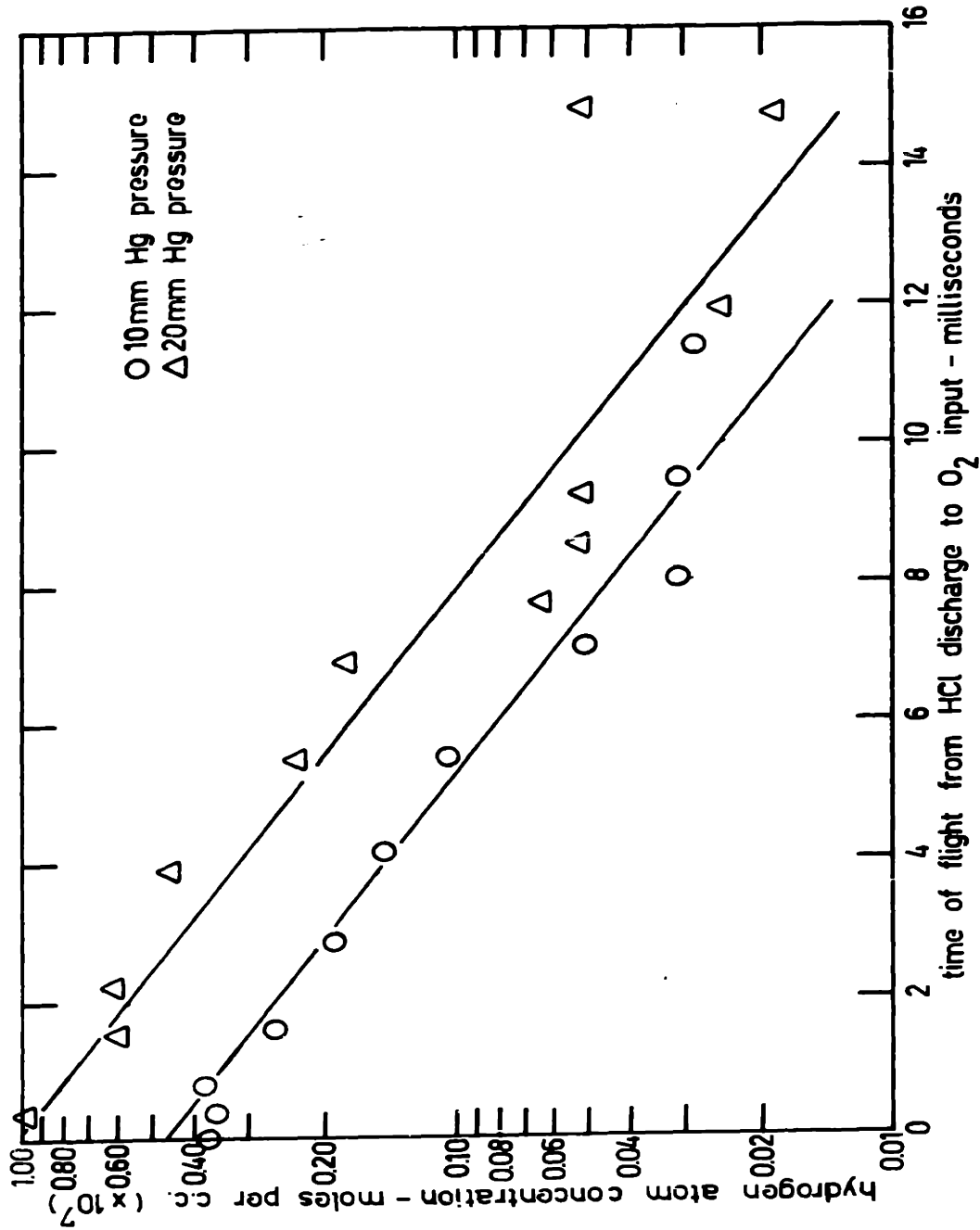


FIGURE 22. HYDROGEN ATOM CONCENTRATION VERSUS TIME OF FLIGHT with side-wall injection reactor at 318 watts absorbed and flows of 0.579×10^{-4} moles/sec. O_2 and 2.32×10^{-4} moles/sec. HCl

C. Measurements

A quartz encased thermocouple attached directly to the reactor was used to measure the temperature profile in the region downstream from the discharge. This was the same method of temperature measurement reported by Elias et al (15) and DelGreco and Kaufmann (2) both of whom worked with microwave discharge chemical systems. The results of this temperature probing are shown in Figures 23 and 24. The data in Figure 23 were obtained with oxygen as the gas being subjected to the discharge. The molar flow rate was 0.579×10^{-4} moles per second which was the same rate ordinarily used in operation. Similarly the data in Figure 24 indicate the temperature measurements when hydrogen chloride was the discharged gas at its usual flow rate of 2.32×10^{-4} moles per second. When these measurements were made, the discharge zone itself was being cooled by a room temperature compressed air stream, but no particular effort was made to cool the downstream region where the temperatures were being measured.

Spectra were taken of the discharge region with a Bausch and Lomb optical spectrograph. The best of these spectra are shown in Figure 25. The three spectra shown are first, oxygen alone; second, hydrogen chloride alone; and third, the mixture of hydrogen chloride and oxygen as used under usual operating conditions. In the oxygen

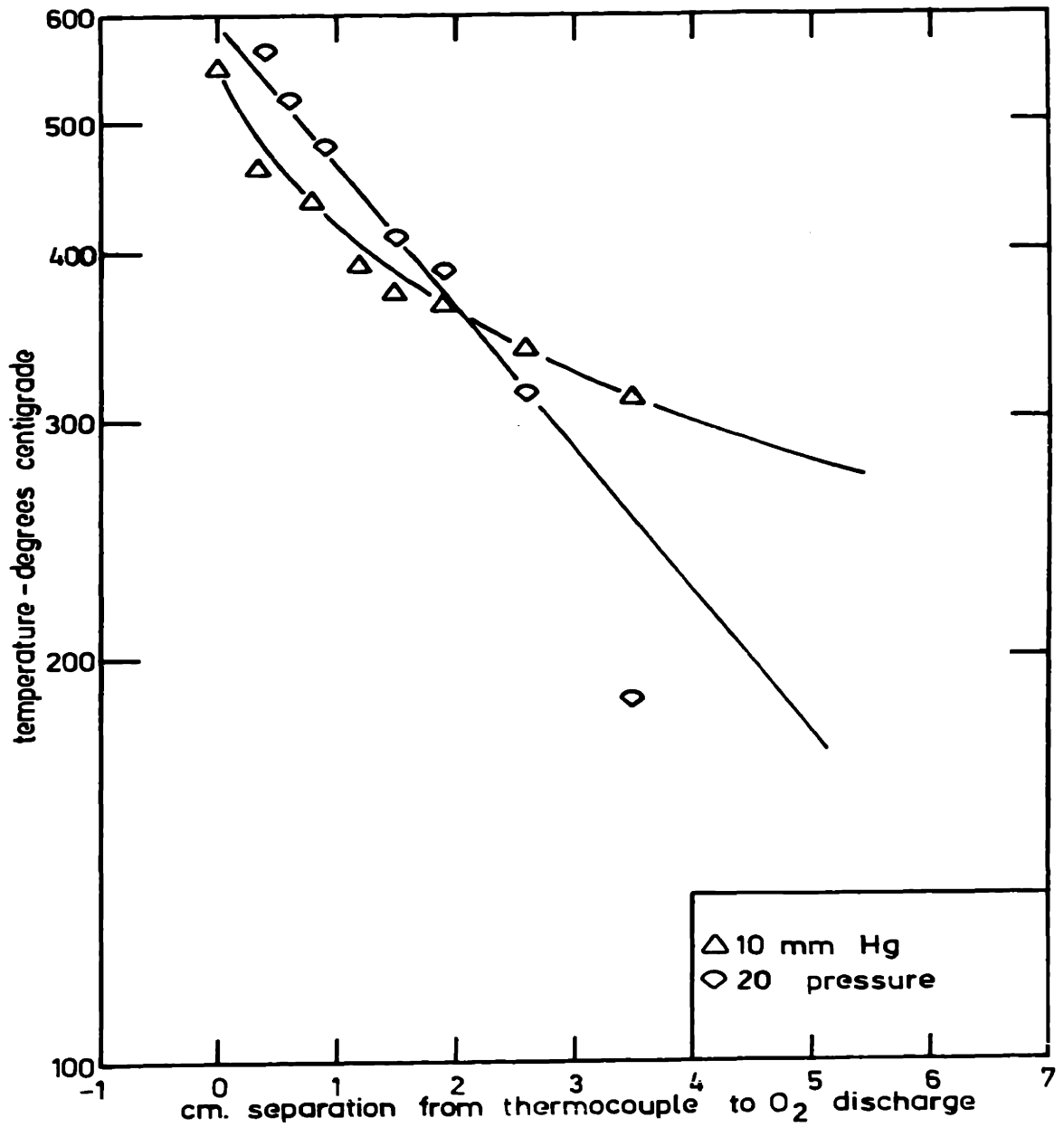


FIGURE 23. TEMPERATURE PROFILE BELOW AN OXYGEN DISCHARGE at 315 watts absorbed and a flow of 0.579×10^{-4} moles/sec. O_2

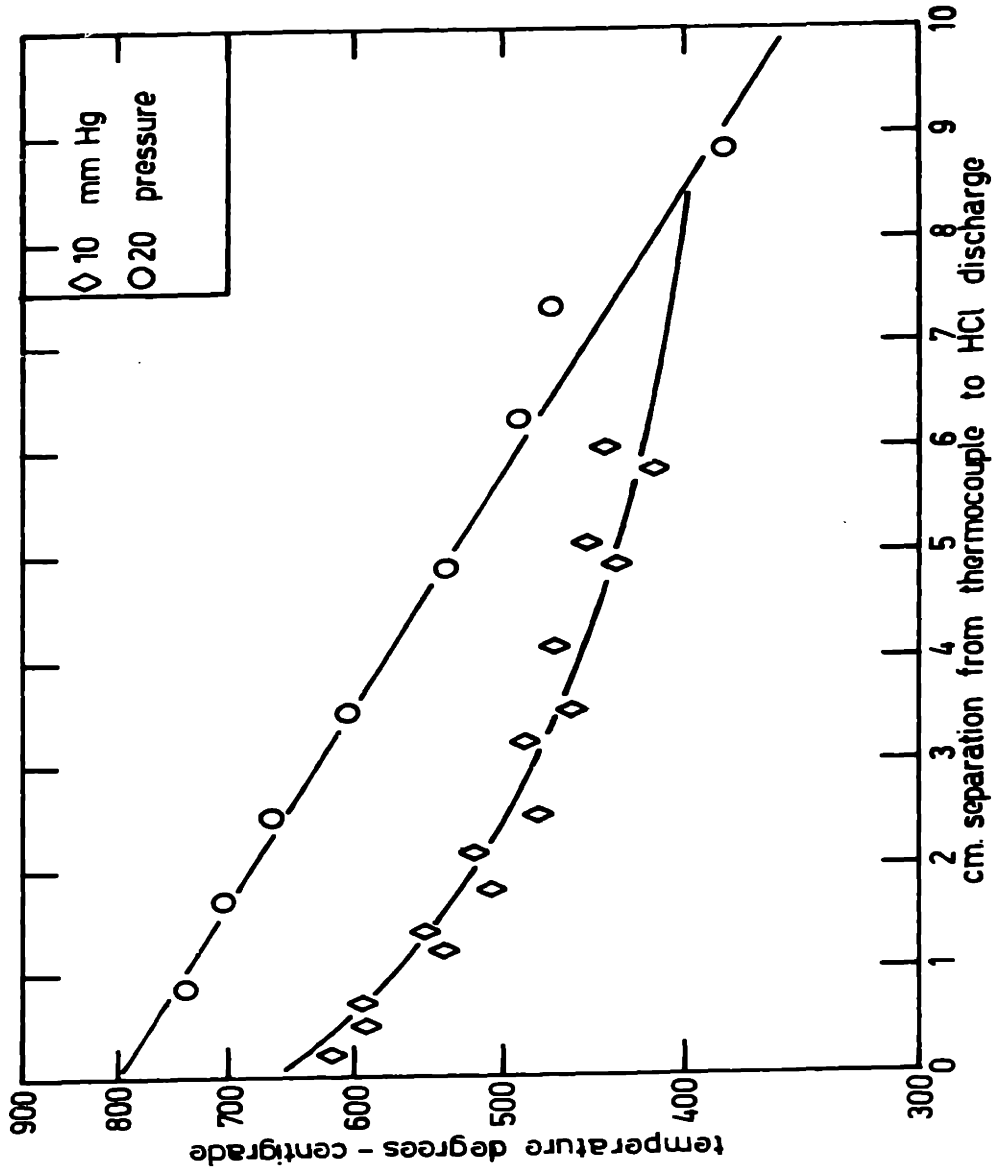


FIGURE 24. TEMPERATURE PROFILE BELOW AN HYDROGEN CHLORIDE DISCHARGE at 320 watts absorbed and a flow of 2.32×10^{-4} moles/sec. HCl

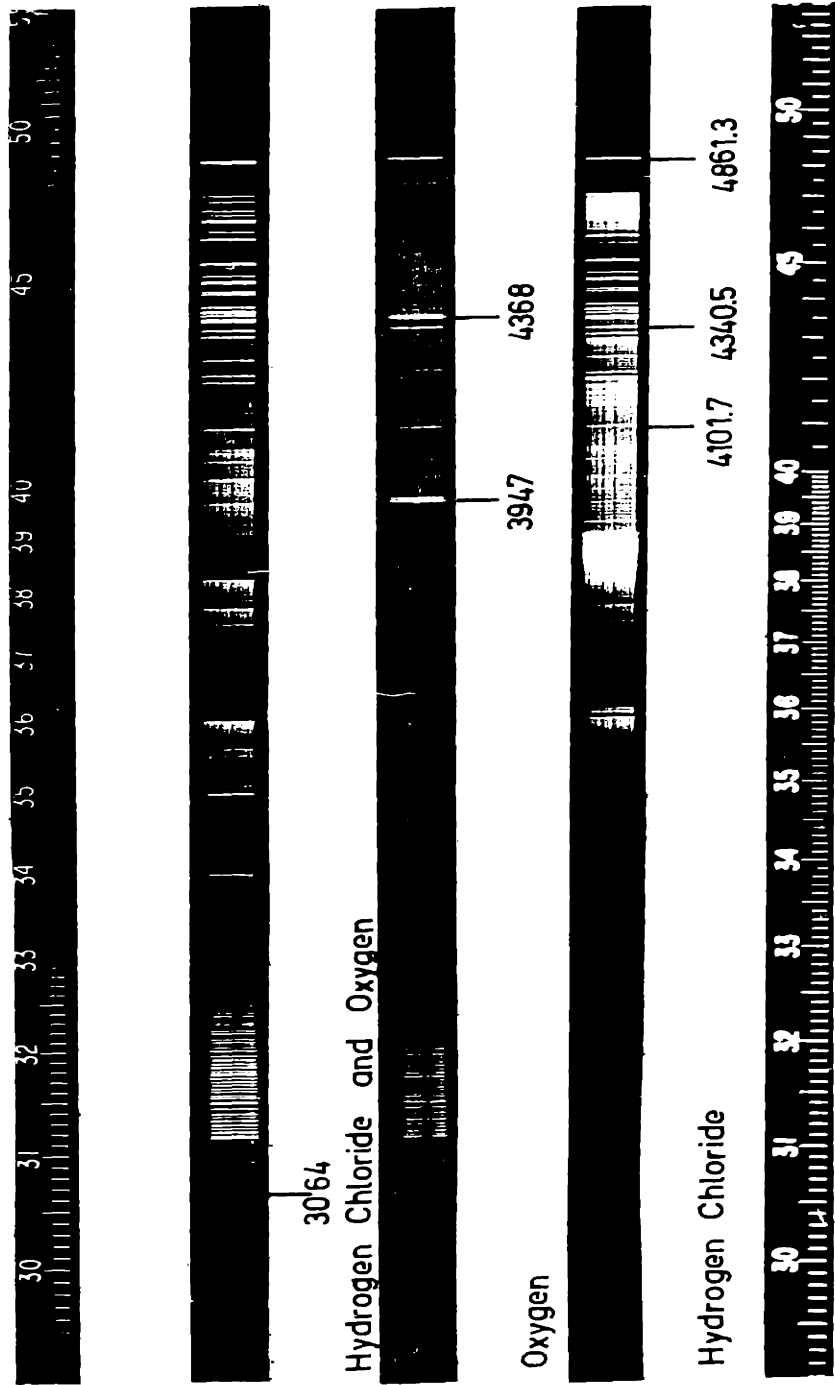


FIGURE 25. SPECTRA OF THE DISCHARGES

spectrum, the lines at 3947A and 4368A particularly stand out. The Balmer lines at 4861.3A, 4340.5A and 4101.7A are visible in the hydrogen chloride spectrum. In the mixed case and to a lesser extent with oxygen, there is a band in the near ultraviolet which has been cut off by the glass lenses used. Its probable band head at 3064A has been marked.

The energy input to the discharge region was monitored during all runs and verified by an independent calorimetric technique as reported in the section on procedure. The results of this energy balance are shown in Table II. As can be seen from that table the agreement is usually within 10% and at worst within 25%.

Efforts to measure the absolute dissociation of oxygen molecules into atoms by a calorimetric method similar to that described by Shaw (36) were not successful. Operation between 2.5 and 2.8 millimeters of mercury pressure with a hydrogen discharge gave the data shown in Table III. The best result of 39.2% hydrogen dissociation compares with Shaw's value of 60% at the same flow rates. When higher operating pressures were used, the instrument gave null readings. Even at low pressures, operation with oxygen led to deterioration of the filaments and had to be abandoned. Table III does show an order of magnitude

TABLE II

Energy Balance
(All values in watts)

Run #	H oil/sec	H reaction/sec	Power Absorbed	Error
347	471	3.24	398	-70
348	490	2.60	398	-89
349	310	2.72	355	+48
350	595	2.12	540	-53
351	280	2.97	274	-3
352	214	2.99	196	-15
353	264	3.12	201	-60
354	341	3.16	2.76	-62
355	383	3.36	358	-22
356	488	3.22	518	+33
357	615	3.28	622	+10
358	672	1.98	630	-40

TABLE III

Calorimetric Data

Run #	Gas Fed	Press mm Hg	Abs'd Power	Moles each Filament	Moles Recombined on 10^6 sec	#1	#2	#3	Total Moles Atoms Recombined/sec	Moles Fed/sec	Phosphoric Acid	% Diss.
C-1	H ₂	2.5	77	0.162	0.116	0.0694			0.347×10^{-6}	138×10^{-6}	No	0.251
C-2	H ₂	2.5	77	0.880	0.463	0.579			1.922×10^{-6}	138×10^{-6}	No	1.39
C-3	O ₂	2.8	80	0.631	-	-			0.631×10^{-6}	58.1×10^{-6}	No	1.09
C-4	H ₂	2.7	103	12.4	6.42	3.56			22.38×10^{-6}	133×10^{-6}	Yes	16.8
C-5	H ₂	2.6	75	13.7	7.87	6.25			27.82×10^{-6}	133×10^{-6}	Yes	20.9
C-6	H ₂	2.8	197	35.4	10.9	5.8			52.1×10^{-6}	133×10^{-6}	Yes	39.2

increase in atomic yields when the walls were poisoned with phosphoric acid.

The tunable cavity built to measure the electron density and field strength did not function properly. When an iris was used to couple the cavity to the waveguide, the resonance peak was inverted; and when a loop type coupler was used, two large peaks of equal magnitude were observed. Figures 26 and 27 show these effects as well as the presence of small spurious resonant peaks near the main one. A microwave absorbent material placed behind the plunger to smooth the curves resulted in their being badly distorted. This effect is shown in Figure 28.

Discharges maintained within the cavity using an uncooled quartz tube as a container were ill-defined and not amenable to the integration technique necessary to determine the electron density by the methods of Rose et al (39). Furthermore, at the pressures of normal operation, 10 - 20 millimeters of mercury, it proved difficult to light and maintain the discharge off resonance as is required to determine the "Q" of the loaded cavity. (See Appendix G for more details.)

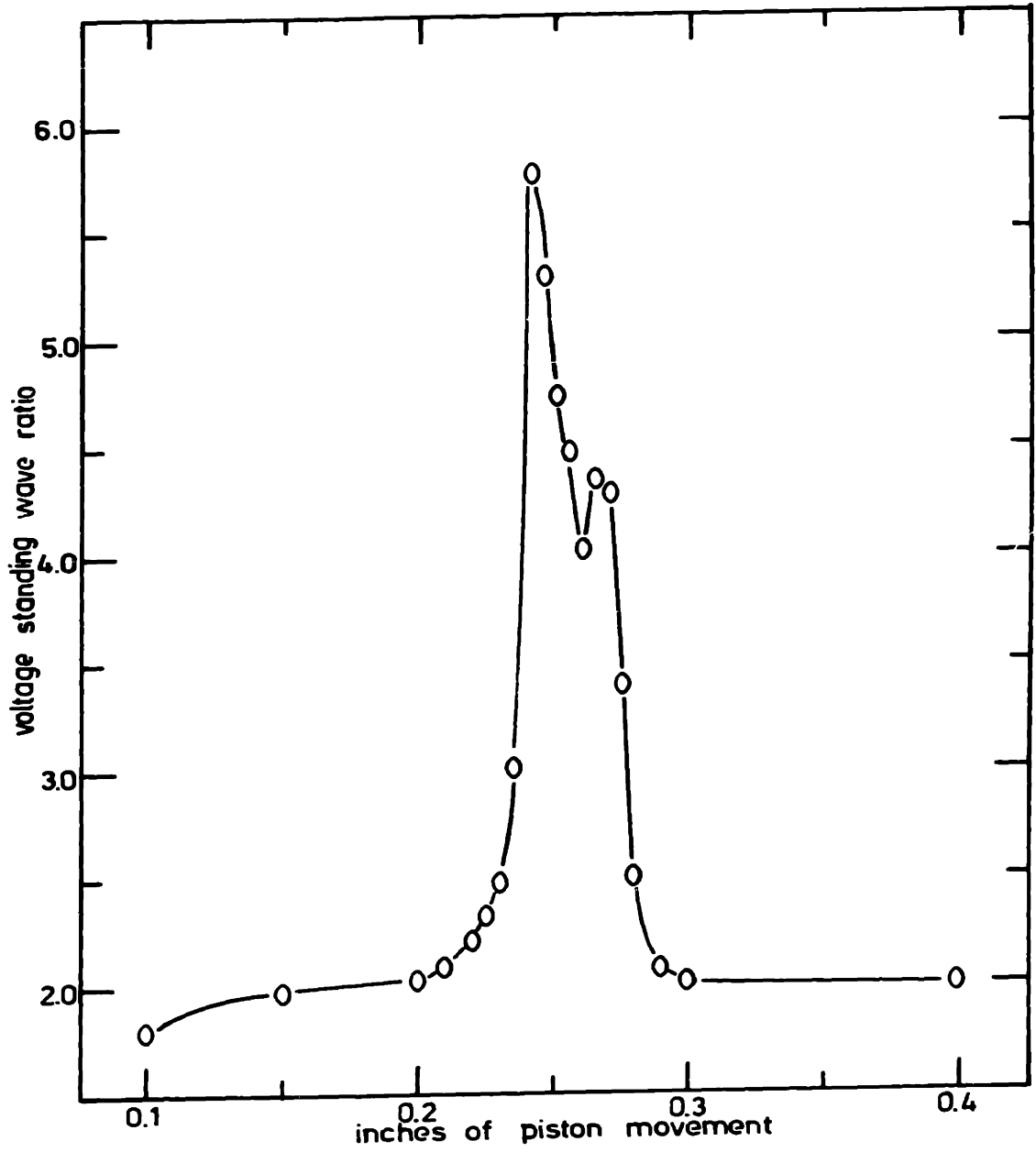


FIGURE 26. CAVITY RESONANT CURVE WITH IRIS COUPLING

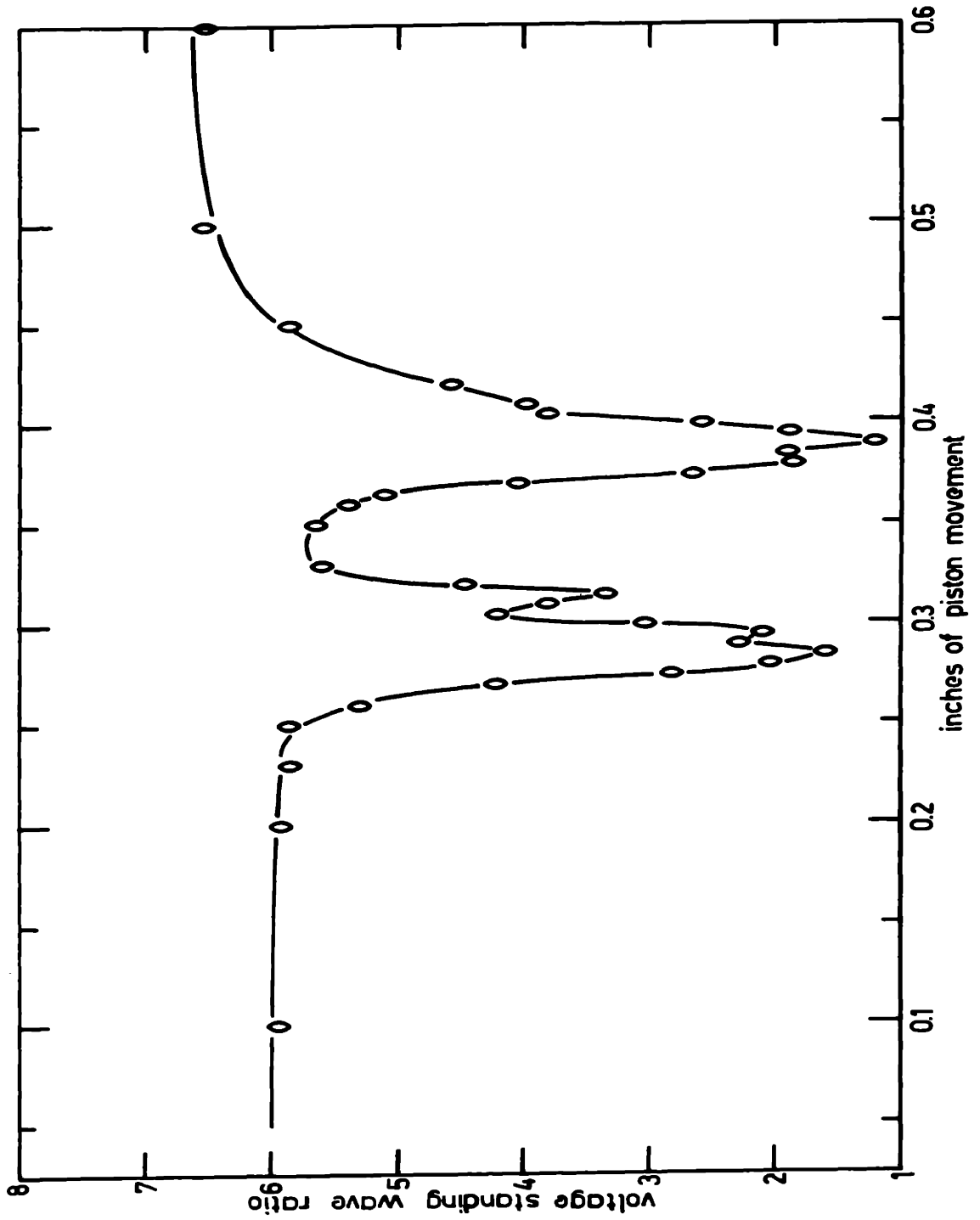


FIGURE 27. CAVITY RESONANT CURVE WITH LOOP COUPLING

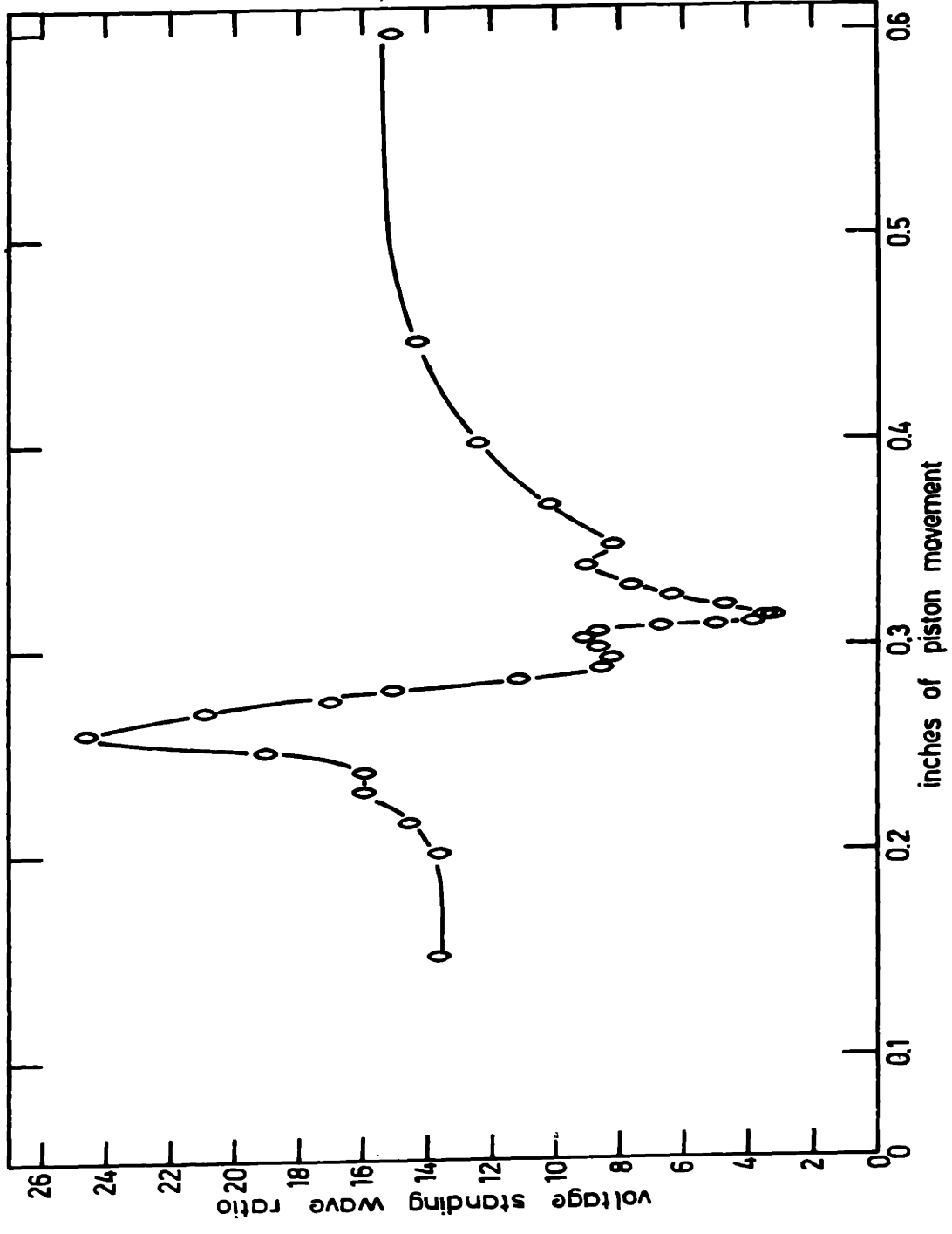


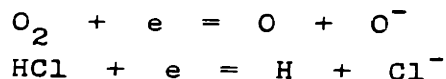
FIGURE 28. CAVITY RESONANT CURVE WITH IRIS COUPLING AND MICROWAVE ABSORBENT MATERIAL

VI. DISCUSSION OF RESULTS

A. Premixed Reactants

1. Effects of Pressure and Power In a plasma the electron's energy determines the probability or cross section for the formation of the necessary active specie for chemical reaction. This cross section is not, however, a single-valued function of the electron energy, but rather passes through a maximum. Physically the reason for such a maximum is that the cross section represents the wave mechanical interaction between the impinging electron and the particle being activated. If the electron moves either too slowly or too quickly there is little energy exchange.

In the discharge itself, the activation process is thought to be a combination of the two reactions below:



For the dissociative attachment process in oxygen McDaniel (40) presents cross section data as a function of electron energy. This data has been reproduced in Figure 29. Since the points on this curve were obtained using monoenergetic electron beam techniques, there is a very sharp maximum. Fox (41) has shown that a similar curve exists for the dissociative attachment process in hydrogen chloride.

william w. cooper iv Sc.D. thesis 10/10/66

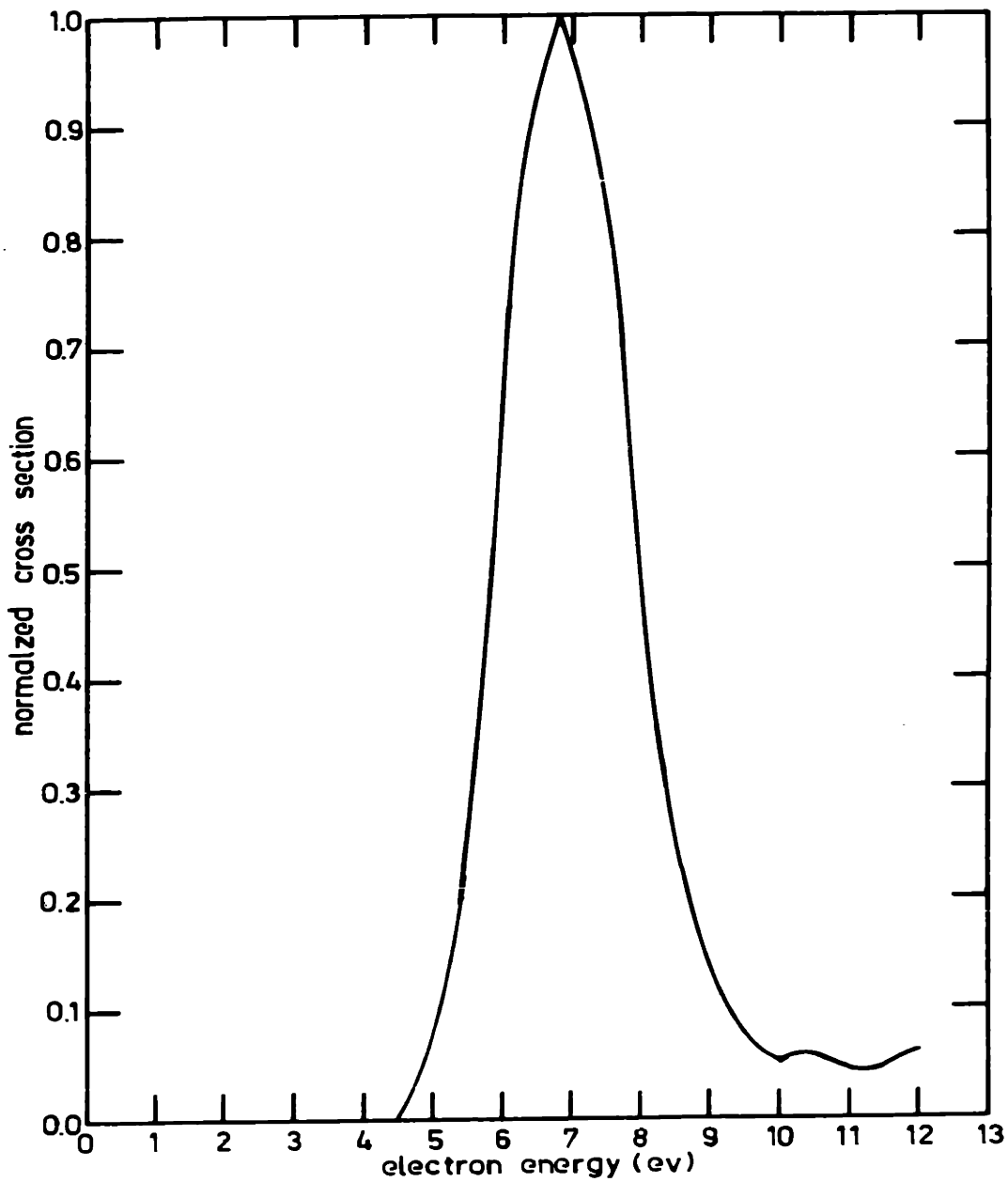


FIGURE 29. DISSOCIATIVE ATTACHMENT CROSS SECTION OF OXYGEN

It was demonstrated in the introduction (See page 22) that the electron energy or temperature is a function of E/p , but not necessarily a simple one. Brown (42) presents data for oxygen and hydrogen chloride which show that the ratio of electron to gas temperature is a monotonically increasing function of E/p . Thus for a constant gas temperature, the electrons become progressively more energetic as E/p increases. Because of this direct relationship between E/p and the electrons' energy, the cross section for the reaction may be plotted as a function of E/p . This curve will pass through a maximum as does that in Figure 29; but because the electrons have a distribution of energies, the peak will not be as sharp. Since there are various peaks for the different possible activation processes, control of E/p implies control over the particular reactive species being formed in the discharge. Other investigators (1) in the area of plasma chemistry have experimentally demonstrated the importance of this fact.

With this background on the importance of E/p as the proper variable, the next question that arises is how to control it. There are two ways of doing this. One is by varying the pressure at which the discharge is operating, and the other is by varying the power input to the discharge. The first of these is straightforward, but there may be difficulties with the second. In an empty waveguide, the

power density is proportional to the electric field strength squared. However, if the guide contains a plasma, the power input is proportional to the product of the electric field strength squared and the electron density. Hence, as more power is fed into the plasma, it can serve to increase either the electron density or the field strength. Lathrop (43) has considered this problem for a hydrogen plasma where as the power increases the electron density may rise sufficiently so that a decrease in the electric field actually results. Because of the high electron affinity of oxygen and chlorine, it seems unlikely that such a decline is occurring in the work reported here. In fact preliminary data obtained by Bell (37) on the hydrogen chloride oxygen system in a radio frequency discharge indicate that as the power increases the field strength also increases.

The microwave data showing the variations in yield as a function of power and pressure are consistent with a model in which E/p controls the chemical reaction. As shown in Figure 13, the percent conversion passes through a maximum at constant power as the pressure is varied from four to forty millimeters of mercury. If the electric field strength were not a function of power, the curves traced out on such a plot at different power levels should superpose. As can be seen from Figure 13, this is not the case. The maximum in yields for the 342 watt curve occurs at about 20 milli-

meters pressure; whereas, that for the 208 watt curve occurs at about 14 millimeters of mercury pressure. According to the theory, these maxima, both about 52%, should be at the same value of E/p . If the power is proportional to the electric field strength squared, an approximation to E/p may be obtained simply by taking the square root of the power and dividing this number by the pressure. This procedure gives 0.925 at the maximum of the 342 watt curve and 1.03 at the maximum of the 208 watt curve. This agreement to within 10% is quite good.

The data taken at a fixed pressure but with varying power must now be reconciled with this pressure data. As can be seen from Figure 11, at 20 millimeters of mercury pressure, the absolute magnitude of the power absorbed in the discharge had little effect on the yields obtained. Close inspection of the curve shows only a 3.5% increase in the magnitude of the yield as the power absorbed increased from 130 to 710 watts. This behavior is in contrast to that at 10 millimeters shown in Figure 12 where an increase in power over the same range led to a 20 percentage point decline in the yield.

To explain the data, consider first the 208 and 342 watt power levels on the 20 millimeter pressure curve in Figure 11. The small increase in the yield as the power is increased between these two levels is consistent with

that observed at the same pressure level in Figure 13. This increase in yield with power may be interpreted as arising from an increase in E/p which at this position of the cross section curve favors higher conversion. If this interpretation be correct, then the same effect should be observable in Figure 13 when E/p is increased by a pressure reduction. At the 208 watt absorbed power level this is indeed the case. A reduction in pressure from the 20 millimeter position leads to an increase in the yields. However, at the 342 watt level, the 20 millimeter position is at the maximum so that any change in pressure leads to a reduction in yield. The scatter in the data may mask the small effect here.

The plot in Figure 12 showing the data taken at 10 millimeters pressure may also be interpreted the same way. Here moving from the 208 to 342 watts absorbed power level, the yield declines from 49% to 45%. This is consistent with the decline from 49% to 46% observed over the same power change at a constant pressure of 10 millimeters in Figure 13. This decrease with power may be explained as resulting from an increase in E/p which at this position of the cross section curve favors lower yields. If these data reflect such a decrease in cross section with rising E/p , then a decline should also be observed when this variable is increased by reducing the pressure. As the data in

Figure 13 show, this is in fact the case. At both power levels a decrease in pressure from the 10 millimeter position leads to a decline in the yields.

Since Figure 13 in effect reflects the cross section curve as a function of E/p , the relative magnitude of the slopes in Figures 11 and 12 can be explained in terms of it. As can be seen at the 20 millimeter level in Figure 13, the slope is small showing a small change in yields with E/p . This is reflected in Figure 11 where varying the power over a wide range has only a small effect on yield. Conversely in Figure 13 at 10 millimeters, the slopes are steep so that a small change in E/p has more effect. Figure 12 reflects this as a sharper decline in yields with increasing power.

Since the work with the tunable cavity was not successful, it has not been possible to actually measure the electric field strength and subject these theories to a quantitative test. Further work should be directed to taking these measurements and putting the hypotheses presented here on a firmer basis.

2. Economics

The amount of power being fed into the gases greatly exceeds that required to dissociate all of the reactant material. For example, with the usual flow rate of

0.579×10^{-4} moles per second of oxygen, only 28.4 watts would be needed to break it all into atoms. This compares with 111 watts, the minimum amount of absorbed power necessary to maintain the discharge.

In an effort to make more efficient use of this power, the diameter of the reactor was increased. Because of its smaller surface to volume ratio a larger reactor has a lower rate of loss of electrons to the walls per unit volume. As the results in Table I on page 53 show, increasing the diameter did not reduce the power required to break down the gas. The lack of any effect of diameter or more specifically surface area on the power required for breakdown indicates that the discharge is recombination or attachment rather than diffusion controlled. That is to say, the bombarding electrons are lost by homogeneous electron capture in the gas phase rather than by diffusion to the walls. At the relatively high pressures of this work, this loss mechanism was not unexpected; and Brown mentions its importance (42). It is also consistent with the dissociative attachment activation scheme presented in the previous section.

A further drawback in the operation of the larger diameter reactor was that at the 20 millimeter pressure level the discharge did not completely fill the tube. This meant that there was open space available to the reactants for flowing through the discharge zone without ever having

been broken down by the field. Such an effect is analogous to channeling in more conventional chemical engineering equipment. Consequently at 20 millimeters pressure with the large 22 millimeter inside diameter tube, there was a reduction in yields. This effect can also be noted in Table I on page 53.

Since more than enough energy was being put into the gas to break the molecular bonds, the flow rates were increased in an attempt to make more efficient use of this energy. This increase in flow rates did lead to a reduction in the energy consumption per pound of chlorine formed. All results of the work at increased flow rates are shown in Table IV. They were first doubled, and then quadrupled. The lowest amount of energy required was 2.3 kilowatt-hours per pound of chlorine formed. This compares with 3.7 kilowatt-hours per pound under the usual flow rates of 2.32×10^{-4} moles per second of hydrogen chloride and 0.579×10^{-4} moles per second of oxygen.

Further reduction in energy requirements could probably be obtained by pushing the flow rates still higher. Although an increase in power was necessary to just maintain the discharge as the flows were increased, this minimum only slightly more than doubled from 110 to 250 watts as the flows were quadrupled. The limitation was the sample trapping system which simply could not condense all of the product stream at these increased flow rates.

Still further reductions in energy requirements might

TABLE IV
Energy Requirements

Run #	Flow Rate ml/min @ 1 atm		Press mm Hg	% Conv	Watts Power Absorbed	kw-hr per lb Cl ₂
	HCl	O ₂				
435	680	170	20	41.4	185	3.45
436	680	170	20	45.0	266	4.57
437	680	170	20	38.5	340	6.8
438	680	170	20	48.2	420	6.72
439	680	170	10	47.6	165	2.67
440	1360	340	20	42.8	265	2.38
441	1360	340	20	45.6	338	2.86
442	1360	340	20	51.1	420	3.17
443	1360	340	10	33.3	252	2.91
444	1360	340	20	47.4	408	3.33
445	1360	340	10	21.3	170	3.08
446	1360	680	20	51.9	340	2.54
447	1360	340	20	23.1	179	5.65
448	1360	340	30	35.6	338	3.68
449	1360	680	20	44.5	262	2.28
450	1360	680	20	49.9	407	3.16
451	1360	340	10	36.8	384	4.04
452	1360	340	10	37.9	311	3.17

be attained by using a generator which has a pulsed output rather than a continuous one. In this way a sharp peak of power would be used to break down the gas at intervals corresponding to the residence time of the reactant materials in the reactor. The repetition rate determined this way on the basis of the work here would be on the order of 100 pulses per second. The proper combination of intensity and duration would have to be determined empirically. Averaged over the pulses, the total energy input could be lower than that for continuous operation. However, the chemical energy input required to produce enough active species for the desired conversion limits the economies to be gained by the pulsing technique. On the basis of the oxygen atom dissociation's being the activation process, the limit is 0.436 kilowatt-hours per pound of chlorine formed. This represents an energy level five times lower than the best so far obtained.

There are other losses in the system which no effort was made to reduce. The largest resulted from the mismatch between the plasma and the waveguide. Proper design of the resonant section and the use of a double stub tuner would enable this source of loss to be tuned out of the system. Under present operation this mismatch results in a reflection of power which is absorbed in the isolator section and lost completely as far as useful work is concerned. With

a voltage standing wave ratio of three, 25% of the incident power is lost in this manner.

The use of air rather than oxygen presents another way of possibly achieving more economical operation. As shown in Figure 14, it is possible to operate with air and obtain reasonable conversions. There is a decrease in yield associated with its use, but in this investigation no extensive work was done to find the optimum operating conditions using an air feed. The determining factor would be a balance of the increased cost of using pure oxygen against the cost of the reduced yields with an air feed. A further possible problem with the use of air as an oxidant is the formation of nitrogen oxides. This has been reported by previous investigators, notably McCarthy (7); and in this work, blue dinitrogen trioxide was noted in the cold trap when air was used as a feed material.

With the equipment used in this investigation, the most efficient use of the power input occurred when the discharge was being sustained just on the verge of extinction; and the flow rates were straining the capacity of the sampling system. These operating conditions are consistent with those found by McCarthy (7) for most efficient operation in the formation of acetylene from methane in a microwave discharge.

3. Quench Two zones are present in Figure 15 where the data resulting from experiments performed with a nitrogen quench are presented. The first of these, nearest the discharge, is a region where the yields are lower than those obtained at the same power level of 358 watts with no quench. (See Figure 11) In light of the results of the work with an air feed, here the nitrogen, in addition to cooling the gases, is probably taking part in the reaction. As with the air feed, this decline in yield is caused by combination of the nitrogen with the active oxygen present. By indicating the region in which these active species are present, the curve serves to give an indication of the position of the reaction zone. The fact that the yields never fall as low as they do with an air feed shows that some of the reaction is taking place in the discharge itself. This picture of the reaction occurring downstream from the discharge is consistent with data to be presented in the next section which show that oxygen atoms are present there.

In the plateau-like region which begins two and one half centimeters downstream from the discharge, the quench has no effect on yields. The gas temperature in this region is 425 °C which corresponds to an equilibrium conversion of 43%. (See Appendix B.) Since the actual conversions observed are 50%, the evidence indicates that the yield is being controlled by the extent of active species formation in the

discharge. The only other explanation is that the forward reaction is faster than the quench step (10^{-3} seconds) and the yields increase as the gases cool. This seems unlikely in view of the well known difficulty in carrying out this reaction without a catalyst.

B. Separated Feeds

1. Reactors Three different designs of reactor were used for the experiments in which the flows of hydrogen chloride and oxygen were separated. The first of these, shown in Figure 16-A, impinged the flow of the gas not passed through the discharge onto the plasma zone. Figure 17 illustrates the data taken with this equipment and shows how the yields correlate with the relative position of the input of the hydrogen chloride gas. The lack of any change in slope as the pressure increased from 10 to 20 millimeters implies that the decay rate at 20 millimeters pressure was slower than that at the 10 millimeter pressure. Such a phenomenon is inconsistent with either a homogeneous loss mechanism depending on collisions in the gas phase or a heterogeneous mechanism depending on wall collisions. In either case the collision rate and, hence, the loss rate are higher at the higher pressure.

Because of this inconsistency, experiments with nitric oxide and oxygen were performed to ascertain the mixing pattern in the reactor. With these gases at one atmosphere, no discharge, and the same relative flow rates as in usual operation, there was a brown plume of nitrogen dioxide five centimeters long above the injection tube for the second gas. This showed that in usual operation the hydrogen chloride was being blown back up into the discharge region

rather than the active species' traveling down the tube and reacting when it reached the point of injection.

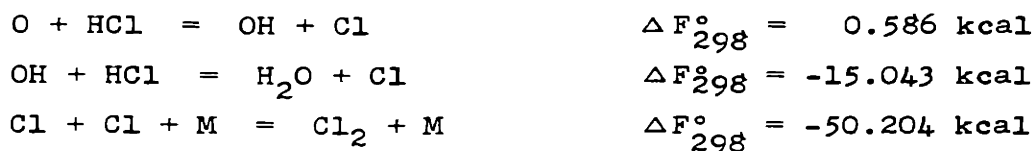
The second design, shown in Figure 16-B, was constructed to overcome this difficulty. The end of the injector tube was closed off, and four holes were drilled in the sides of the tube as close to the end as possible. In this way, the gas flow was directed toward the sides of the reactor rather than directly at the discharge zone. Results with this modified design were also unsatisfactory. As can be seen from Figure 18, the yields dropped off drastically from 31% to 3.5% as the position of the hydrogen chloride input was moved only one centimeter away from the discharge region. This effect can be explained as the deactivating effect of the bluff end of the injector tube. Active species from the discharge zone impinged onto this tip and were recombined or otherwise deactivated. Because of these negative results, runs with this reactor were made only at 20 millimeters pressure.

The final design with^{which} most data were taken is illustrated in Figure 16-C. This reactor avoided all the problems associated with the first two designs by having the second gas injected laterally through four holes equally spaced around the outside wall. Data taken with this reactor and shown in Figures 19, 20, 21, and 22 demonstrate conclusively that the active species required for reaction

have a finite lifetime outside the discharge zone and that reaction may take place in this plasma free region rather than be restricted to the discharge zone itself.

2. Kinetics The observation that reaction can occur when only one of the reactant gases is subjected to the action of the discharge must be explained in terms of a kinetic scheme for reaction. The active energy carrying species must have a lifetime on the order of ten milliseconds to explain the data. Since ions are quite short lived they are not considered further as the crucial energy carrier. For example, using data from Phelps and Pack (44), the collisional detachment lifetime of O_2^- was estimated to be 0.5×10^{-3} seconds.

It is well established that oxygen atoms are the major product of a microwave discharge in oxygen (45,46). Smaller amounts of the $^1\Delta_g$ metastable state are also formed (17). The kinetic scheme proposed below is reasonable in view of these facts and the experimental observation that oxygen atoms and hydroxyl radicals appear in the spectra taken of the discharge. This sequence explains well the data taken when oxygen was the only gas subjected to the activating effect of the discharge. The free energy change of each step is also given (47).



Harteck (48) has previously reported the first of these reactions to be the primary process with which oxygen atoms formed in a silent discharge react with hydrogen chloride.

The metastable $^1\Delta_g$ has the required long lifetime, on the order of hours for a radiative transition (49); but as the free energy change for the reaction below shows, it does not have sufficient energy to break the H-Cl bond.



Ozone is another species which fulfills the lifetime criterion; but in not being energetic enough, it suffers from the same drawback as the metastable state. The initiating scheme and its free energy change are shown below:



In all these schemes, only that beginning with atomic oxygen has sufficient energy to overcome the strong H-Cl bond and have close to a favorable free energy change for the initiating step alone.

A new initiating step is needed to explain the data which show reaction occurring when the oxygen is injected downstream from a hydrogen chloride discharge. DelGreco and Kaufman (2) and Foner and Hudson (50) report the reaction of hydrogen atoms with oxygen molecules via a third body collision. Their reaction sequence is shown below with the free energy changes for each step.



This scheme assumes that the hydrogen chloride dissociates in the discharge to form hydrogen atoms. As mentioned previously, Fox (41) reports an energy requirement of 0.66 electron volts or +15.2 kcal for the dissociative recombination process: $\text{HCl} + e = \text{H} + \text{Cl}^-$. This process is consistent with the mechanism postulated here. With the formation of oxygen atoms and hydroxyl radicals, this scheme merges into that proposed for the oxygen discharge on page 94; and the atoms and radicals can react with the remaining hydrogen chloride to form chlorine.

These reaction sequences must also be able to explain the experimental results with mixed feeds. As a basis for comparison in Figures 19 and 21, the yields obtained with the sidewall injection reactor may be extrapolated to zero input position for the second gas. When hydrogen chloride is the activated gas, Figure 21 indicates this extrapolated yield to be 50% at both 10 and 20 millimeters pressure; and when oxygen is activated, Figure 19 shows it to be 17% at 10 millimeters pressure and 35% at 20 millimeters pressure. These figures compare with the 46-48% yields obtained using a mixed feed at the same 320 watt absorbed power level. Since experiment shows that premixing the gases does not sum the yields achieved unmixed, hydrogen chloride and oxygen both cannot be activated to the same extent when mixed as when passed through the discharge alone. The explanation of these observations lies in the relative cross sections for

the activation processes. Because Figure 21 shows higher yields at zero separation than Figure 19, the data indicate that hydrogen chloride is more efficiently activated than oxygen. This finding is consistent with data on their relative electron collision cross sections reported by Brown (42). To break the H-Cl bond via dissociative attachment, the electrons need only reach an energy of 0.66 electron volts compared to 3.6 electron volts for the same process in oxygen. This activation of the hydrogen chloride provides a sink for electrons as soon as they have obtained an energy of 0.66 electron volts. When this energy is reached, they are removed from the swarm by an inelastic collision with the hydrogen chloride, the net effect of which is to truncate the high energy tail of the electron distribution function. In this way, electrons are prevented from gaining enough energy to dissociate the oxygen molecules. Hence, when feeds are mixed, the yields approach those obtained when the more easily activated hydrogen chloride is passed alone through the discharge.

3. Recombination Because of the paucity of data in the literature on hydrogen chloride, support for the mechanism postulated for reaction must come from data taken when oxygen was the gas passed through the discharge. If indeed oxygen atoms are the active species for reaction, then their

loss rate between the base of the discharge and the point of injection of the hydrogen chloride should be equivalent to either their homogeneous recombination rate or their wall recombination rate.

The homogeneous recombination of oxygen atoms in the gas phase is thought to proceed in a two step process (51). These steps are indicated in Equations (19) and (20) below.



A stationary state is then assumed for the O_3 concentration to arrive at the rate expression:

$$d[O]/dt = -[O]\{2k_1[O_2]^2\} \quad (21)$$

For small oxygen atom concentrations and a fixed pressure this equation may be integrated to give:

$$[O]/[O]_0 = \exp(-2k_1[O_2]^2 t) \quad (22)$$

A plot of the logarithm of $[O]/[O]_0$ versus t should give a straight line of slope $2k_1[O_2]^2$. By performing this operation at varying pressures and, hence, slopes, the slopes themselves can be plotted against $[O_2]^2$ to obtain the rate constant k_1 .

To apply this model to the system, it is necessary to assume that the added hydrogen chloride instantly removes all oxygen atoms at the point of its addition. Then using the kinetic scheme postulated in the previous section, the oxygen atom concentration at the point of the hydrogen chloride input may be calculated. (See Appendix A) These kinetics

indicate a one to one correspondence between chlorine molecule formation and oxygen atom disappearance, The time appearing in Equation (22) above is the actual time of flight from the base of the discharge to the point of titration with hydrogen chloride.

Figure 20 shows that this model does not fit the data very well. Although the lines are straight as predicted, the postulated effect of pressure on the slopes does not appear. The lack of such a pressure effect suggests that a wall loss process is dominant in removing the active species. A number of workers have reported (52, 53) this as a loss mechanism for oxygen atoms and obtained values for the recombination coefficient of oxygen atoms on various surfaces. Since the system under consideration here has laminar flow with Reynolds numbers (See Appendix C) varying from 36 to 72, the transport of these atoms to the walls must be by diffusion.

4. Diffusion It is possible to model the reactor being used as a semi-infinite cylinder and consider the decay in oxygen atom concentration within a slug of material as it moves down the tube away from the discharge. The detailed calculations are shown in Appendix D and follow closely those of Wise and Ablow (54). The differential equation which expresses the material balance on an annular ring within the reactor is written as Equation (23) on the following page.

$$\frac{\partial^2 n}{\partial r^2} + \frac{1}{r} \frac{\partial n}{\partial r} - \frac{v_z}{D} \frac{\partial n}{\partial z} = 0 \quad (23)$$

There are three assumptions going into this equation. The first is that the velocity profile which for laminar flow is given by the expression:

$$v = v_0 (1 - (r/r_0)^2) \quad (24)$$

can be expressed as some average v_z . This simplification allows the analytic integration of Equation (23) above. The other two assumptions are that the magnitude of the diffusive flux in the axial direction is negligible compared to the convective flux and that the reverse is true in the radial direction with diffusive term being important. The appropriate boundary conditions for the problem are:

$$\begin{aligned} @ r = 0, & \quad n \text{ is finite} \\ @ z = 0, & \quad n = n_0 \\ @ r = r_0, & \quad \partial n / \partial r = -\gamma n u / 4D. \end{aligned}$$

The last of these conditions matches the diffusive flux at the wall to the wall recombination rate. Here "u" is the mean value of the peculiar speed of the oxygen atoms and is equal to $(8kT/m)^{1/2}$. With these boundary conditions, the solution is:

$$\frac{n}{n_0} = 2 \sum_{i=1}^{\infty} \frac{\exp(-Da_i^2 z / v_z r_0^2) J_0(a_i r / r_0)}{a_i (1 + b^2 a_i^2) J_1(a_i)} \quad (25)$$

In the above solution, "b" is a dimensionless variable given by:

$$b = 4D / \gamma u r_0 \quad (26)$$

and the a_i 's are solutions to the transcendental equation:

$$J_0(a_i) = ba_i J_1(a_i) \quad (27)$$

The other symbols have their usual meanings with "n" being the oxygen atom density; m, the oxygen atom mass; r_0 , the reactor radius; D, the diffusivity; n_0 , the density at the base of the discharge; z, the distance downstream from the discharge; and J_0 and J_1 , the Bessel functions of zero and first order.

Since the velocity in the reactor can be determined from the known molar flow rates and the temperature, the only unknowns in Equation (25) are the diffusivity, D, and the recombination coefficient, b . Because both appear directly in "b" and indirectly in the " a_i 's", it is difficult to get useful information from Equation (25) as it is. In order to simplify the equation, the radial variation in the density is removed by integrating over the cross section of the tube. Since this "r" variation is of no interest and not measurable with the techniques used, no essential information is lost in the process. All terms except $J_0(a_i r/r_0)$ are unaffected by the integration which effectively averages this Bessel function over the cross section. As indicated in Equation (D-24) of Appendix D, this average is $J_1(a_i)/a_i$. The final result of the averaging of Equation (25) is shown as Equation (28) below.

$$\frac{n(z)}{n_0} = 4 \sum_{i=1}^{\infty} \frac{\exp(-Da_i^2 z/v_z r_0^2)}{a_i^2 (1 + b^2 a_i^2)} \quad (28)$$

As shown in Appendix D, the exponential is large except for very small z ; and the first term in the series forms a satisfactory approximation. In addition for "b" large compared to unity, it is also shown there that $a_1 = (2/b)^{\frac{1}{2}}$. Substituting this approximation into Equation (28) results in:

$$\frac{n(z)}{n_0} = \frac{2b \exp(-2Dz/br_0^2 v_z)}{(1 + 2b)} \quad (29)$$

Taking the logarithm of both sides of Equation (29) gives:

$$\ln[n(z)/n_0] = \ln[2b/(1 + 2b)] - (2D/br_0^2)t \quad (30)$$

where the time of flight "t" has been substituted for z/v_z . The slope of the line, $-(2D/br_0^2)$, can be further reduced with the help of Equation (26) to $\gamma u/2r_0$. This result is independent of the diffusivity and, hence, the pressure.

If this simplified model is correct, then a plot of the yields versus time of flight on a semilogarithmic plot should be a straight line with a slope independent of pressure. As can be seen from Figures 20 and 22, this result agrees with the experimental data. The data shown there plot as parallel lines on the semilogarithmic scale and do not show a change in slope with pressure as would be expected if the loss process were homogeneous recombination.

5. Mass Balance This same result could have been obtained in a more direct and physically more obvious way by making

a mass balance on a volume element of the gas as it moves down through the tube after the discharge. Let "n" be the atomic concentration in such a wafer-like element at any time. The rate at which these particles collide with the wall is given by kinetic theory (55) as $nu/4$ collisions per square centimeter per second where "u" is the mean peculiar speed of the particles. The area available for collision is $2\pi r dz$ and the element has a volume of $\pi r^2 dz$. Let γ denote the efficiency of recombination, that is the number of recombinations per collision. Then the rate of change of density in this volume element as it moves along will be given by Equation (31) below.

$$dn/dt = -\gamma(nu/4)(2\pi r dz/\pi r^2 dz) = -\gamma nu/2r_0 \quad (31)$$

This equation integrates to:

$$\ln(n/n_0) = -(\gamma u/2r_0)t \quad (32)$$

Plotted on a semilogarithmic scale this equation also has a slope of $-(\gamma u/2r_0)$ which agrees exactly with the result found via simplification of the rigorous diffusion equation.

Physically what allows this simplification is the inefficiency of the walls as recombining surfaces. Because they are so poor, only a very small concentration gradient is established in the radial direction; but because of the high diffusivity, estimated at $40 \text{ cm}^2/\text{sec}$ for oxygen atoms (See Appendix C.), at these low pressures there is sufficient flux to the walls to account for the loss.

6. Test of the Diffusion, Wall Recombination Model If this model is correct, it should be possible to calculate , the recombination coefficient, from the slopes of the plot in Figures 20 and 22. The only other information necessary is the radius of the tube and the mean peculiar speed of the oxygen or hydrogen atoms. The former can be easily measured and is 0.55 centimeters. The latter can be calculated from a knowledge of the temperature in the region downstream from the discharge.

From the kinetic theory this mean peculiar speed is given by (55):

$$u = (8kT/\pi m)^{\frac{1}{2}} \quad (33)$$

For the purposes of calculation on the oxygen data an average value of 625°K was used. This gives a mean peculiar speed of 9.05×10^{-4} cm/sec. With this value and the measured slope of 107 seconds^{-1} for the lines in Figure 20, the oxygen wall recombination coefficient is calculated to be 13.0×10^{-4} . For hydrogen chloride the corresponding temperature is 685°K which results in a coefficient of 8.62×10^{-4} . The details of these calculations are shown in Appendix A.

The number obtained with the oxygen data compares with a value of 7.1×10^{-4} reported by Greaves and Linnett (53) for recombination on quartz and with a value of 1.9×10^{-4} reported by Dickens et al (62) for recombination on pyrex. No value was found in the literature with which to compare the recombination coefficient for hydrogen chloride.

The agreement between the oxygen recombination coefficient calculated from the experimental data and that reported in the literature provides support for the proposed mechanism which postulates the oxygen atom as the active species initiating reaction. The steeper slopes of the lines in Figure 22 indicate a faster decay of the hydrogen atoms than is the case for the oxygen. Because of its higher peculiar velocity, four times that of oxygen at the same temperature, hydrogen atoms will collide with the wall more often than oxygen atoms. If the recombination efficiencies and temperatures are similar the slope should be about four times as steep; whereas in fact it is 2.8 times as great as that with oxygen. Were chlorine atoms the active species, the decay should be slower than with oxygen.

7. Recommendations for Future Work The reaction scheme presented above should be additionally tested by passing pure hydrogen gas through the discharge zone to produce the atoms and then mixing the products downstream with the hydrogen chloride and oxygen reactants. If the reaction occurs via the mechanism presented, the formation of OH and O radicals in the second and third steps should lead to their reaction with the hydrogen chloride present. In this case, any chlorine formation would positively confirm the hydrogen atom's being the initiating active species. Safety considerations prevented this experiment from being carried out.

An absolute measurement of the oxygen or hydrogen atom concentration in the region below the discharge was not possible with the equipment used in this work. Calorimetric methods can be applied to the problem; and as is discussed in Section C-4 below, there is reason to believe work in that area would be productive. Data should be taken for both hydrogen and oxygen atoms and the results plotted as a function of position downstream from the discharge. This data and the data in Figures 20 and 22 could then be compared and interpreted in terms of the exact numerical solution of Equation 23 as suggested below.

Additional theoretical work should test this diffusion model by carrying out a numerical integration of Equation 23 in dimensionless form using the true velocity profile. The resulting values of the atom concentration averaged at several cross sections could be plotted as a function of downstream distance or time. These theoretical plots would be suitable for comparison with those obtained from the experimental data.

A further experimental test of the model would involve operation with reactors of varying diameter. As was shown in subsection 4 above, the slope of the lines in Figures 20 and 22 is given by $(\gamma u / 2r_0)$; hence, operation with reactors of different radius provides a means of taking independent measures of this group. Then using the temperature data appropriate to each reactor to calculate "u", the value of γ may be obtained from the slope and the radius. This

number for γ should be compared with those taken with reactors of different radii. Because of varying microscopic areas from tube to tube, these value for γ would probably agree only to within an order of magnitude.

C. Measurements and Errors

1. Temperature As shown in the apparatus section, temperatures downstream from the discharge were measured with an iron-constantan thermocouple placed inside a quartz thermowell. This is the same method used by two other groups of workers (15, 2) on similar systems with no reported difficulty. An objection to this procedure for measuring temperatures in this region is that there are excited species present which can recombine on the thermowell walls to give erroneously high readings. An estimate of the magnitude of this effect may be obtained by considering the temperature difference required to dissipate by a convective flux into the gas all the enthalpy released on the probe. The calculation presented in Appendix E shows that this error is on the order of 2°K.

The temperatures actually measured this way were used for the calculations carried out to draw the plots of the data in Figures 20 and 22. In these plots the time of flight was calculated taking into account the temperature variation along the tube. These calculations and associated

plots are given in detail in Appendix A. It can be seen there from Figures A-1 through A-4 that the effect of the temperature on the bulk gas velocity is greatest in the region closest to the discharge. The subsequent integration smooths out the velocity variation so that the time of flight versus distance plot in these same figures approaches a straight line as it would be if the temperature were truly a constant. The average temperature used in calculation of the mean peculiar speeds is that temperature which corresponds to the average velocity indicated by the slope in the linear portion of the time versus distance plots in Figure A-1 through A-4. For the oxygen this temperature is the 625°K which has been used in all preceding calculations. For hydrogen chloride the corresponding temperature is 685°K.

2. Spectra The spectra shown in Figure 25 were all taken at 20 millimeters pressure and at the usual flow rates for the respective gases. The oxygen spectrum shows clearly the 3947A and 4368A lines attributable to oxygen atoms. (56) It also shows the long wavelength portion of the 3064A OH radical band as well as some of the hydrogen Balmer lines. These lines show the presence of water vapor in the oxygen. The exposure time used for making this spectrum was much longer than that for the spectrum of the mixed feed or the hydrogen chloride alone. The presence of oxygen atoms in the spectrum lends further support to the postulated mechanism

of reaction requiring oxygen atoms for an initiating step.

The hydrogen chloride spectrum shows all of the Balmer lines except the first which is cut off by the long wavelength sensitivity of the plate. The presence of hydrogen atoms is a necessary condition for the mechanism postulated when hydrogen chloride is the sole gas being activated. The other lines at the long wavelength end of the spectrum are due largely to chlorine atoms. The very bright band near 3900A results from the CH bond and indicates hydrocarbon impurities in the hydrogen chloride. This is to be expected with the commercial grade of gas used. Such gas customarily is a by product stream from the chlorination of hydrocarbons. This band disappears when oxygen is added to the system.

The spectrum of the mixed system is largely a superposition of the separate ones. The hydroxyl bands are much brighter as would be expected if the radical is being formed as a reaction intermediate. Because of the much shorter exposure it is difficult to see the oxygen atom lines, especially that at 3947A. While by themselves the spectra do not say anything about the mechanism of reaction, the fact that they show the postulated intermediates to be present in the discharge zone is further evidence that the postulated mechanisms are correct.

3. Power Measurements For economic evaluation accurate measurements of the power actually dissipated in the discharge

region is essential. In this work the power shown as being absorbed in the discharge includes as errors any that is lost by radiation from the open slit in the waveguide and any that is lost as heat in the walls of the waveguide or the reactor tube. The technique of monitoring the temperature rise in the cooling oil jacketing the reactor verified the power meter readings usually to within 10%. (See Table II) since the method of measurement used always approached balance on the potentiometer used for the oil change in temperature reading from the same side, most of the errors are biased in the same direction. An error of one-half degree in the measurement of the cooling oil temperature change would completely account for the 25% error in Run 353 where the agreement is worst.

4. Calorimetry The original motivation for the calorimeter was to obtain a direct measure of the extent of the oxygen of hydrogen chloride dissociation in the discharge region. The details of the technique are explained in Appendix F. Basically it depends on the enthalpy release of the species recombining on its surface. Initially work was begun using hydrogen gas in an effort to duplicate the data obtained by Shaw (36) using a duplicate instrument.

Table III shows all the data taken with the instrument. As can be seen from that data, coating the wall with phosphoric acid greatly increased the number of atoms reaching the calorimeter. Even so the largest amount measured 39.2%

dissociation did not match the 90% reported by Shaw. It was found that the technique was unsuited to use with oxygen because the filaments oxidized with a consequent change in resistance and current flow.

The more than ten fold increase in the measured hydrogen atom production when the walls were coated with phosphoric acid again points to a wall loss process as being the important one for removal of the active species.

When the pressure was raised to that of usual operation, 10 or 20 millimeters of mercury, this calorimetric technique failed altogether. At these higher pressures even with a phosphoric acid coated wall, the atomic species had decayed to negligible values by the time they reached the position of the first filament. A redesigned calorimeter would allow the probes to be moved closer to the discharge, but because of the lack of success with oxygen this modification was not attempted.

Elias Ogryzlo, and Schiff (15) report a selectivity of certain metal oxides for recombination of oxygen atoms and deactivation of metastable states. Future work should use their methods and determine the exact composition of the discharge products. Then using a cavity or other technique for measuring the field strength the value of optimum E/p could be found for most efficient atom production and operation. The greatest problem with this calorimetric procedure is the extension to high pressures.

Presumably this could be overcome by a combination of wall coating for deactivation and design for close proximity of discharge and probes.

5. Tunable Cavity Thorough discussion of the techniques developed by Brown and other workers (39, 57, 58) on the use of a resonant cavity as a microwave diagnostic tool is given in Appendix G. Basically these techniques depend on the measurement of the cavity Q and its resonant frequency. Since the frequency of the microwave equipment available for this work was fixed the cavity design was such that it rather than the generator could be tuned. The cavity was constructed to resonate in the TE_{111} mode. On a mode chart (59) this choice is relatively far removed from any interfering resonances. Also the Q of the cavity is not greatly affected by the position of the plunger used for tuning.

The resonance curves in Figures 26-28 show that the cavity did not function as had been hoped. The resonance curve showed spurious peaks so that the Q could not be easily determined and the frequency shift with and without a plasma could not be measured. There are several reasons for this behavior. A major problem as illustrated by comparing Figures 26 and 28 is associated with the tuning of the cavity itself. The free space behind the plunger was taking part in the resonant process as shown by the fact

that padding this region with a microwave absorbent material had such an effect on the resonant curve.

Another point of difficulty was coupling the cavity to the waveguide. Plots of the position of the voltage minimum versus plunger position shown in Figure 30 indicated that the cavity was over coupled to the waveguide. Ideally at resonance the cavity should be a purely resistive load as far as the waveguide and generator are concerned. This problem of proper matching is one that would have to be solved before the cavity diagnostic techniques could be applied. A possible method of attack is to use coaxial line rather than waveguide as the transmission line. With coaxial line, coupling to a cavity may be easily done with a simple loop linking the magnetic fields. Variation of the degree of coupling may be obtained either by turning the loop or changing its size.

To avoid the problem of spurious resonances, dramatically illustrated in Figure 27, a cavity should be designed to function with a variable frequency generator. Since this cavity size would be fixed there would be no odd empty spaces inside it to participate in resonance. This design would also solve another problem encountered with a cavity oscillating in the TE_{111} mode. Here it was found that the discharge region inside the quartz tube was not well defined. Because the electric field is concentrated in an ill-defined spheroid at the center of the cavity,

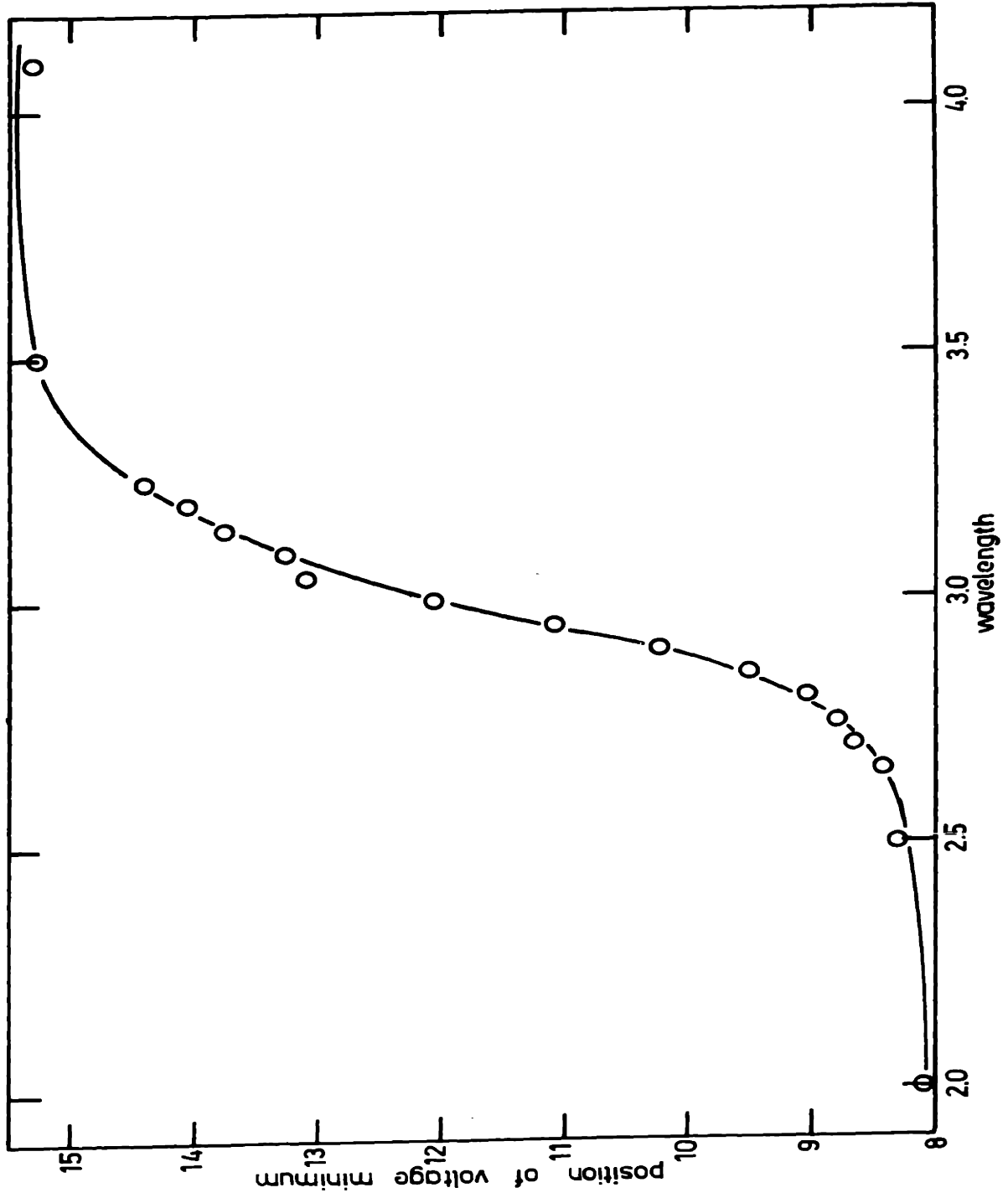


FIGURE 30. PHASE CURVE - ARBITRARY SCALES

it is not possible to apply the integration techniques developed by Rose and Brown (39). With a TM_{010} cavity this problem would be avoided. In this mode the electric field is uniform along the axis of the cavity with no component on the axial direction. Hence the discharge should be uniform along the centrally located quartz tube. Since there is no variation in the field strength along the axis this cavity cannot be tuned by a movable plunger. However if the generator is tunable that presents no problem.

VII. CONCLUSIONS

1. Chlorine may be formed in yields of over 50% from the oxidation of hydrogen chloride in a microwave discharge
2. Oxygen or hydrogen atoms form the active initiating species.
3. The results may be interpreted in terms of E/p being the proper variable for control of the chemical yields.
4. Quench data indicates the extent of reaction is controlled by the active species formation in the discharge.
5. Decay of the active species takes place on the surface of the reactor.
6. Spectra show oxygen atoms, hydrogen atoms, and hydroxyl radicals to be present in the discharge.
7. Air may be used as the oxidizing agent at reduced yields.
8. Energy requirements are as low as 2.3 kilowatt-hours/pound of chlorine with indications they may be further reduced.

VIII. RECOMMENDATIONS

1. Further efforts should be made to apply cavity or other techniques to the measurement of the electric field strength.
2. A tunable generator and a cavity operating in the TM_{010} mode should be used for further work.
3. Operation with pulsed microwave power should be investigated as a means of more economic operation.
4. Separated feed reactors of varying diameter should be used to test the effects of radius in the diffusion model.
5. The calorimetric techniques should be developed for obtaining a direct measure of the active species concentration at these pressures.
6. Passing hydrogen through the discharge and mixing downstream with hydrogen chloride and oxygen presents a way of testing the hypothesis that hydrogen atoms are the initiating species.
7. A computer solution of the diffusion equation incorporating the laminar velocity profile should be carried out.
8. A better sample collection system should be developed so that the apparatus may be operated at higher flow rates.

APPENDIX A

In the following discussion, the procedure is a titration aimed at determining the active specie concentration downstream from the discharge. The physical situation is one in which either oxygen or hydrogen chloride is passed through the discharge using the reactor shown in Figure (16-C). Downstream, this gas is mixed with the second undischarged reactant. The concentrations of oxygen or hydrogen atoms referred to are those at the inlet point of the second unactivated gas.

A. Details of Calculations for Oxygen Discharge

Consider a region downstream from an oxygen discharge and let:

C = total molar concentration at a pressure p

M = moles of O₂ molecules fed to the system per second²

Y = the flow of oxygen atoms per second

F = the moles of HCl fed to the system per second

X = conversion of HCl to Cl₂

Then since each reacted oxygen molecule decomposes to two atoms in the discharge, the actual molar flow rate of oxygen molecules is $M - Y/2$. From the stoichiometry of the kinetic

scheme, each oxygen atom leads to the conversion of two hydrogen chloride molecules to chlorine. Thus the conversion may be written as:

$$X = 2Y/F \quad (A-1)$$

Since the total molar flow is $M + Y/2$, the sum of the oxygen molecular and atomic flows, in the gas phase, the mole fraction of oxygen atoms is $Y/(M + Y/2)$. Substituting for Y and noting that for stoichiometric feeds $F = 4M$, the oxygen atom mole fraction becomes:

$$Y/(M + Y/2) = \frac{FX/2}{M + FX/4} = \frac{2MX}{M + MX} = \frac{2X}{1 + X} \quad (A-2)$$

The total molar concentration may be determined from the perfect gas law and is:

$$\frac{N}{V} = \frac{P}{760RT} \quad (A-3)$$

Multiplying this density by the oxygen atom mole fraction gives for the oxygen atom concentration:

$$n = \left(\frac{2X}{1 + X} \right) \left(\frac{P}{760RT} \right) \quad (A-4)$$

The velocity of the gases may be determined by dividing the total volumetric flow rate by the cross sectional area. The volumetric flow rate is given by the product of the total molar flow rate and the volume per mole. This is:

$$[M + Y/2] \left[22,400 \left(\frac{760}{P} \right) \left(\frac{T}{273} \right) \right] = M[1 + X] \left[22,400 \left(\frac{760}{P} \right) \left(\frac{T}{273} \right) \right] \text{ cm}^3/\text{sec} \quad (A-5)$$

Noting that M equals 0.579×10^{-4} moles of oxygen per second and that the cross sectional area is 0.95 square centimeters, simplifying Equation (A-5) results in the velocity's being given by:

$$v = 3.8 (T/p) (1 + X) \text{ cm/sec} \quad (\text{A-6})$$

The temperature as a function of position below the discharge has been plotted in Figure 23. Using this plot and Equations (A-4) and (A-6), the velocity and density may also be determined as functions of position. Figures (A-1) and (A-2) show the reciprocal of this velocity plotted versus the separation between the hydrogen chloride input and the discharge. By graphically integrating this reciprocal velocity plot, the time of flight from the discharge base to this hydrogen chloride input position may be determined. Figures (A-1) and (A-2) also indicate the results of this integration. All pertinent values have been collected in Tables (A-1) and (A-2). Finally the oxygen atom concentration has been plotted against the time of flight in Figure 20.

B. Details of Calculations for Hydrogen Chloride Discharge

Consider a region downstream from an hydrogen chloride discharge and let:

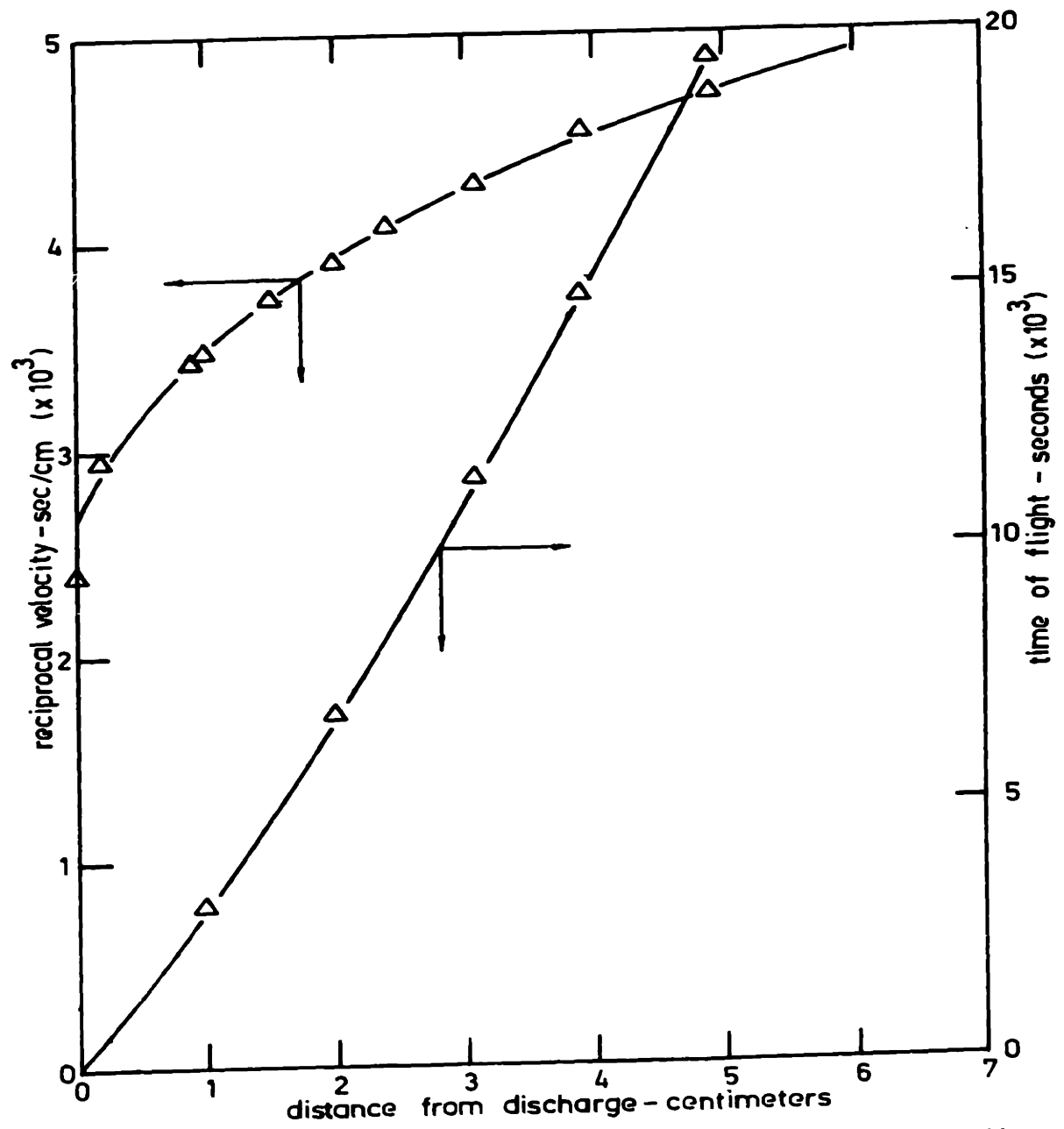


FIGURE A-1. OXYGEN VELOCITY - TIME DATA AT 10 mm Hg

william w. cooper iv Sc.D. thesis 10/11/66

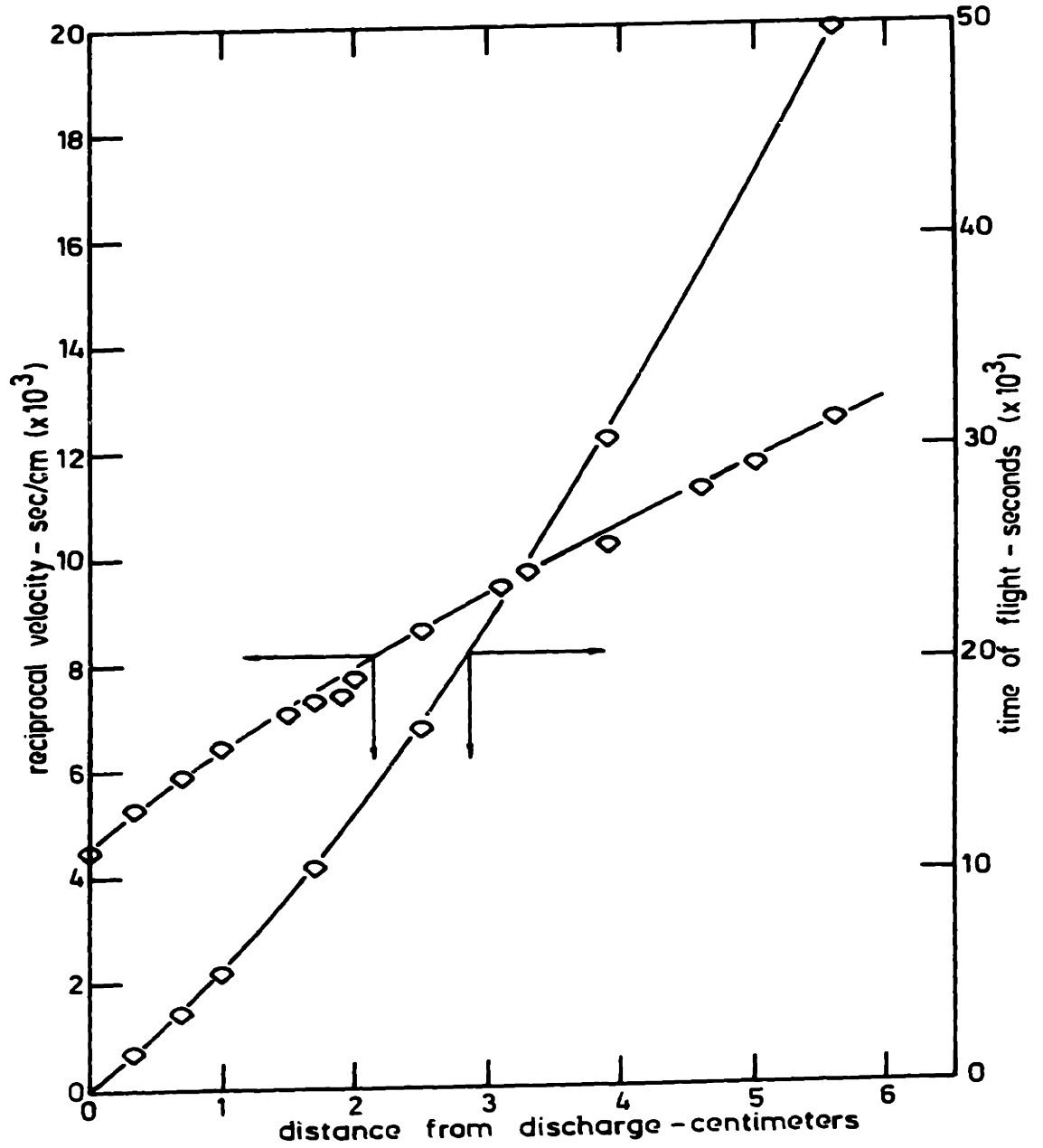


FIGURE A-2. OXYGEN VELOCITY-TIME DATA AT 20mm Hg

TABLE A-1

Oxygen Atom Data at 10 mm Hg Pressure

Run #	Position d cm	Conversion X	Temp °K	Velocity v cm/sec	1/v	Moles O atoms/cc	Time of Flight Sec
494	4.9	0.0118	555	213	4.70×10^{-3}	0.0675×10^{-7}	19.49×10^{-3}
495	3.9	0.0177	573	221	4.53×10^{-3}	0.0976×10^{-7}	14.91×10^{-3}
496	3.1	0.0383	594	234	4.27×10^{-3}	0.1995×10^{-7}	11.39×10^{-3}
497	2.4	0.0471	618	246	4.07×10^{-3}	0.234×10^{-7}	8.3×10^{-3}
498	1.5	0.0766	658	269	3.72×10^{-3}	0.347×10^{-7}	4.8×10^{-3}
499	0.9	0.103	698	292	3.42×10^{-3}	0.430×10^{-7}	2.7×10^{-3}
500	0.2	0.147	778	339	2.95×10^{-3}	0.529×10^{-7}	0.55×10^{-3}
501	0.0	0.346	813	416	2.40×10^{-3}	1.015×10^{-7}	0.0
502	1.0	0.0971	690	288	3.47×10^{-3}	0.412×10^{-7}	3.13×10^{-3}
503	2.0	0.0706	633	257	3.89×10^{-3}	0.334×10^{-7}	6.85×10^{-3}

TABLE A-2

Oxygen Atom Data at 20 mm Hg Pressure

Run #	Position d cm	Conversion X	Temp °K	Velocity v cm/sec	l/v	Moles O atoms/cc	Time of Flight Sec
482	4.6	0.0059	466	89	11.23×10^{-3}	0.0808×10^{-7}	38.0×10^{-3}
483	1.9	0.0947	648	135	7.41×10^{-3}	0.858×10^{-7}	11.6×10^{-3}
485	5.6	0.00296	418	79.7	12.53×10^{-3}	0.044×10^{-7}	49.8×10^{-3}
486	5.0	0.00598	448	85.6	11.69×10^{-3}	0.0826×10^{-7}	42.6×10^{-3}
487	3.9	0.0089	513	98	10.21×10^{-3}	0.0733×10^{-7}	30.6×10^{-3}
488	3.3	0.00891	538	103	9.71×10^{-3}	0.1054×10^{-7}	24.4×10^{-3}
489	2.5	0.0236	596	116	8.63×10^{-3}	0.248×10^{-7}	16.90×10^{-3}
490	1.7	0.0884	663	137	7.30×10^{-3}	0.788×10^{-7}	10.42×10^{-3}
491	0.7	0.156	773	170	5.90×10^{-3}	1.122×10^{-7}	3.68×10^{-3}
492	0.35	0.224	813	189	5.29×10^{-3}	1.444×10^{-7}	1.72×10^{-3}
493	0.0	0.358	860	222	4.51×10^{-3}	1.97×10^{-7}	0.0
503'	1.0	0.124	726	155	6.45×10^{-3}	0.975×10^{-7}	5.5×10^{-3}
504	1.5	0.0854	683	141	7.09×10^{-3}	0.740×10^{-7}	9.0×10^{-3}
505	2.0	0.0676	637	129	7.75×10^{-3}	0.639×10^{-7}	12.7×10^{-3}
506	3.1	0.0118	550	106	9.44×10^{-3}	0.136×10^{-7}	22.4×10^{-3}

C = the total molar concentration at a pressure p

F = the moles of HCl fed to the system per second

Y = the flow of either H or Cl atoms per second

X = the conversion of HCl to Cl₂

The actual hydrogen chloride molar flow rate will be F - Y, and the total flow rate will be F + Y. Since according to the kinetic scheme, the dissociation of each hydrogen chloride molecule leads in addition to the reaction of one other, the conversion will be given by:

$$X = 2Y/F \quad (A-7)$$

The mole fraction of hydrogen atoms at any time is Y/(F + Y) which reduces with the aid of Equation (A-7) to X/(2 + X). Multiplying the expression for the total molar concentration given in Equation (A-3) by this mole fraction gives for the hydrogen atom density:

$$n_h = [X/(2 + X)] [P/(760RT)] \quad (A-8)$$

The velocity may again be determined by dividing the total volumetric flow rate by the cross sectional area. The total molar flow rate is F + Y and with the use of Equation A-7 this becomes:

$$F + Y = F + FX/2 = F(2 + X)/2 \quad (A-9)$$

Hence the volumetric flow rate is :

$$F \left[\frac{2 + X}{2} \right] (22,400) \left(\frac{T}{273} \right) \left(\frac{760}{P} \right) \text{cm}^3/\text{sec} \quad (A-10)$$

Noting that the molar flow rate of hydrogen chloride is 2.32×10^{-4} moles/sec and that the cross sectional area is 0.95 square centimeters the velocity becomes:

$$v_h = 7.62 \frac{T}{P} (2 + X) \text{ cm/sec} \quad (\text{A-11})$$

The temperature profile below an hydrogen chloride discharge has been plotted in Figure 24. With the help of this plot and Equations A-8 and A-11, the density and bulk velocity of the hydrogen atoms below the discharge may be computed. The reciprocal of this velocity has been plotted in Figures A-3 and A-4 versus the position downstream from the discharge. By graphically integrating this reciprocal velocity plot, the time of flight from the discharge base to the oxygen input position may be determined. The right hand scale in Figures A-3 and A-4 indicates the results of this integration. The pertinent values have all been collected in Tables A-3 and A-4. Finally the hydrogen atom concentration has been plotted against the time of flight as shown in Figure 22.

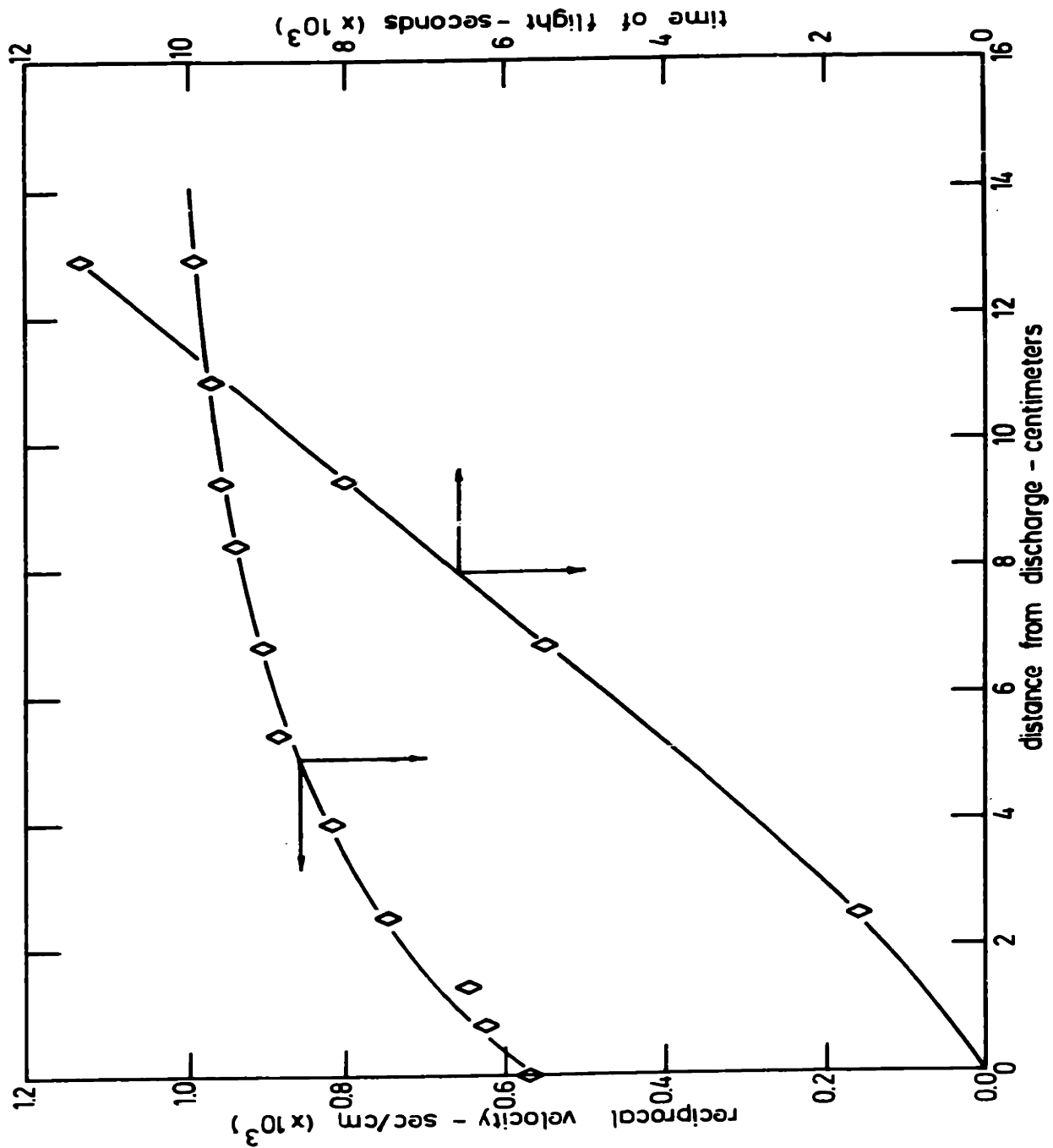


FIGURE A-3. HYDROGEN CHLORIDE VELOCITY DATA AT 10 mm Hg PRESSURE

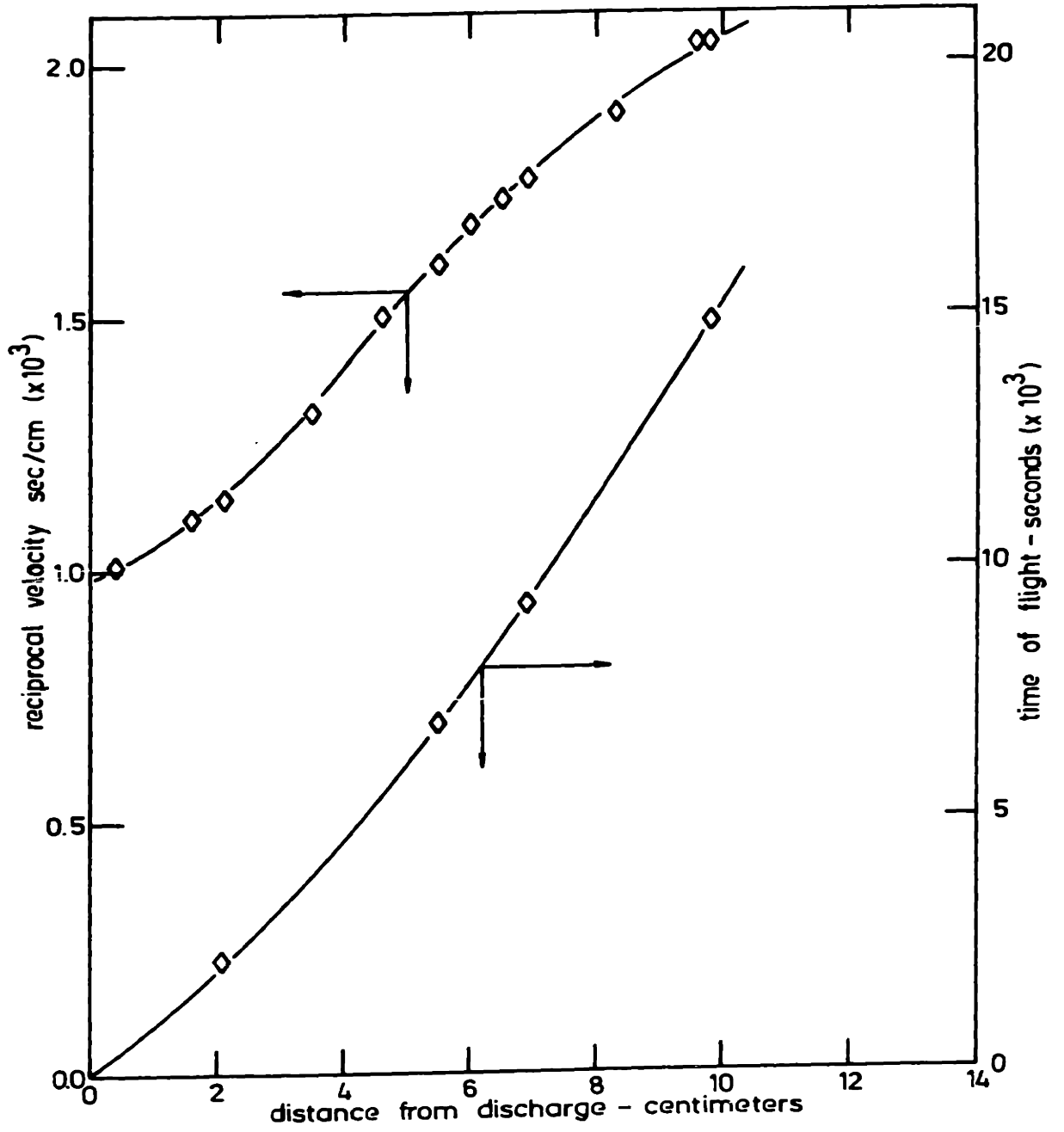


FIGURE A-4. HYDROGEN CHLORIDE VELOCITY TIME DATA AT 20 mm Hg PRESSURE

TABLE A-3
Hydrogen Atom Data at 10 mm Hg Pressure

Run #	Position d cm	Conversion X	Temp °K	Velocity v cm/sec	1/v	Moles H atoms/cc	Time of Flight Sec
509	1.4	0.479	815	1540	0.649×10^{-3}	0.380×10^{-7}	0.80×10^{-3}
510	2.5	0.288	770	1342	0.749×10^{-3}	0.262×10^{-7}	1.59×10^{-3}
511	4.0	0.192	730	1219	0.820×10^{-3}	0.192×10^{-7}	2.86×10^{-3}
513	5.4	0.139	710	1157	0.864×10^{-3}	0.147×10^{-7}	4.17×10^{-3}
516	0.8	0.468	848	1596	0.627×10^{-3}	0.358×10^{-7}	0.40×10^{-3}
517	0.0	0.534	910	1757	0.569×10^{-3}	0.371×10^{-7}	0.0
518	6.8	0.0945	695	1109	0.903×10^{-3}	0.104×10^{-7}	5.52×10^{-3}
527	9.4	0.0266	676	1042	0.960×10^{-3}	0.031×10^{-7}	8.03×10^{-3}
528	10.9	0.0294	665	1029	0.972×10^{-3}	0.031×10^{-7}	9.48×10^{-3}
529	8.4	0.0441	682	1063	0.940×10^{-3}	0.0506×10^{-7}	7.07×10^{-3}
530	12.9	0.0235	650	1003	0.997×10^{-3}	0.0286×10^{-7}	11.37×10^{-3}

TABLE A-4
Hydrogen Atom Data at 20 mm Hg Pressure

Run #	Position d cm	Conversion X	Temp °K	Velocity v cm/sec	1/v	Moles H Atoms/cc	Time of Flight Sec
514	4.6	0.127	824	668	1.50×10^{-3}	0.233×10^{-7}	5.47×10^{-3}
519	9.8	0.0207	636	489	2.04×10^{-3}	0.0516×10^{-7}	14.83×10^{-3}
520	6.9	0.0236	733	564	1.77×10^{-3}	0.0511×10^{-7}	9.28×10^{-3}
521	3.5	0.285	875	762	1.31×10^{-3}	0.458×10^{-7}	3.90×10^{-3}
522	1.6	0.440	975	907	1.10×10^{-3}	0.594×10^{-7}	1.55×10^{-3}
523	0.4	0.471	1050	987	1.01×10^{-3}	0.977×10^{-7}	0.39×10^{-3}
524	5.5	0.0911	787	626	1.60×10^{-3}	0.178×10^{-7}	6.91×10^{-3}
525	8.3	0.0105	686	525	1.90×10^{-3}	0.0244×10^{-7}	11.95×10^{-3}
526	6.5	0.0237	749	577	1.73×10^{-3}	0.0502×10^{-7}	8.58×10^{-3}
531	2.1	0.437	945	875	1.14×10^{-3}	0.610×10^{-7}	2.23×10^{-3}
532	2.1	0.0308	767	594	1.68×10^{-3}	0.0635×10^{-7}	7.73×10^{-3}
533	9.6	0.0074	640	490	2.04×10^{-3}	0.0185×10^{-7}	14.48×10^{-3}

C. Calculation of δ :

The slope in Figure 20 is 107 reciprocal seconds. This number is equal to $(\gamma u/2R)$. From Figure A-2 the slope of the γ versus d plot is approximately 112 cm/sec and in Figure A-1 the slope is 251 cm/sec. At 20 millimeters Equation A-6 shows that the velocity is given by:

$$v = 0.19T(1 + X) \quad (A-6)$$

and at 10 millimeters this is:

$$v = 0.38T(1 + X) \quad (A-6)$$

Substituting the value of v from the slopes of Figures A-1 and A-2 and neglecting X compared to 1 gives temperatures of 590 and 660°K. These average to 625°K. Using this average temperature the mean peculiar velocity may be calculated.

$$u = \left(\frac{8kT}{\pi m}\right)^{\frac{1}{2}} = \frac{(8)(1.38 \times 10^{-16})(625)}{(\pi)(26.8 \times 10^{-24})} = 9.05 \times 10^{-4} \quad (A-12)$$

Hence:

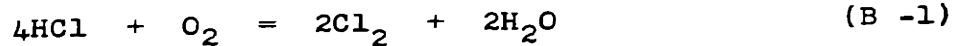
$$\gamma = \frac{2R(\text{slope})}{u} = \frac{2(0.55)(107)}{9.05 \times 10^{-4}} = 13.0 \times 10^{-4} \quad (A-13)$$

The calculation for HCl proceeds in exactly the same way and gives $\delta = 8.62 \times 10^{-4}$.

APPENDIX B

Thermodynamics

For the Deacon Reaction written as:



the equilibrium constant may be written as:

$$K_p = \frac{(P_{\text{Cl}_2})^2 (P_{\text{H}_2\text{O}})^2}{(P_{\text{HCl}})^4 (P_{\text{O}_2})} \quad (\text{B-2})$$

where a standard state of one atmosphere has been assumed. By taking as a basis a feed of four moles of hydrogen chloride and one mole of oxygen, the following equation may be set up for the equilibrium constant in terms of the total pressure and moles of chlorine formed. The symbol "X" denotes the latter.

$$K_p = \frac{X^4(10 - X)}{16p(2 - X)^5} \quad (\text{B-3})$$

Then using data available in Sconce's book (60) for the temperature variation of K_p , the equilibrium conversions to chlorine may be plotted as a function of temperature. Figure (B-1) show this plot. Figures (B-2) and (B-3) show for comparison the actual temperature profile in the region downstream from a mixed feed discharge.

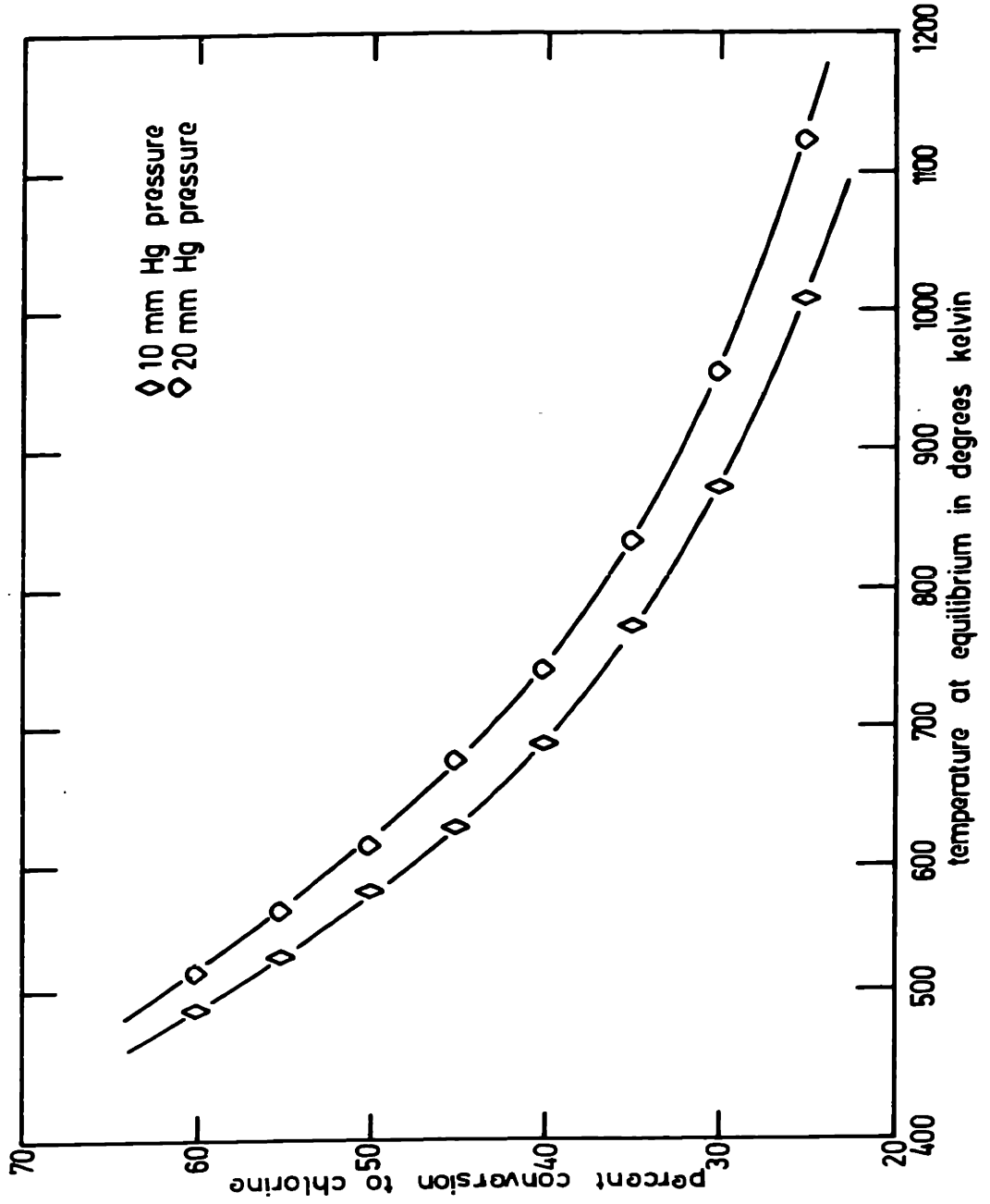


FIGURE B-1. CONVERSION VERSUS EQUILIBRIUM TEMPERATURE

william w cooper iv Sc.D. thesis 10/11/66

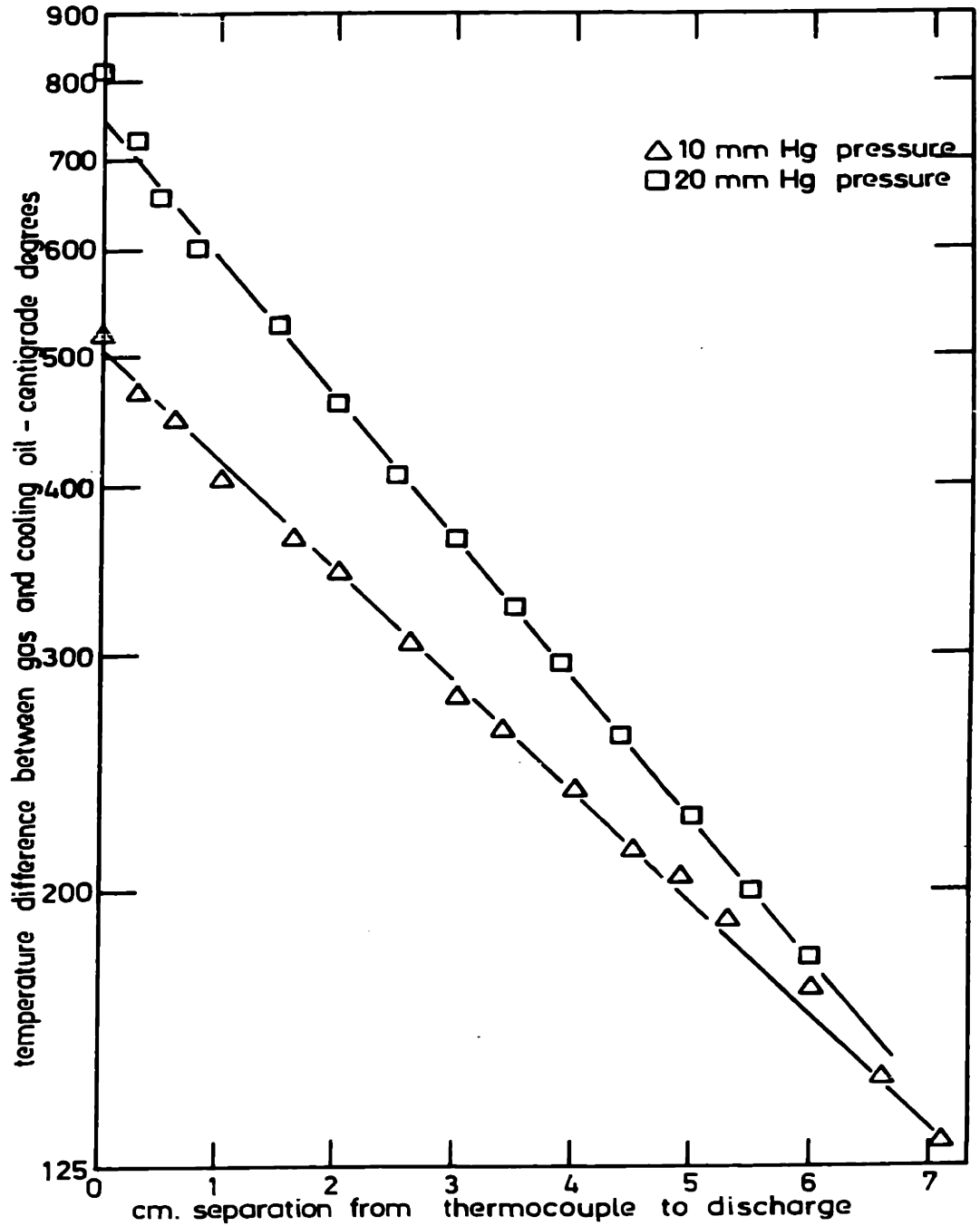


FIGURE B-2. TEMPERATURE PROFILES at 275 watts with mixed feeds

APPENDIX C

A. Reynolds Number

The Reynolds number is given by the formula:

$$Re = dv\rho/\mu \quad (C-1)$$

In the present work the diameter, d , is 1.1 centimeters. To a first approximation the viscosity, μ , is independent of pressure, and varies as the square root of the temperature. For oxygen at 283°C, its value is 323×10^{-6} poise. (65) The gas density at 10 millimeters pressure is:

$$\rho = p/RT = (10)/(760)(82)(566) = 2.83 \times 10^{-7} \text{ moles/cc} \quad (C-2)$$

Taking a molecular weight of 32, this becomes 90.6×10^{-7} gms/cc. With a total feed of 425 ml/min at one atmosphere, the volumetric flow rate is:

$$V = 425/60 \times 566/273 \times 760/10 = 1120 \text{ cc/sec.} \quad (C-3)$$

Since the diameter is 1.1 centimeters, the linear velocity is:

$$v = 1120/(0.55)^2 = 1180 \text{ cm/sec.} \quad (C-4)$$

Substituting Equations (C-2) and (C-4) into Equation (C-1) yields:

$$Re = (1.1)(1180)(90.6 \times 10^{-7})/(323 \times 10^{-6}) = 36.4 \quad (C-5)$$

At twice the pressure this number will be approximately doubled.

B. Estimate of Diffusivity

The Gilliland correlation (61) is:

$$D = 0.0069 \frac{T^{3/2}}{p (V_A^{1/3} + V_B^{1/3})^2} \sqrt{1/M_A + 1/M_B} \quad (C-6)$$

Where D is in ft²/hr, T in °R, p in atm, M_{A,B} the molecular weight, and V_{A,B} tabulated volumetric parameters.

Let p = 20 mm or 0.0263 atm and T = 625°K or 1120 °R so that T^{3/2} = 37,200.

For oxygen V_O = 7.4 so that V_O^{1/3} = 1.95 and V_{O₂} = 14.8 so that V_{O₂}^{1/3} = 2.45. Thus:

$$(V_O^{1/3} + V_{O_2}^{1/3})^2 = 19.35 \quad (C-7)$$

Also for oxygen M_O = 16 and M_{O₂} = 32 so that 1/M_O = 0.0625 and 1/M_{O₂} = 0.03125. Thus:

$$\sqrt{1/M_O + 1/M_{O_2}} = 0.306 \quad (C-8)$$

Substituting into Equation (C-6) yields:

$$D = \frac{(0.0069)(37,200)(0.306)}{(0.0263)(19.35)} = 155 \text{ ft}^2/\text{hr} \quad (C-9)$$

or

$$D_{O-O_2} = (155)(929)/(3600) = 40.0 \text{ cm}^2/\text{sec} \quad (C-10)$$

APPENDIX D

A. Derivation of Diffusion Equation

Consider a material balance on the annular volume element shown in Figure D-1. Let the active specie flux in the radial direction be given by N_r and in the axial direction by N_z .

The rate at which mass enters the volume element is:

$$N_z 2\pi r \Delta r \Big|_z + N_r 2\pi r \Delta z \Big|_r \quad (D-1)$$

and at which it leaves is:

$$N_z 2\pi r \Delta r \Big|_{z+\Delta z} + N_r 2\pi r \Delta z \Big|_{r+\Delta r} \quad (D-2)$$

Setting these rates equal and evaluating the increments by the first term of a Taylor's series gives:

$$\frac{\partial N_z}{\partial z} + \frac{1}{r} \frac{\partial (r N_r)}{\partial r} = 0 \quad (D-3)$$

But the fluxes are given by:

$$N_r = \cancel{x(N_r + M_r)} - cD\partial x/\partial r \cong -D\partial n/\partial r \quad (D-4)$$

$$N_z = \cancel{x(N_z + M_z)} - cD\partial x/\partial z \cong nv_z \quad (D-5)$$

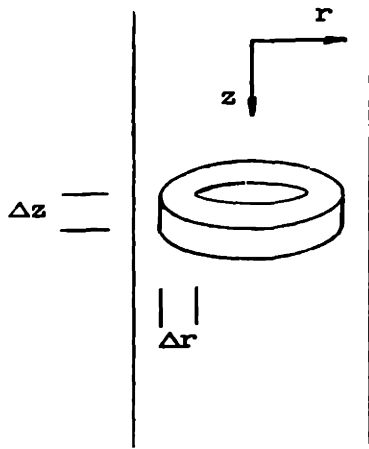


Figure D-1. Annular volume element

where M represents the flux of everything except the active specie. Here it has been assumed that the diffusive flux in the radial direction is predominant and that the convective flux predominates in the axial direction.

With the substitution of Equations (D-4) and (D-5) into (D-3), the following partial differential equation results:

$$\frac{\partial^2 n}{\partial r^2} + \frac{1}{r} \frac{\partial n}{\partial r} - \frac{v_z}{D} \frac{\partial n}{\partial z} = 0 \quad (D-6)$$

If the flow in the tube is laminar, v_z will be a function of radial position given by:

$$v_z = v_0 (1 - (r/r_0)^2) \quad (D-7)$$

If this expression is used in Equation (D-6), it is not possible to integrate it analytically. Because of this difficulty, it is assumed that v_z represents some average velocity which is a constant. With this simplification the integration proceeds directly via separation of variables.

Let $n = \sum RZ$, where R is a function of r only and Z is a function of z only. When RZ is substituted for n in (D-6), there results:

$$\frac{1}{R} \frac{\partial^2 R}{\partial r^2} + \frac{1}{rR} \frac{\partial R}{\partial r} = \frac{1}{Z} \frac{v_z}{D} \frac{\partial Z}{\partial z} \quad (D-8)$$

Setting each side of Equation (D-8) equal to $(a/r_0)^2$ yields:

$$\frac{d^2 R}{dr^2} + \frac{1}{r} \frac{dR}{dr} + \frac{(a)^2 R}{(r_0)^2} = 0 \quad (D-9)$$

$$\frac{dZ}{Z} = - \frac{D(a)^2}{v_z(r_0)^2} dz \quad (D-10)$$

The general solutions are:

$$\begin{aligned} R &= AJ_0(ar/r_0) + BY_0(ar/r_0) \\ Z &= X \exp(-Da^2 z / v_z r_0^2) \end{aligned} \quad (D-11)$$

These solutions are subject to three boundary conditions. The first is that the solution be finite at $r = 0$. This requires the integration constant, "B", to be zero since $Y_0(r)$ is infinite when $r = 0$. Because of this requirement, Equation (D-11) above reduces to:

$$R = AJ_0(ar/r_0) \quad (D-13)$$

The second boundary condition expresses the fact that the loss of the active specie to the wall via diffusion must equal the recombination rate on the wall. Since the collision rate with the wall per unit area is equal to $nu/4$, this balance may be expressed by the equation:

$$-Ddn/dr = \gamma nu/4 \quad (D-14)$$

Here "u" is the mean peculiar speed given by $(8kT/\pi m)^{1/2}$, and γ is the wall recombination coefficient.

To simplify (D-14) the dimensionless variable, "b," defined by:

$$b = 4D/\gamma ur_0 \quad (D-15)$$

is introduced. In terms of this variable Equation (D-14) reduces to:

$$dn/dr = -n/br_0 \quad (D-16)$$

and using the fact that $n = \sum RZ$, (D-16) further reduces to:

$$dR/dr = -R/br_0 \quad (D-17)$$

When (D-13) is substituted into (D-17), the following transcendental equation results:

$$J_0(a_i) = ba_i J_1(a_i) \quad (D-18)$$

Thus:

$$n = \sum_{i=1}^{\infty} X_i \exp(-Da_i^2 z/v_z r_0^2) J_0(a_i r/r_0) \quad (D-19)$$

Application of the third boundary condition expressing a uniformity of active atoms at the base of the discharge allows determination of the X_i 's. This condition states that at $z = 0$, n equals a constant, n_0 . Using these values (D-19) becomes:

$$n_0 = \sum_{i=1}^{\infty} X_i J_0(a_i r/r_0) \quad (D-20)$$

By multiplying both sides of (D-20) by $(r/r_0)J_0(a_i r/r_0)$, integrating from 0 to r_0 , and making use of the orthogonality properties of Bessel functions, there results:

$$n_0 J_1(a_i)/a_i = \frac{1}{2} X_i (1 + b^2 a_i^2) J_1(a_i) \quad (D-21)$$

Solving this for X_i and substituting into (D-19) gives the final solution to Equation (D-6).

$$\frac{n}{n_0} = 2 \sum_{i=1}^{\infty} \frac{\exp(-Da_i^2 z/v_z r_0^2) J_0(a_i r/r_0)}{a_i (1 + b^2 a_i^2) J_1(a_i)} \quad (D-22)$$

B. Average over the Radius

To eliminate the "r" variation in Equation (D-22), it is averaged over the variable r/r_0 .

$$\frac{n(z)}{n_0} = \frac{\int_0^1 (n/n_0)(r/r_0)d(r/r_0)}{\int_0^1 (r/r_0)d(r/r_0)} = \frac{\int_0^1 2 \sum_{i=1}^{\infty} \frac{\exp(-Da_i^2 z/v_z r_0^2) J_0(a_i r/r_0) (r/r_0) d(r/r_0)}{a_i (1 + b^2 a_i^2) J_1(a_i)}}{\int_0^1 (r/r_0)d(r/r_0)} \quad (D-23)$$

Using the facts that:

$$\int_0^1 J_0(a_i r/r_0) (r/r_0) d(r/r_0) = (1/a_i) J_1(a_i) \quad (D-24)$$

and

$$\int_0^1 (r/r_0) d(r/r_0) = \frac{1}{2} \quad (D-25)$$

there results:

$$\frac{n(z)}{n_0} = 4 \sum_{i=1}^{\infty} \frac{\exp(-Da_i^2 z/v_z r_0^2)}{a_i^2 (1 + b^2 a_i^2)} \quad (D-26)$$

C. Magnitude of Terms

The first two terms in the series in Equation (D-26) are:

$$\frac{n(z)}{n_0} = 4 \left[\frac{\exp(-Da_1^2 z/v_z r_0^2)}{a_1^2 (1 + b^2 a_1^2)} + \frac{\exp(-Da_2^2 z/v_z r_0^2)}{a_2^2 (1 + b^2 a_2^2)} + \dots \right] \quad (D-27)$$

Consider the relative values of these two terms at a distance downstream from the discharge such that z/v_z equals one millisecond. Under a pressure of 20 millimeters and at a temperature of 625°K the Gilliland correlation gives a value of the diffusivity, D , of approximately $40 \text{ cm}^2/\text{sec}$. Under these same conditions the peculiar speed, u , is $9.05 \times 10^4 \text{ cm/sec}$. Dickens' value of δ reported in the literature (62) is 1.9×10^{-4} . Putting these values along with a tube radius of 0.55 cm. into Equation (D-15) results in a value of 26.8 for the dimensionless variable, b . With this value of "b" the transcendental equation, (D-18), may be solved for a_1 and a_2 .

In Figure (D-2), $J_0(a)$ and $26.8aJ_1(a)$ have both been plotted versus "a." The intersections of these lines give 0.275 and 3.94 respectively as the values for a_1 and a_2 . With these numbers substituted into Equation (D-27), the first term reduces to 0.236 and the second to 0.74×10^{-5} . Thus it has been shown numerically that the first term in the series of Equation (D-26) provides a satisfactory approximation.

D. Approximation for a_1

The transcendental equation which determines the value of the " a_i 's" has been written as Equation (D-18).

$$J_0(a_i) = ba_i J_1(a_i) \quad (\text{D-18})$$

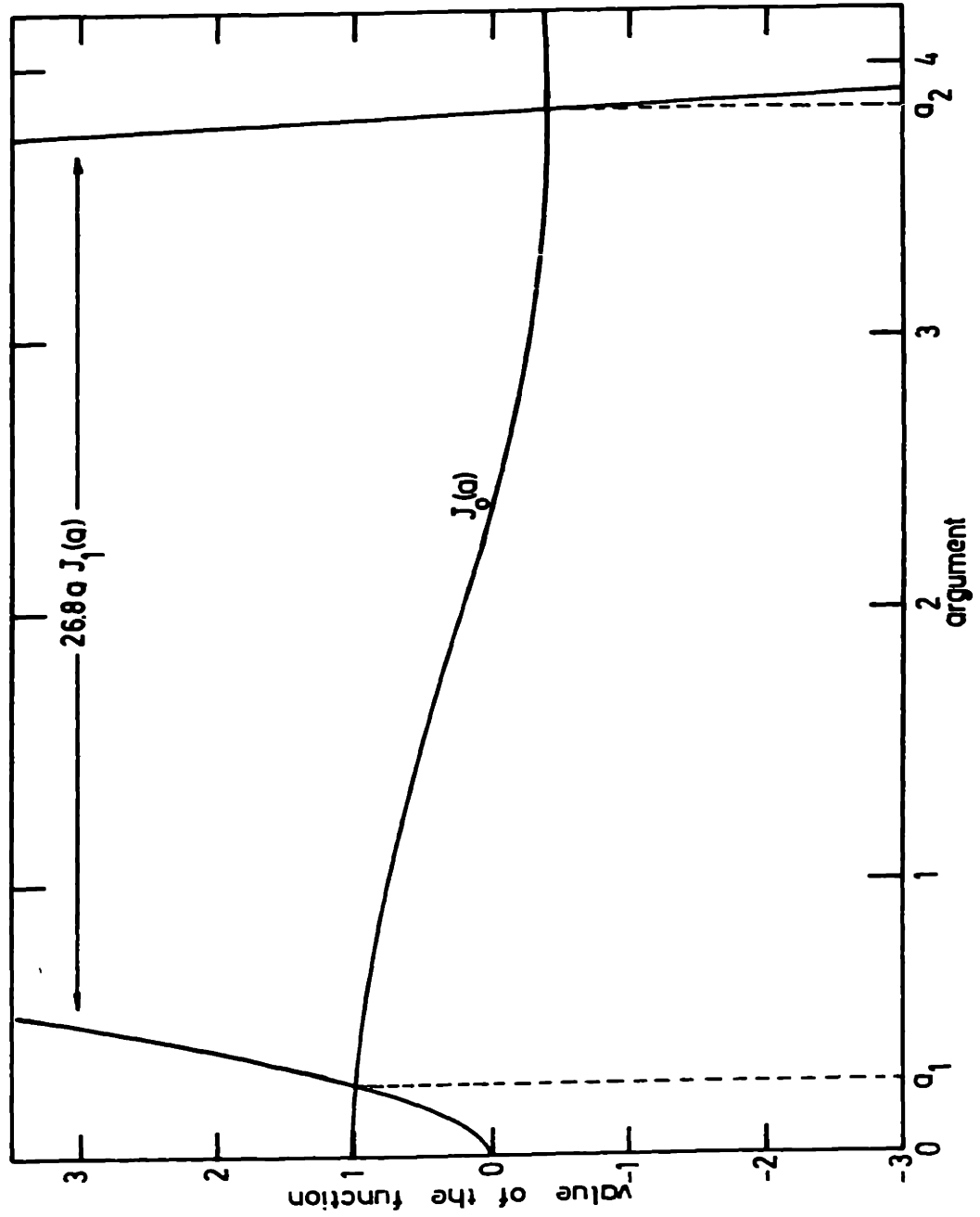


FIGURE D-2 TRANSCENDENTAL EQUATION PLOT

Using the definition of Bessel functions, this equation may be expanded as below:

$$1 - (a/2)^2 + (1/2!)^2(a/2)^4 - \dots = b \left[a^2/2 - (1/2!)a^4/2^3 + \dots \right] \quad (D-28)$$

Collecting terms of the same power in "a" results in:

$$1 - (a^2/2)(b + 1) + (1/2!)(a^4/2^3) \left[b + (1/2)(1/2!) \right] - \dots \quad (D-29)$$

Since only the smallest eigenvalue, a_1 , is of interest, the first two terms form a sufficiently good approximation. In addition if "b" is large compared to unity, the result is:

$$a_1 \cong (2/b)^{\frac{1}{2}} \quad (D-30)$$

APPENDIX EError Estimate of Measured Temperature

Consider a region one centimeter downstream from the discharge. From Table A-2, at 20 millimeters pressure the gas velocity is 155 cm/sec. Figure 20 shows the oxygen atom concentration to be 1×10^{-7} moles of atoms per cubic centimeter and Figure 23 shows a temperature of 463°C . The dissociation enthalpy of the oxygen molecule is 115 kcal/mole.

Since the thermocouple's quartz well is 4 millimeters in diameter, it projects an area of $\pi (0.2)^2 = 0.126$ square centimeters. Hence, the total flux of atoms impinging on the probe is given by the product of this area, their density, and velocity. This is:

$$(0.126)(1 \times 10^{-7})(155) = 19.6 \times 10^{-7} \text{ moles O atoms/sec.} \quad (\text{E-1})$$

The total enthalpy of recombination available is:

$$(115/2)(19.6 \times 10^{-7}) = 1.13 \times 10^{-4} \text{ kcal/sec.} \quad (\text{E-2})$$

But if the recombination coefficient, γ , is 10^{-3} , this heat load is reduced to:

$$\Delta H_r = 1.13 \times 10^{-7} \text{ kcal/sec.} \quad (\text{E-3})$$

Bird, Stewart, and Lightfoot (63) list heat transfer coefficients for forced convection in the range of 10-100 kcal/m²-hr-^oC. Taking the lowest value of 10 this reduces to

2.78×10^{-7} kcal/cm²-sec-°C. The area available for convective transfer is the hemispherical end of the probe which is 0.252 cm².

Then using Newton's law of cooling which may be expressed as:

$$Q_h = hA \Delta T \quad (E-4)$$

the enthalpy of recombination is set equal to the convective heat flux and the equation solved for the required temperature difference.

$$\Delta T = (1.13 \times 10^{-7}) / (0.252)(2.78 \times 10^{-7}) = 1.62^\circ\text{K} \quad (E-5)$$

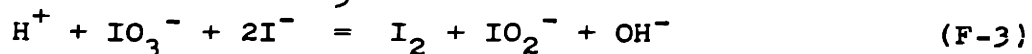
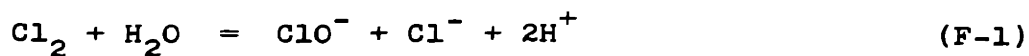
This number then provides an estimate of how much hotter than the gas stream the thermocouple would have to be to dissipate the heat left there by the recombining oxygen atoms.

APPENDIX F

Sample Calculations

A. Wet Analysis

The reactions occurring are listed below:



The chlorine containing product gases are dissolved in an alkaline solution. The pH of this solution is then adjusted to eight and the titration with potassium iodide begun. As long as the strong oxidant ClO^- is present, the iodide is oxidized to the iodate. When it is exhausted, however, the iodate may oxidize the iodide to free iodine. The alkaline solution suppresses this reaction until there is an excess of iodide. The starch indicator shows a very sharp color change as soon as any free iodine is formed by reaction (F-3).

The titrating potassium iodide solution is 0.1N. As can be seen from Equations (F-1) and (F-2) each equivalent of ClO^- corresponds to one mole of Cl_2 and each equivalent of KI added corresponds to three of ClO^- . Also since only one quarter of the total solution is analyzed, this must be multiplied by four. Hence, the total moles of chlorine produced is given by:

$$\text{Cl}_2 = (\text{ml KI}/10^3)(0.100)(3)(4) \quad (\text{F-4})$$

The total moles of Cl_2 that could possibly be formed are:

$$\text{Cl}_2 \text{ pos} = (\text{ml HCl}/2)(1/22,400)(273/298) \quad (\text{F-5})$$

The percent conversion to chlorine is then given by:

$$\% = \frac{(\text{ml KI})(0.100)(3)(4)(2)(22,400)(298)(100)}{(\text{ml HCl})(1,000)(273)} = 5.88 \times 10^3 (\text{ml KI}/\text{ml HCl}) \quad (\text{F-6})$$

Since the runs were timed so that 2000 ml of HCl were always fed, Equation (F-6) becomes:

$$\% = 2.94(\text{ml KI}) \quad (\text{F-7})$$

B. Energy Balance

Figure (F-1) shows the required physical property data of the reactor cooling oil. To perform the balance, in Run 352 the following data were taken:

Oil Temp	= 19.5°C	C_p oil	= 0.464 cal/gm-°C
ΔT oil	= 1.72°C	ρ oil	= 0.779 gm/cc
KI	= 15.4 ml	Power abs	= 196 watts

With a temperature change of 1.72°C and a flow rate of 82.5 cc/sec the power removed by the oil was:

$$(82.5)(0.779)(0.464)(1.72)(4.18) = 214 \text{ watts} \quad (\text{F-8})$$

william w cooper iv Sc.D. thesis 11/5/66

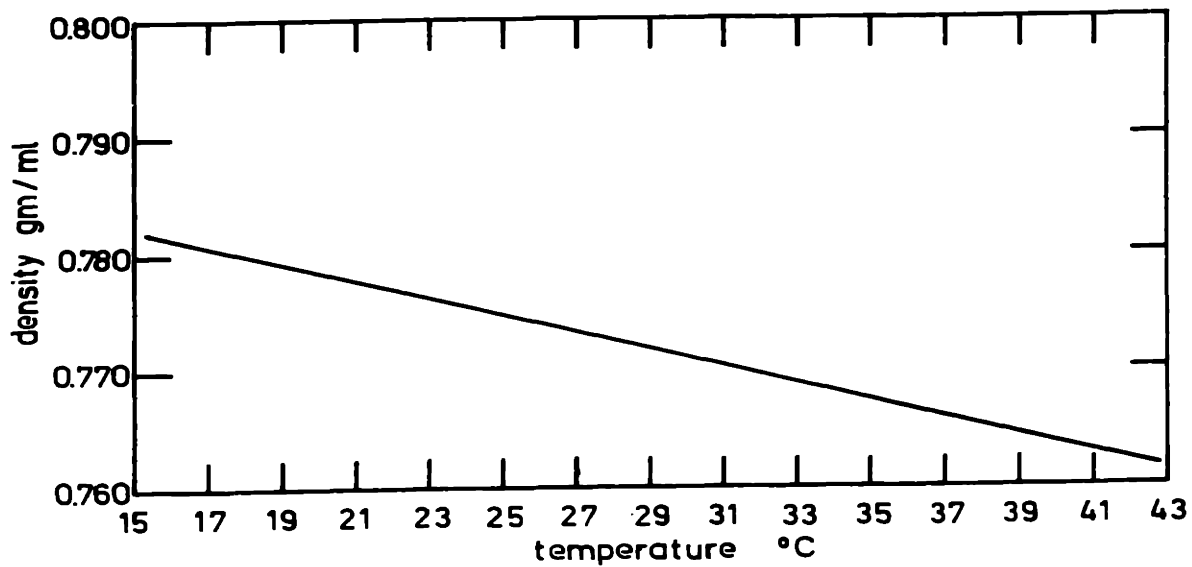
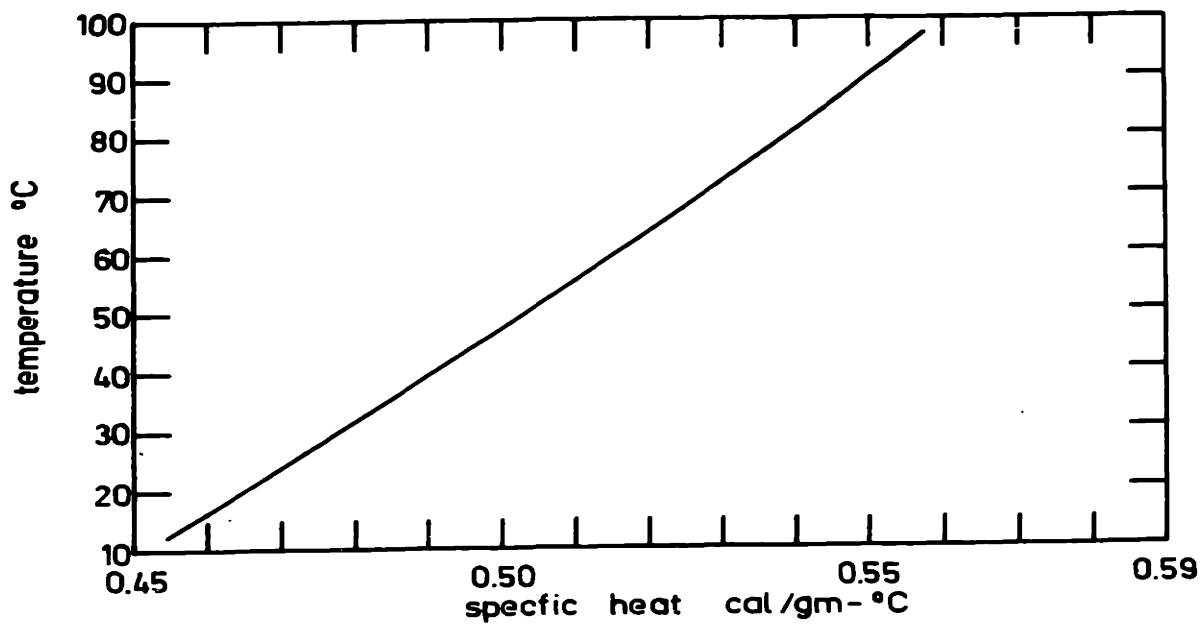


FIGURE F-1. BAYOL-35 PHYSICAL PROPERTY DATA

The reaction occurring is:



For each mole of Cl_2 formed, the heat release is one half this so in view of Equation (F-4) the power release via reaction is:

$$\text{Power} = (\text{ml KI})(12 \times 10^{-4})(4.18)(13,672) = 2.99 \text{ watts} \quad (\text{F-10})$$

Adding this to the microwave power input of 196 watts gives a total input of 199 watts compared with an output of 214 watts in the oil.

C. Calorimetry

The data for Run C-4 will be considered for filament #1. The current and voltage at bridge balance with no discharge were 0.451 amps and 20.8 volts. With a discharge, these declined to 0.300 amps and 13.4 volts. Since the filament is ohmic, the power dissipation there is given by the voltage current product. The difference in this product with and without a discharge corresponds to the power released by the hydrogen atom recombination.

$$\text{No discharge} \quad (20.8)(0.451) = 9.39$$

$$\text{With discharge} \quad (13.4)(0.300) = \frac{4.02}{5.37}$$

Since the dissociation energy of hydrogen molecules is 43.2×10^4 joules per mole, there are:

$(5.37)/(43.2 \times 10^4) = 12.4 \times 10^{-6}$ moles (F-11)
moles of H_2 recombined. This process is repeated for each filament to get the total which in this case was:

$12.4 \times 10^{-6} + 6.5 \times 10^{-6} + 3.5 \times 10^{-6} = 22.4 \times 10^{-6}$ (F-12)
compared with a total flow of 134×10^{-6} moles per second or a 16.8% dissociation.

D. Voltage Standing Wave Ratio and Absorbed Power Calculation

As was mentioned in the text, a null method was used to determine the voltage standing wave ratio. The pancake attenuator used for this null measurement was calibrated in decibels by the manufacturer. A micrometer screw with markings served to adjust the attenuation.

Initially the screw was set and the probe in the slotted section moved until it was located at a standing wave minimum. The current as registered on a microammeter was noted. The probe was then positioned on a standing wave maximum and the attenuator adjusted so that the microammeter reading was the same as at the minimum. The amount the attenuation had to be increased gave directly the voltage standing wave ration in decibels.

For example, in Run #352 the attenuation was changed 8.7 decibels. Using the relation (64):

$$\text{SWR (db)} = 20 \log_{10} \text{SWR (voltage)} \quad (\text{F-13})$$

the voltage standing wave ratio is found to be 2.72

For this same run the power meter read a nominal 300 watts; but because the coupling from the meter to the waveguide was not exactly 50 decibels but rather 49.2 decibels, the actual incident power was 249 watts. Since the voltage standing wave ration was 2.72, the absorbed power was:

$$P_{\text{abs}} = \frac{(249)(4)(2.72)}{(2.72 + 1)^2} = 196 \text{ watts} \quad (\text{F-14})$$

APPENDIX G

Technique of Electric Field Measurement

Rose and Brown (39) discuss the measurement of the electric field within a discharge contained in a cavity of simple geometry. The definition of "Q" as the ratio of the energy stored to the power dissipated in the cavity per radian is used as the basis for the calculation.

The energy stored is:

$$U = \eta E_o^2 \quad (G-1)$$

where η is a geometrical parameter, and E_o is the amplitude of the electric field. However, the unloaded "Q" of the cavity may be written as:

$$Q_u = \eta E_o^2 \omega_o / P_o \quad (G-2)$$

In terms of it the amplitude of the electric field is:

$$E_o = (P_o Q_u / \eta \omega_o)^{\frac{1}{2}} \quad (G-3)$$

where P_o is the power absorbed at the resonant frequency ω_o .

Determination of Q_u as used in Equation (G-3) follows the method outlined by Brown and Rose (57). This procedure consists first of plotting the standing wave ration in decibels versus the wavelength of power supplied to the cavity. The form of this plot is shown in Figure (G-1) on the following page.

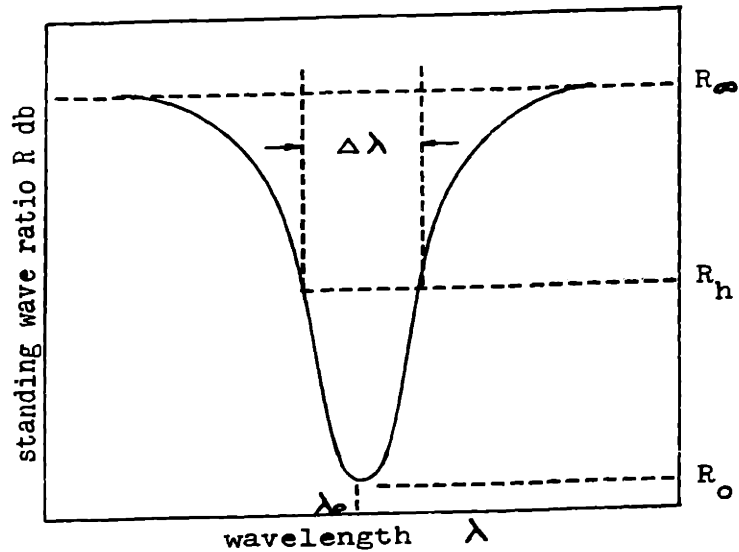


Figure (G-1). Resonance Curve

The ratios R_0 and R_∞ are determined from this curve. Then using plots presented in Brown and Rose's article, R_h can be found. Knowing R_h a $\Delta\lambda$ can be measured from the resonance curve corresponding to Figure (G-1) as its width when $R = R_h$. From $\Delta\lambda$ a quantity, Q_L , may be found according to the relation:

$$Q_L = \lambda_0 / \Delta\lambda \quad (G-4)$$

Next another plot in the same article relating Q_u/Q_L to R_0 for various R 's is used to obtain Q_u .

All that remains is the calculation of \mathcal{R} . Rose and Brown have worked this out for the case of the TM_{010} mode, but the calculations would proceed similarly for any other. The stored energy at the maximum of the sinusoidal time

variation of the electric field is:

$$U = \frac{1}{2} \epsilon_0 \int_0^{r_0} E^2 dv \quad (G-5)$$

Since for the particular mode the electric field configuration is known, this integral may be evaluated and an answer determined in the form of Equation (G-1). From this, η is determined and finally from Equation (G-3), the field strength. This method for the determination of the electric field requires a knowledge of the power absorbed at resonance. This quantity can be ascertained as outlined in Appendix F.

APPENDIX H

Nomenclature

- a_i = eigenvalues of the transcendental equation - dimensionless
- A = area - square centimeters
- b = composite dimensionless variable
- c = concentration - moles per cubic centimeter
- C_p = heat capacity - calories per gram per degree Centigrade
- d = diameter - centimeters
- D = diffusivity - centimeters squared per second
- E = electric field strength - volts per centimeter
- E_o = amplitude of the electric field - volts per centimeter
- f = frequency - reciprocal seconds
- F = force - dynes
- ΔF = free energy change - kilocalories
- h = heat transfer coefficient - kilocalories per square centimeter per second
- ΔH = enthalpy change - kilocalories
- k = Boltzmann's constant - 1.38 ergs per degree Kelvin
- k_i = rate constant in kinetic equation - various dimensions of the form moles to some power per unit time
- m = mass of electron or active particle - grams
- M = molecular weight - grams per mole
or mass of particle with which electrons collide
- n = active species density - moles per cubic centimeter

- n_o = active species density at base of discharge - moles per cubic centimeter
- N = number density of gas molecules - number per cubic centimeter
- N_i = molar flux - moles per square centimeter per second
- p = pressure - either in atmospheres or millimeters of mercury
- p_o = standard pressure at one atmosphere - dimensions consistent with p
- P = power - watts or ergs per second
- q = the electronic charge - 1.602×10^{-19} coulombs
- Q = electron elastic collision cross section - square centimeters
- Q_u = unloaded cavity quality factor - dimensionless
- Q_l = loaded cavity quality factor - dimensionless
- Q_h = heat flux - kilocalories per second
- r = radial position in reactor - centimeters
- r_o = reactor radius - centimeters
- t = time - seconds
- T = temperature - degrees Kelvin
- T_e = electron temperature - degrees Kelvin
- T_g = gas temperature - degrees Kelvin
- T_o = standard temperature - 273° Kelvin
- u = mean peculiar velocity - centimeters per second
- v = velocity - centimeters per second
- \bar{v} = average electron speed - centimeters per second
- v_z = axial velocity - centimeters per second
- W = work - ergs

- x = mole fraction - dimensionless
- U = stored energy - joules
- γ = recombination coefficient - dimensionless
- δ = fraction of an electron's energy dissipated on collision
- ϵ_0 = electron kinetic energy - ergs
- ν_m = collision frequency for momentum transfer - reciprocal seconds
- η = geometrical energy parameter - joule-centimeters squared per volt squared
- μ = viscosity - poise
- λ = wavelength - centimeters
- ω = angular frequency - radians per second

APPENDIX I

Location of Original Data

The original data upon which this thesis is based are contained in four bound notebooks with numbered pages. These are kept on file by Professors Harold S. Mickley and Raymond F. Baddour in the Department of Chemical Engineering at the Massachusetts Institute of Technology.

APPENDIX J

Literature Citations

1. Lunt, R. Winstanley and Meek, C.A. "The Energy Balance and Energy Efficiencies for the Principal Electron Processes in Hydrogen" Proc. Roy. Soc. A157, 146 (1936)
2. Del Greco, Frank P. and Kaufman, Fredrick "Lifetime and Reactions of OH Radicals in Discharge Flow Systems" Discussions of the Faraday Society 33, 128 (1962)
3. Iwasyk, J. M., "The Carbon-Hydrogen System at Temperatures above 2500°C," Sc.D. Thesis in Chemical Engineering, M.I.T., Cambridge, Mass. (1960)
4. Bronfin, Barry R., "Fluro-carbon Synthesis in a High-Intensity Carbon Arc," Sc.D. Thesis in Chemical Engineering, M.I.T., Cambridge, Mass. (1953)
5. Blanchet, Jean L., "Reactions of Carbon Vapor with Hydrogen and with Methane in a High-Intensity Arc," Sc.D. Thesis in Chemical Engineering, M.I.T., Cambridge, Mass. (1963)
6. Leutner, Hans W., "The Production of Cyanogen from the Elements using a Plasma Jet," Ind. and Eng. Chem. Proc. Design and Dev. 1, 166 (1962)
7. McCarthy, R. L., "Chemicals Synthesis from Free Radicals Produced in Microwave Fields," J.Chem. Phys. 22, 1360 (1954)
8. Herlin, Melvin A. and Brown, Sanborn C., "Breakdown of a Gas at Microwave Frequencies," Phys. R_ev. 74, 291 (1948)
9. Brown, Sanborn C., "High-Frequency Gas-Discharge Breakdown," Proc. I. R. E. 39, 1493 (1951)
10. Herlin, Melvin A. and Brown, Sanborn C., "Electrical Breakdown of a Gas between Coaxial Cylinders at Microwave Frequencies," Phys. Rev. 74, 910 (1948)
11. Shaw, T. M., "Dissociation of Hydrogen in a Microwave Discharge," J. Chem. Phys. 30, 1366 (1959)

12. Bak, B. and Rastrup-Anderson, J., "Microwave Discharge Production of Hydrogen Atoms," Acta. Chem. Scand. 16, 111 (1962)
13. Shaw, Thomas M., "Effect of Water Vapor on the Dissociation of Hydrogen in an Electrical Discharge," J. Chem. Phys. 31, 1142 (1959)
14. Young, R. A.; Sharpless, R. L.; and Stringham, R. J., "Catalyzed Dissociation of N_2 in Microwave Discharges," J. Chem. Phys. 40, 117 (1964)
15. Elias, L.; Ogryzlo, E. A.; and Schiff, H. J., "The Study of Electrically Discharged O_2 by means of an Isothermal Calorimetric Detector," Can. J. Chem. 37, 1680 (1959)
16. Kaufman, F. and Kelso, J. R., "Catalytic Effects in the Dissociation of Oxygen in Microwave Discharges," J. Chem. Phys. 32, 301 (1960)
17. Ogryzlo, E. A., "Halogen Atom Reactions: I The Electrical Discharge as a Source of Halogen Atoms," Can. J. Chem. 39, 2556 (1961)
18. Foner, S. N. and Hudson, R. L., "Metastable Oxygen Molecules Produced by Electrical Discharges," J. Chem. Phys. 25, 601 (1956)
19. McTaggart, F. K., "Reactions of Carbon Monoxide in a High Frequency Discharge," Aust. J. Chem. 17, 1182 (1964)
20. McTaggart, F. K., "Reduction of the Alkali and Alkaline Earth Halides in a High-Frequency Discharge: I Hydrogen Discharge," Aust. J. Chem. 18, 937 (1965)
21. McTaggart, F. K., "Reduction of the Alkali and Alkaline Earth Halides in High-Frequency Discharges: II The Role of electrons," Aust. J. Chem. 18, 949 (1965)
22. Vastola, F. J. and Wightman, J. P., "The Rearrangement of Acetylene, Benzene, Ethane, Ethylene, Methane, and Naphthalene in a Microwave Discharge," J. Appl. Chem. 14, 69 (1964)
23. Vastola, F. J.; Walker, P. L.; and Wightman, J.P., "The Reaction between Carbon and the Products of Hydrogen, Oxygen, and Water Microwave Discharges," Carbon 1, 11 (1963)
24. Coates, Arthur D., "Microwave Induced Dissociation of n-Hexane," U.S. Dept. Com. Office Tech. Serv. AD4C9436

25. Streitwieser, Ander Jr. and Ward, Harold R., "Organic Compounds in a Microwave Discharge: II Initial Studies with Toluene and Related Hydrocarbons," J. Am. Chem. Soc. 85, 539 (1963)
26. Smith, W. C. and Engelhardt, V. A., "Chemistry of Sulphur Tetrafluoride: V Preparation of Sulphur Oxytetrafluoride and Sulphur Hexafluoride by Oxidation of Sulphur Tetrafluoride," J. Am. Chem. Soc. 82, 3838 (1960)
27. Emeleus, H. J. and Tittle, B., "Synthesis of Pentafluoro-Sulphur Chloride and Sulphur Oxide Tetrafluoride in the Microwave Discharge," J. Chem. Soc. (London) 1963 1644 (1963)
28. Shriver, D. and Jolly, W. L., "The Microwave Synthesis of Digermanium Hexachloride," J. Am. Chem. Soc. 80, 6692 (1958)
29. Frazer, Jack W. and Holzmann, R. T., "Microwave Excitation as a Synthetic Tool: Preparation of Diboron Tetrachloride," J. Am. Chem. Soc. 80, 2907 (1958)
30. Root, Marcia A., "The Reaction of Tetrafluoromethane in a Microwave Induced Glow Discharge," S. B. Thesis in Chemical Engineering, M.I.T., Cambridge, Mass. (1964)
31. Kontaratos, N. and Demetriades, S. T., "Electrical Breakdown of Gases at Elevated Temperatures," Phys. Rev. 137(6A), 1685 (1965)
32. Vasilev, S. S., "The Energy Balance and Stationary Distribution of Energy under Physico-Chemical Processes in Electrical Discharges," Zh. Fiz. Kjim. 24, 1107 (1950)
33. Massey, J. T. and Cannon, S. M., "Constricted Discharges in the Rare Gases: I. Spectroscopic and Electrical Measurements," J. Appl. Phys. 36, 361 (1965)
34. Brown, S. C. and MacDonald, A. D., "Limits for the Diffusion Theory of High Frequency Gas Discharge Breakdown," Phys. Rev. 76, 1629 (1949)
35. Fehsenfeld, F. C.; Evenson, K. M.; and Broida, J. P., "Microwave Discharge Cavities Operating at 2450 MHz," Rev. Sci. Instr. 36, 294 (1965)
36. Shaw, T. M., "Studies of Microwave Gas Discharges: Production of Free Radicals in a Microwave Discharge," General Electric Technical Information Report Number TIS R58EIM 115, General Electric Microwave Laboratory, Power Tube Department, Palo Alto, California

37. Bell, Alexis T., Personal Communication with the author at the Department of Chemical Engineering, Massachusetts Institute of Technology
38. Charlot, G. and Bezier, Denise, Quantitative Inorganic Analysis, Wiley, New York (1957)
39. Rose, David J. and Brown, Sanborn C., "Methods of Measuring the Properties of Ionized Gases at High Frequencies: II. Measurement of Electric Field," J. Appl. Phys. 23, 719 (1952)
40. McDaniel, Earl W., Collision Phenomena in Ionized Gases Wiley, New York (1964)
41. Fox, R. E., "Negative Ion Formation in Hydrogen Chloride by Electron Impact," J. Chem. Phys. 26, 1281 (1957)
42. Brown, Sanborn C., Basic Data of Plasma Physics, M.I.T. Press, Cambridge, Mass. (1959)
43. Lathrop, J. W., "Characteristics of Steady State Maintaining Fields in a Microwave Discharge," Ph.D. Thesis in Physics, M.I.T., Cambridge, Mass. (1952)
44. Phelps, A. V. and Pack, J. L., "Collisional Detachment in Molecular Oxygen," Phys. Rev. Letters 6, 111 (1961)
45. Kaufman, F. and Kelso, J., "Reactions of Atomic Oxygen and Atomic Nitrogen with Oxides of Nitrogen," Seventh International Symposium on Combustion, London and Oxford (1958) p. 58
46. Linnett, J. W. and Marsden, D. G. H., "The Kinetics of the Recombination of Oxygen Atoms at a Glass Surface," Proc. Roy. Soc. (London) A234, 489 (1955)
47. Janaf Thermochemical Data, Dow Chemical Company, Thermal Laboratory, Midland, Michigan (1962)
48. Harteck, P. und Kopsch, U., Z. fur Physik, Chem. B12, 327 (1931) "Gasreaktionen mit atomarem Sauerstoff"
49. Arnold, S. J.; Finlayson, N.; and Ogryzlo, E. A., $1\Delta_g^*$, "Some Novel Energy-Pooling Processes Involving O_2 ($1\Delta_g^*$)," J. Chem. Phys. 44, 2529 (1966)
50. Foner, S. N. and Hudson, R. L., "Mass Spectrometry of the HO_2 Free Radical," J. Chem. Phys. 36, 2681 (1962)

51. Clyne, M. A. A.; Thrush, B. A.; and Wayne, R. P.; "Some Reactions of Ozone in Discharge Flow Experiments," Nature 199, 1057 (1963)
52. Dickens, P. G.; Schofield, D.; and Walsh, J.; "Recombination of Atoms at Surfaces: Part 8. The Three Dimensional Diffusion Equation," Trans. Faraday Soc. 56, 225 (1960)
53. Greaves, J. C. and Linnett, J. W., "The Recombination of Oxygen Atoms at Surfaces,": Trans. Faraday Soc. 54, 1323 (1958)
54. Wise, Henry and Ablow, Clarence, "Diffusion and Hetrogeneous Reaction: I. The Dynamics of Radical Reactions," J. Chem. Phys. 29, 634 (1958)
55. Chapman, S. and Cowling, R. G., The Mathematical Theory of Non-Uniform Gases, University Press, Cambridge, second edition (1961)
56. Pearse, R. W. B. and Gaydon, A. G., The Identification of Molecular Spectra, Chapman and Hall L.T.D., London (1963)
57. Brown, Sanborn C. and Rose, David J., "Methods of Measuring the Properties of Ionized Gases at High Frequencies: I. Measurements of Q," J. Appl. Phys. 23, 711 (1952)
58. Rose, David J. and Brown, Sanborn, C., "Methods of Measuring the Properties of Ionized Gases at High Frequencies: III. Measurement of Discharge Admittance and Electron Density," J. Appl. Phys. 23, 1028 (1952)
59. Heald, M. A. and Wharton, C. B., Plasma Diagnostics with Microwaves, Wiley, New York (1965)
60. Sconce, J. S. (ed), Chlorine, Its Manufacture, Properties, and Uses, A.C.S. Monograph Series, Reinhold, New York (1962)
61. Sherwood, Thomas K, and Pigford, Robert L., Absorption and Extraction, McGraw-Hill, New York (1952)
62. Dickens, P. G.; Gould, R. D.; Linnett, J. W.; and Richmond, A., "Recombination of Oxygen Atoms in the Gas Phase," Nature 187, 686 (1960)
63. Bird, R. Bryon; Stewart, Warrem E.; and Lightfoot, Edwin N., Transport Phenomena, Wiley, New York (1960)
64. Slater, John C., Microwave Electronics, Van Nostrand, Princeton (1950)

APPENDIX K

Biographical Note

The author was born on June 24, 1941 in Salisbury, Maryland. He attended public schools in Massachusetts through the eighth grade. His secondary education was at the Lawrence Academy in Groton, Massachusetts where he studied under the Huntley N. Spaulding Scholarship.

He entered the Massachusetts Institute of Technology in September 1959. These undergraduate studies were financially assisted by an Alfred P. Sloan Foundation Scholarship. During the course of his work, the author was elected to the Tau Beta Pi Association, the Society of the Sigma Xi, and Phi Lamda Upsilon. He received his Bachelor of Science degree in Chemical Engineering in June 1963,

Graduate education under a National Science Foundation Cooperative Fellowship was begun in the fall of 1963 and the degree of Master of Science in Chemical Engineering was awarded to him in September 1964. After receiving this degree, he continued his studies under the same fellowship.

